THEORETICAL EXAMINATION OF PASSING SIGHT DISTANCE IN THREE DIMENSIONS WITH APPLICATION TO MARKING NO-PASSING ZONES

A Dissertation

by

MEHDI AZIMI

Submitted to the Office of Graduate Studies of
Texas A&M University
in partial fulfillment of the requirements for the degree of

DOCTOR OF PHILOSOPHY

Approved by:

Chair of Committee,	H. Gene Hawkins
Committee Members,	Dominique Lord
	Yunlong Zhang
	Russell Feagin
Head of Department,	John Niedzwecki

December 2012

Major Subject: Civil Engineering

ABSTRACT

Rural two-lane highways constitute the majority of the road system in the United States. Over 62 percent of the Texas Department of Transportation (TxDOT) center line highway miles are two-lane highways. No-passing zones, which are indicated by solid lines separating the traffic moving in opposite directions, tell drivers where there are segments of two-lane highways that do not have sufficient sight distance to safely perform passing maneuvers.

This study describes a method for automating the process for locating no-passing zones using global positioning system (GPS) data. The author developed a new analytical algorithm to evaluate three-dimensional passing sight distances that will work for any arbitrary alignment of two-lane highway. The algorithm was incorporated into a computer model that uses GPS data as the input and results in the locations for no-passing zones. The steps involved in the process include collecting the GPS data, converting it to a form that models the roadway center line, evaluating the availability of passing sight distance, and determining the locations where no-passing zone markings should be placed. The resulting automated system processes GPS coordinates and converts them into easting and northing values, smoothes GPS data and evaluates roadway alignments for possible sight restrictions that indicate where no-passing zones should be located. The automated system was tested on three highway segments using two different GPS receivers, and the results obtained were in general agreement with the existing locations of no-passing zone markings. The verification results indicate that the

algorithm and the computer program developed in this dissertation can be used to determine the availability of passing sight distance and locate no-passing zones.

DEDICATION

This dissertation is dedicated to my lovely wife, Noushin. It would not have happened without her support, encouragement, patience, and love. I am forever indebted to her.

ACKNOWLEDGEMENTS

I would like to express my sincere gratitude and deep appreciation to my advisor, Dr. H. Gene Hawkins, for his constant support and guidance throughout my study and throughout the completion of this dissertation, and also for providing funding for the entire period of my PhD study. As my mentor, he has truly had a profound impact on my life.

I would like to thank my committee members, Dr. Dominique Lord, Dr. Yunlong Zhang, and Dr. Russell Feagin for all their time, suggestions, constructive advice, and critical reviews of this dissertation.

I am greatly indebted to the Texas A&M Transportation Institute (TTI) for providing me an invaluable research experience. I also wish to thank my colleagues and friends, including Cameron Williams, Adel Khodakarami, and Hongmin Zhou, for their friendship and also their help and healthy discussions during my study.

Last, but not least, I would like to express my deep gratitude to my wife, parents, sister, and brother for their love and support.

The author recognize that support for this research was provided by a grant from the U.S. Department of Transportation, University Transportation Centers Program to the Southwest Region University Transportation Center, which is funded, in part, with general revenue funds from the State of Texas.

TABLE OF CONTENTS

LIST OF FIGURES

Page

LIST OF TABLES

Page

CHAPTER I

INTRODUCTION

Two-lane, two-way highways are an important element of the transportation system and they make up a large percent of the total highway mileage. Over 62 percent of the 80,000 center line highway miles on the TxDOT system are rural two-lane highways (*1*). A unique feature of two-lane highways is that in order to pass a slower-moving vehicle, a faster-moving vehicle must cross into the oncoming lane (at locations where adequate sight distance exists and there are no oncoming vehicles). Pavement markings (solid center lines) and traffic signs are used to indicate the location of no-passing zones where driving to the left of the center line is prohibited. The no-passing zones indicate locations where the sight distance is less than the minimum passing sight distance. This study used GPS data and applied theoretical approaches to evaluate three-dimensional (3D) sight distances in order to develop a method for automating the process for locating no-passing zones.

PROBLEM STATEMENT

Identifying highway segments that do not have adequate passing sight distance can be a challenging task because of the amount of the time necessary to locate the segments (no-passing zones) and the hazards involved in working on the highway in the presence of moving traffic. Various methods for measuring passing sight distance in the field and determining the location of no-passing zones have been developed and used. Most of

the methods used by highway agencies require work crews to operate in the roadway to physically evaluate sight distances in the field. As a result, there may be one or more weaknesses in the current methods due to the amount of time required, accuracy obtained, and/or related safety issues presented. Therefore, new methods that efficiently locate no-passing zones, define the no-passing zones accurately, and do so safely are needed. GPS has the potential to meet these needs; however, processes for gathering roadway GPS data, smoothing GPS data, mathematically locating no-passing zones from GPS data, and implementing the results in the field must be addressed. The author believed that a system (prototype) enabling work crews to drive on two-lane roadways with GPS receivers to automatically determine no-passing zones could be developed by focusing on these issues.

RESEARCH OBJECTIVES

The goal of the research was to develop a safe, reliable, fast, and accurate system that automates the process for locating no-passing zones and is applicable to roadways with changes in both horizontal and vertical alignment. To this end, the research entailed the following objectives:

- Identify the processes necessary to smooth GPS data and geometrically model roadway surface
- Create algorithms for evaluating sight distances and locating no-passing zones from modeled roadway surfaces due to horizontal and vertical sight obstructions

- Develop a computer model, a software package, and a prototype model that can be used by engineers in the field to establish the location of no-passing zones

RESEARCH ORGANIZATION

This research developed a method for automating the process for locating no-passing zones by developing a new theoretical approach to address the three-dimensional alignment concepts. The following paragraphs describe the organization of this dissertation.

Chapter II: Background

Chapter II presents the background for the research including information about passing sight distance, no-passing zone, and GPS. The passing sight distance background includes the definition of passing sight distance, the origin of the American Association of State Highway and Transportation Officials (AASHTO) Green Book passing sight distance, and the origin of the Manual on Uniform Traffic Control Devices (MUTCD) passing sight distance. The no-passing zone background includes the definition of no-passing zone and a review of the current location methods for no-passing zones. In the GPS section, different technology, the accuracy of GPS data, and the application of GPS in highway engineering are reviewed.

Chapter III: Theoretical Approach

Chapter III first presents a method for converting GPS data to be used in the model as well as a method for smoothing the GPS data and geometric modeling of highways. Then, it outlines the development of new algorithms for evaluating sight distances. The three main algorithms deal with the vertical sight distance, horizontal sight distance, and three-dimensional sight distance. Furthermore, two other new algorithms are presented that are used in the main algorithms: one for converting the center of travel lane to the roadway center line, and the other one for modeling the right and the left visual clear zone boundaries. Finally, the chapter discusses how the algorithms can be incorporated into a computer model to locate no-passing zones on two-lane highways.

Chapter IV: Software Package Development

This chapter describes the procedure for coding the no-passing zone computer model and creating the no-passing zone (NPZ) program. The interface of the computer program is explained and illustrated in the chapter, as well.

Chapter V: Data Collection and Experimental Work

Data collection and experimental work of the research are presented in this chapter according to three main steps: data collection site selection, field operation and data collection, and data post-processing and reduction. Each step is explained in detail, and the process for preparing the input files for the NPZ computer program is described.

Chapter VI: Results and Model Validation

This chapter summarizes the results of the no-passing zone model developed in the previous chapters and compares the results to the existing pavement marking (no-passing zones) in the field.

Chapter VII: Conclusions

Chapter VII summarizes the research efforts and presents the conclusion for the conducted research effort.

CHAPTER II

BACKGROUND

The criteria for marking no-passing zones are contained in the MUTCD (*2*). Location of a no-passing zone for a new highway can be determined from a set of plans (graphical method), but the location needs to be confirmed in the field due to potential differences between the plans and the actual construction. Locating no-passing zones in the field typically involves surveying activities or field measurements. In the field measurements, the common method is using two vehicles or targets with specific heights (such as a driver's eye and an object) that are connected by a rope (associated with the appropriate passing sight distance) in order to check the available sight distance along the highway. Both methods are time consuming, expensive, and subject to error, and they can significantly impact other vehicles traveling on the roadway. Furthermore, these procedures place workers in the presence of moving traffic. In addition to determining the location of no-passing zones for a new highway, the location needs to be reestablished whenever the speed limit changes, when obstacles are placed that block the sight distance in the vertical or horizontal plane, and sometimes when the pavement is resurfaced. There is a need to develop an automated method of locating no-passing zones that is ready for implementation by transportation agencies. Previous research efforts have addressed some aspects related to this need (*3-9*), but they either consider only special cases or the approaches are not feasible or ready for implementation. This research intended to develop a method for locating no-passing zones that is based on

GPS and considers both horizontal and vertical alignment perspectives of the roadway. Such an automated system can save time and cost, avoid human errors, and be safer compared to the current methods of field measurements. In the process of developing such a system, the author found several related topics that deserved review. This chapter presents pertinent background information in areas related to this research effort.

PASSING SIGHT DISTANCE

Sight distance, the length of roadway visible to a driver, has been recognized as a key element in highway geometric design. The AASHTO Green Book states that the designer should provide sufficient sight distance for the drivers to control operation of their vehicles before striking unexpected objects in the traveled way (*10*). Two-lane highways should also have sufficient sight distance to provide opportunities for faster drivers to occupy the opposing traffic lane for passing other vehicles without risk of a crash where gaps in opposing traffic permit. Two-lane rural highways should generally provide such passing sight distance at frequent intervals and for substantial portions of their length (*10*).

There were originally two types of passing sight distance criteria for two-lane highways that were used by highway agencies: geometric design passing sight distance and marking criteria passing sight distance. The AASHTO Green Book and MUTCD both cover the subject of passing sight distance. The contents of these documents are briefly covered below.

AASHTO GREEN BOOK

The 2004 AASHTO publication "A Policy on Geometric Design of Highways and Streets" (*11*), also known as the 2004 Green Book, presents a simple but conservative model for determining the passing sight distance based on the results of field studies conducted between 1938 and 1958 (*12*). The model incorporates three vehicles and is based on five assumptions:

1. The vehicle being passed (the overtaken vehicle) travels at a constant (uniform) speed.
2. The passing vehicle follows the slow vehicle into the passing section.
3. Upon entering the passing section, the passing driver requires a short period of time to perceive that the opposing lane is clear and to begin accelerating.
4. The passing vehicle travels at an average speed that is 10 mph faster than the vehicle being passed while occupying the left lane.
5. When the passing vehicle returns to its lane, there is an adequate clearance distance between the vehicle and an oncoming vehicle in the other lane.

The 2004 AASHTO minimum passing sight distance is the sum of four distances, as follows (Figure 1 gives a graphical explanation of these elements):

$$S = d_1 + d_2 + d_3 + d_4 \quad (1)$$

- Element d_1 (initial maneuver distance) is the distance traversed during perception and reaction time and during initial acceleration to the point of encroachment on the left lane. It is defined by the following equation:

$$d_1 = 1.47\, t_1 \left(V - m + \frac{a\, t_1}{2}\right) \quad (2)$$

where t_1 = time of initial maneuver (sec), V = average speed of passing vehicle (mph), m = difference in speed of passed and passing vehicle (mph), and a = average acceleration (mph/sec).

- Element d_2 (occupancy distance) is the distance traveled while the passing vehicle occupies the left lane and is defined by the following equation:

$$d_2 = 1.47\, V\, t_2 \quad (3)$$

where V = average speed of passing vehicle (mph), and t_2 = time passing vehicle occupies the left lane (sec).

- Element d_3 (clearance distance) is the distance between the passing vehicle at the end of its maneuver and the opposing vehicle. Based on the studies, the clearance distance is between 100 and 300 ft.

- Element d_4 (encroachment distance) is the distance traversed by an approaching vehicle during a passing maneuver. The encroachment distance is calculated by multiplying the speed of the opposing vehicle (normally assumed to be the speed of the passing vehicle) by two-thirds of the time the passing vehicle occupies the left lane:

$$d_4 = 1.47\, V \left(\frac{2}{3}\, t_2\right) = \frac{2}{3}\, d_2 \quad (4)$$

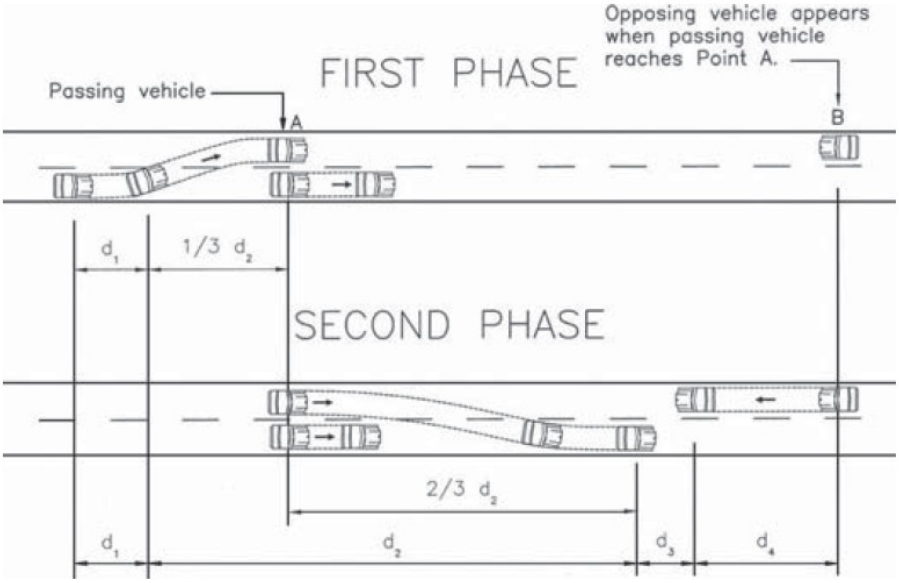

Source: Exhibit 3-4, Reference (*11*)

Figure 1. Elements of passing sight distance for two-lane highways, presented in 2004 AASHTO Green Book

Table 1 summarizes the results of field observations directed toward quantifying the various aspects of the passing sight distance.

Table 1. Elements of safe passing sight distance for design of two-lane highways, presented in 2004 AASHTO Green Book

Component of Passing Maneuver	Speed Range (mph)			
	30-40	40-50	50-60	60-70
	Average Passing Speed (mph)			
	34.9	43.8	52.6	62.0
Initial Maneuver				
a=average acceleration (mph/sec)	1.40	1.43	1.47	1.50
t_1=time (sec)	3.6	4.0	4.3	4.5
d_1=distance traveled (ft)	145	216	289	366
Occupation of Left Lane				
t_2=time (sec)	9.3	10.0	10.7	11.3
d_2=distance traveled (ft)	477	643	827	1030
Clearance Length				
d_3=distance traveled (ft)	100	180	250	300
Opposing Vehicle				
d_4=distance traveled (ft)	318	429	552	687
Total Distance, $d_1+d_2+d_3+d_4$	1040	1468	1918	2383

Source: Exhibit 3-5, Reference (*11*)

The design lengths for passing sight distances for various speeds and the corresponding individual values of d_1, d_2, d_3, and d_4 are shown in Figure 2.

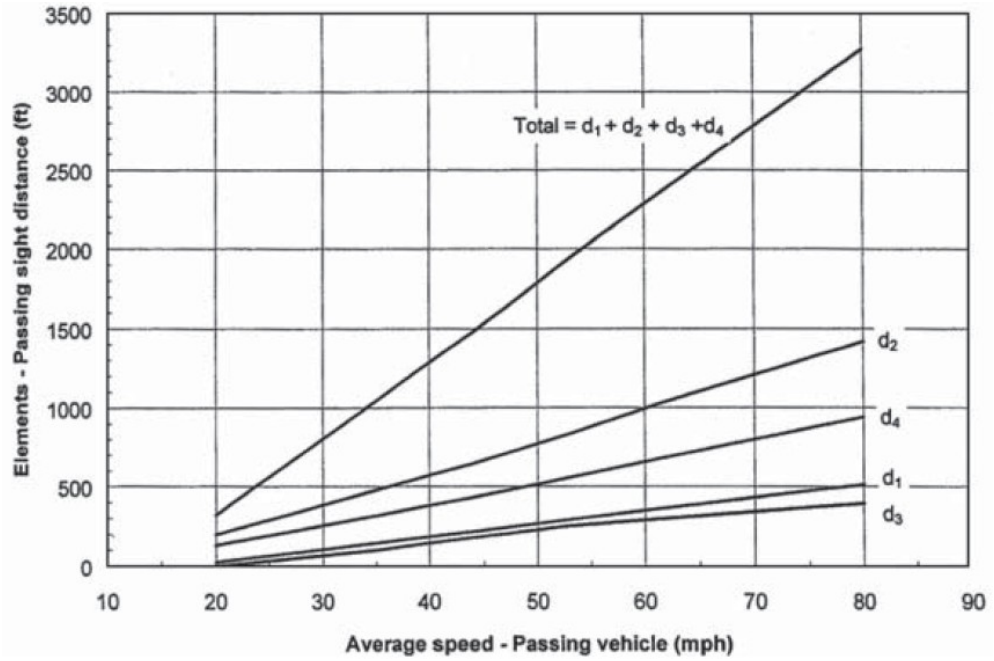

Source: Exhibit 3-6, Reference (*11*)

Figure 2. Total passing sight distance and its components--two-lane highways, presented in 2004 AASHTO Green Book

The 2004 AASHTO Green Book recommends minimum passing sight distances between 710 and 2680 ft for two-lane highways for design speeds ranging from 20 to 80 mph (see Table 2). These values are based on the driver's eye height being 3.5 ft and the height of the object being 3.5 ft.

Table 2. 2004 Green Book passing sight distances for design of two-lane highways

Design Speed (mph)	Assumed Speeds (mph)		Passing Sight Distance (ft)	
	Passed Vehicle	Passing Vehicle	Calculated	Rounded for Design
20	18	28	706	710
25	22	32	897	900
30	26	36	1088	1090
35	30	40	1279	1280
40	34	44	1470	1470
45	37	47	1625	1625
50	41	51	132	1835
55	44	54	1984	1985
60	47	57	2133	2135
65	50	60	2281	2285
70	54	64	2479	2480
75	56	66	2578	2580
80	58	68	2677	2680

Source: Exhibit 3-7, Reference (*11*)

The 2004 AASHTO passing sight distance values presented in Table 2 were used for design purposes only. A research study conducted in 2008 (*12*), found that two-lane highways can be safely designed with the MUTCD passing sight distance criteria (used for marking of passing and no-passing zones on two-lane highways). According to this research study, the 2004 AASHTO Green Book passing sight distance criteria is often considered to be impractical, although it might make the traffic operations more efficient. The study recommended modifications to the text of the 2004 AASHTO Green Book to implement the MUTCD passing sight distance criteria in passing sight distance design. The 2011 AASHTO Green Book (*10*) applied the modifications. Passing sight distance for two-lane highways was revised and is now consistent with the MUTCD (see Table 3).

Table 3. 2011 Green Book passing sight distances for design of two-lane highways

Design Speed (mph)	Assumed Speeds (mph)		Passing Sight Distance (ft)
	Passed Vehicle	Passing Vehicle	
20	8	20	400
25	13	25	450
30	18	30	500
35	23	35	550
40	28	40	600
45	33	45	700
50	38	50	800
55	43	55	900
60	48	60	1000
65	53	65	1100
70	58	70	1200
75	63	75	1300
80	68	80	1400

Source: Table 3-4, Reference (*10*)

MANUAL ON UNIFORM TRAFFIC CONTROL DEVICES

The MUTCD developed by the Federal Highway Administration (*2*), lays out minimum passing sight distance for placing no-passing zone pavement markings on completed highways. The MUTCD criteria were first incorporated in the 1948 MUTCD, were identical to those presented in the 1940 American Association of State Highway Officials (AASHO; now AASHTO) policy on marking no-passing zones (*13*), and were used as warrants for no-passing zones (*12*). The warrants are based on a compromise between delayed and flying passes. A delayed pass is a maneuver in which the passing vehicle slows down before making a pass. A flying pass is a maneuver in which the passing vehicle is not delayed by the slower, passed vehicle. Table 4 presents the sight distances for flying and delayed passes and the minimum sight distances suggested by the 1940 AASHO policy on marking no-passing zones (*13*).

Table 4. Sight distances for flying and delayed passes

V, assumed design speed of the road (mph)	30	40	50	60	70
m, difference in speed between the assumed design speed of the road and the assumed speed of the overtaken vehicle (mph)	10	12.5	15	20	25
V_0, assumed speed of an opposing vehicle comes into view just when the passing maneuver is begun (mph)	25	32.5	40	47.5	55
Sight Distances for Flying Passes (ft)	440	550	660	660	660
Sight Distances for Delayed Passes (ft)	510	760	1090	1380	1780
Suggested Minimum Sight Distances (ft)	500	600	800	1000	1200

Source: Reference (*13*)

In the table, V denotes the assumed design speed of the road and is defined as follows (*13*):

> "*The assumed design speed is considered to be the maximum approximately uniform speed which probably will be adopted by the faster group of drivers but not, necessarily, by a small percentage of reckless ones.*
>
> *The design speed of an existing road or section of road may be found by measuring the speed of travel when the road is not congested, plotting a curve relating speeds to numbers or percentages of vehicles and choosing a speed from the curve which is greater than the speed used by almost all drivers. It may also be found by driving the road until a comfortable maximum uniform speed is found.*"

Table 5 presents changes of the MUTCD criteria for passing sight distance (minimum passing sight distance, height of driver eye, and height of object) over time. The values for minimum passing sight distances have not been changed over time,

although more values were added in 2000 to include all the corresponding speed limit increments of 5 mph. However, the height of driver eye has decreased with time as the vehicle sizes and dimensions changed. The height of eye has been reduced from 4.5 ft in 1948 to 3 ft in 2000. The height of the object also has been decreased with the same range. It means that the available passing sight distances have been decreased for the vehicles over the years.

Table 5. Change of MUTCD passing sight distance criteria over time

		1948	1961	1971	1978 Rev. 3	2000 - 2009
Minimum PSD (ft)	25 mph	-	-	-	-	450
	30 mph	500	500	500	500	500
	35 mph	-	-	-	-	550
	40 mph	600	600	600	600	600
	45 mph	-	-	-	-	700
	50 mph	800	800	800	800	800
	55 mph	-	-	-	-	900
	60 mph	1000	1000	1000	1000	1000
	65 mph	-	-	-	-	1100
	70 mph	1200	1200	1200	1200	1200
Height of Driver Eye (ft)		4.5	4.0	3.75	3.5	3.5
Height of Object (ft)		4.5	4.0	3.75	3.5	3.5

Table 6 lists the 2009 MUTCD recommended minimum passing sight distances for various speeds. Although the current MUTCD adopted the same minimum passing sight distances as the 1940 AASHO policy on marking no-passing zones, it defines the symbol V as 85th-percentile/posted/statutory speed rather than design speed (see Table 6).

Table 6. Minimum passing sight distances for no-passing zones markings

85th Percentile or Posted or Statutory Speed Limit (mph)	Minimum Passing Sight Distance (ft)
25	450
30	500
35	550
40	600
45	700
50	800
55	900
60	1000
65	1100
70	1200

Source: Table 3B-1, Reference (*2*)

As it was discussed earlier (Table 5), the current MUTCD passing sight distance criteria are measured based on 3.5 ft height of driver eye and 3.5 ft height of object (the 3.5 ft height of object allows the driver to see the top of a typical passenger car). In other words, it is assumed that the driver's eyes are at a height of 3.5 ft from the road surface and the opposing vehicle is 3.5 ft tall. The actual passing sight distance is the length of roadway ahead over which the object would be visible. On a vertical curve, it is the distance at which an object 3.5 ft above the pavement surface can be seen from a point 3.5 ft above the pavement (see Figure 3). Similarly, on a horizontal curve, it is the distance measured along the center line between two points 3.5 ft above the pavement on a line tangent to the embankment or other obstruction that cuts off the view on the inside of the curve (see Figure 4).

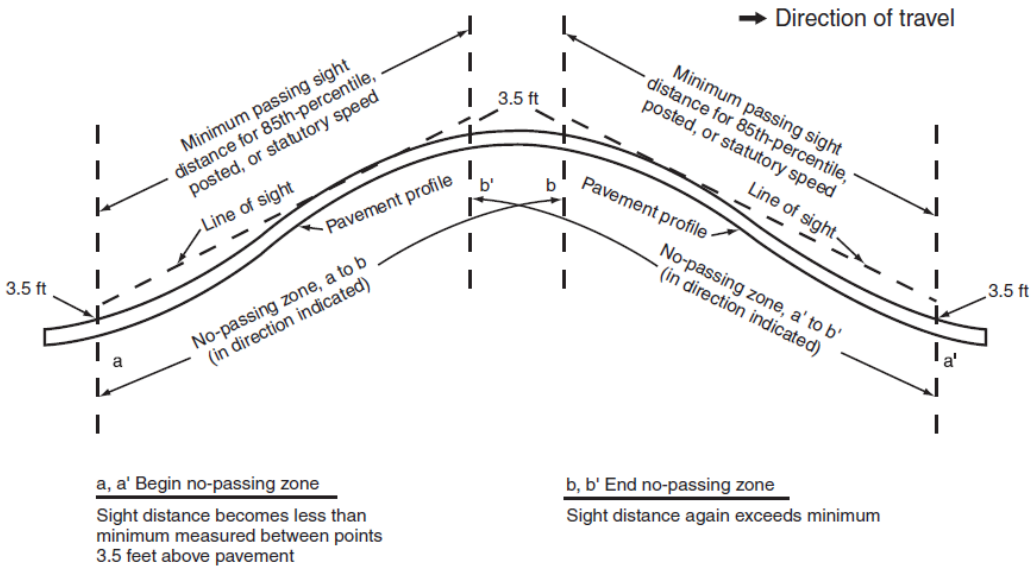

Profile View

Note: No-passing zones in opposite directions may or may not overlap, depending on alignment

Source: Exhibit 3B-4, Reference (*2*)

Figure 3. Passing sight distance at vertical curve

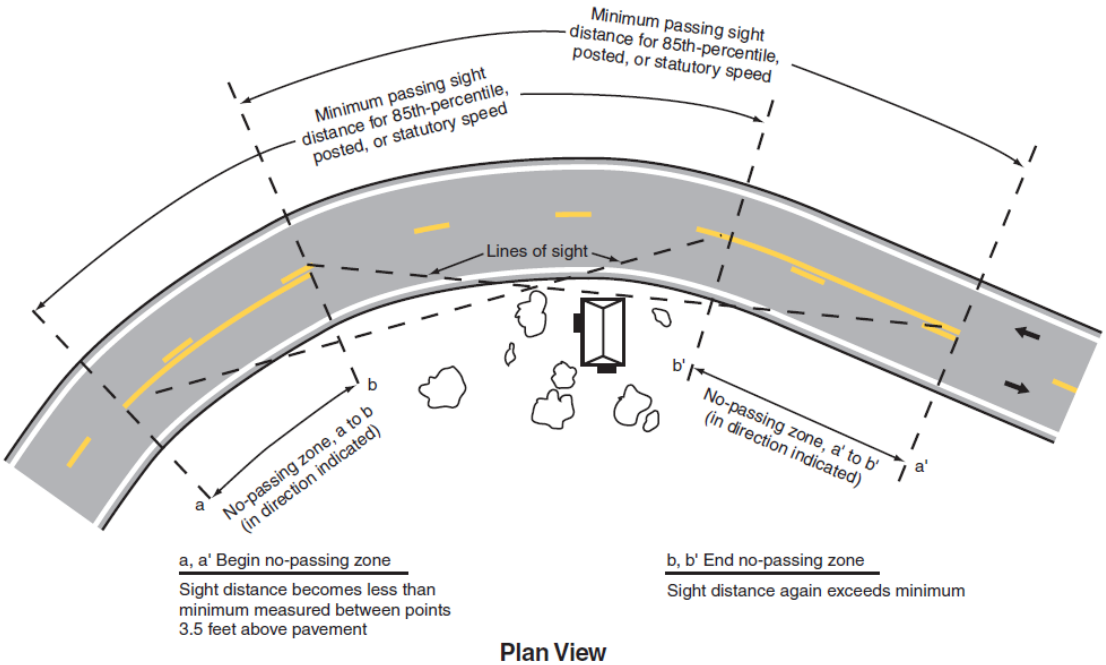

Plan View

Note: No-passing zones in opposite directions may or may not overlap, depending on alignment

Source: Exhibit 3B-4, Reference (*2*)

Figure 4. Passing sight distance at horizontal curve

As was explained, the minimum passing sight distances suggested by the 2004 AASHTO Green Book and the MUTCD are based on different assumptions. The 2004 AASHTO criteria were not used in the marking of no-passing zones. The MUTCD presents considerably shorter passing sight distance values, derived for traffic-operating control needs and for marking standards. Figure 5 compares the passing sight distance values resulting from the 2004 AASHTO Green Book, 2011 AASHTO Green Book, and MUTCD. Glennon (*14*) developed a passing sight distance model based on the kinematic relationships among the passing, passed, and opposing vehicles. Harwood and Glennon (*15*) applied the Glennon model and studied four scenarios: passenger car passing passenger car, passenger car passing truck, truck passing passenger car, truck passing truck. They found a close agreement between the MUTCD criteria for passing sight distance and the sight distance requirements for passenger car passing another passenger car. In passing maneuvers involving trucks, the required passing sight distance was greater than that recommended by the MUTCD but less than that recommended by the 2004 AASHTO Green Book criteria.

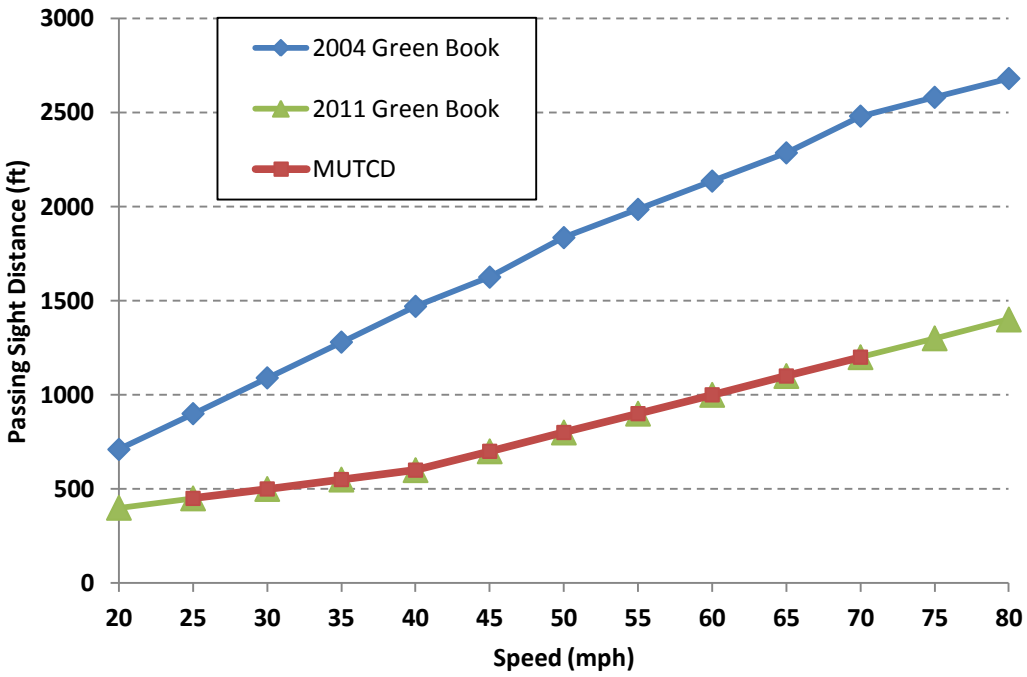

Figure 5. Comparison of minimum passing sight distance values for 2004 and 2011 AASHTO Green Book and MUTCD

NO-PASSING ZONES

No-passing zones, represented by solid lines marked in the center line of two-lane highways, forewarn drivers of the segments of highway that contain sight restrictions and therefore should not be used to make passing maneuvers. The 2009 MUTCD states the following in reference to no-passing zone marking (*2*):

> "*On two-way, two- or three-lane roadways where center line markings are installed, no-passing zones shall be established at vertical and horizontal curves and other locations where an engineering study indicates that passing must be prohibited because of inadequate sight distances or other special conditions.*

On roadways with center line markings, no-passing zone markings shall be used at horizontal or vertical curves where the passing sight distance is less than the minimum shown in the MUTCD table for the 85th-percentile speed or the posted or statutory speed limit."

The beginning of a no-passing zone is the point at which the sight distance first becomes less than that specified in the MUTCD (Table 6). The end of the no-passing zone is the point at which the sight distance becomes greater than the minimum specified in MUTCD. Neither the AASHTO Green Book nor the MUTCD addresses required minimum lengths for passing zones or no-passing zones. However, the MUTCD indirectly sets a minimum passing zone length of 400 ft by providing guidance that was first included in the 1961 edition (*12*) and is still included in the current version of the manual (*2*): "*Where the distance between successive no-passing zones is less than 400 feet, no-passing zone markings should connect the zones*."

Some states have established standards for extending the measured no-passing zones. For example, Iowa recommends that no-passing zones begin 100 ft in advance of the point where sight distance becomes less than that required, but it does not suggest any extension for the ending points of no-passing zones (*16*, *17*).

NO-PASSING ZONE LOCATION METHODS

There are various methods for measuring passing sight distance and determining no-passing zones in the field (*18-20*). Some of the current methods are reviewed in the following sections.

Towed-Target (Rope) Method

This method requires a vehicle towing a target on the end of a rope, chain, or cable. The length of the rope/chain/cable is equal to the minimum passing sight distance and varies based on the posted speed of the highway as suggested in the MUTCD (Table 6). When the target disappears, the vehicle stops and the location of the target is marked on the pavement as the beginning of the no-passing zone for the same direction of traffic. The location of the vehicle can be marked on the pavement as the end of the no-passing zone for the opposing traffic. Then, the vehicle resumes moving forward until the target reappears. The vehicle stops and the location of the target is marked on the pavement as the end of the no-passing zone for the same direction of traffic. The location of the vehicle would be the beginning of the no-passing zone for the opposing traffic.

Distance Measuring Equipment Method

This method employs two vehicles with 3.5 ft driver's eye height, equipped with calibrated distance measuring instruments (DMI), two-way hand-held radios, and a target mounted on the driver side of the rear of the lead vehicle in a way that the top of the target is at 3.5 ft. To set the minimum sight distance interval, both vehicles should park side by side and zero out the DMIs. Then, the lead vehicle moves forward to the minimum passing sight distance defined by the MUTCD (Table 6) and zeros out its DMI again. Now, the vehicles are synchronized. Both vehicles start moving forward with a constant distance (the minimum passing sight distance) and speed. The separation distance of the two vehicles is established by communicating through the radios and

keeping identical readings on the DMIs. When the lead vehicle begins to get out of sight, both vehicles stop at synchronized DMI readings. The trailing vehicle operator marks the pavement to the right of the center line with spray paint or yellow tape for the beginning of the no-passing zone for the same direction of traffic. The lead vehicle marks to the left of the center line for the end of the no-passing zone for the opposing traffic. The two vehicles again proceed forward with identical DMI readings until the target is visible to the trailing vehicle. Both vehicles stop at synchronized DMI readings. The trailing vehicle marks the right of the center line for the end of the no-passing zone for the same direction of traffic. The lead vehicle marks on the left of the center line for the beginning of the no-passing zone for the opposing traffic. Rangefinders help in determining if no-passing zones should be extended. For example, if there is a stop sign after the ending point of a no-passing zone, the crew member can find the distance of the stop sign by targeting it using the rangefinder. If the distance is less than the standard, the no-passing zone is extended.

One-Vehicle Method

This method requires just one vehicle equipped with a DMI and one person. The observer drives slowly through the curve (for example, drives north as shown in Figure 6). When the driver reaches the point at which the vista opens, he or she stops the vehicle and places a mark on the right side of the roadway. This point is the end of the no-passing zone in the direction of travel (point 1 in Figure 6). Then, the driver sets the DMI to zero, travels the required passing sight distance, and stops to place a mark on the

left side of the road. This point is the beginning of the no-passing zone in the opposite direction (point 2). By driving the opposite direction and following the same procedure, points 3 and 4 are marked and the locations of the no-passing zones for the site are determined. Figure 6 illustrates the method for a horizontal curve. The procedure for locating no-passing zones due to vertical curves is the same.

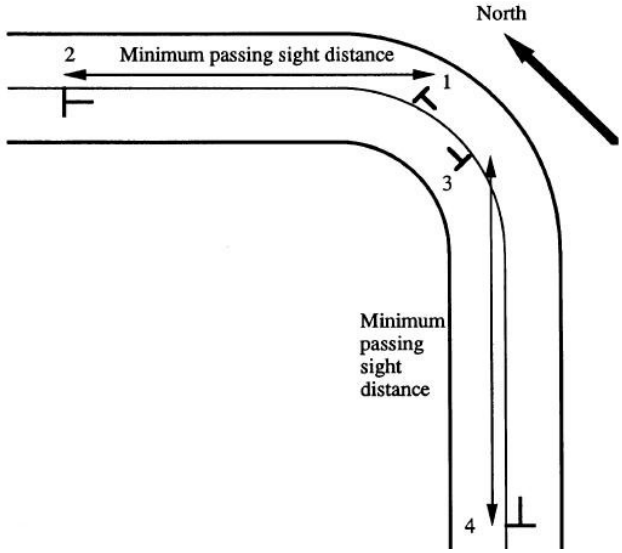

Figure 6. Illustration of the one-vehicle method (*20*)

Two-Vehicle Method

The procedure is similar to the distance measuring equipment method except the separation distance of the two vehicles is maintained using a rope, chain, or cable instead of DMIs. The length of the rope/chain/cable is equal to the minimum passing sight distance and varies based on the posted speed of the highway as suggested in the MUTCD (Table 6).

Walking (Two-Person) Method, Hand Measuring Wheel Method

These methods are the same as the two-vehicle method except the work is done by two crew members on foot. In the walking (two-person) method, the crew members use a rope, a chain, or a cable. However, in the hand measuring wheel method, they use a measuring wheel to maintain their separation distance.

Chalkline Method

This method requires the use of chalkline that is stretched between two crew members to keep the desired distance apart (similar to the walking method).

New Jersey Cone Method

This method employs a two-member crew driving one vehicle on the highway. When an out-of-sight area appears to be ahead, the vehicle stops and the crew members begin to place the traffic cones at 100 ft intervals. The placement of the cones must be started before the area of the reduced sight distance and continued along the segment with the length longer than the minimum passing sight distance (Table 6). Then, the crews move along the segment and check if the cones are in sight.

Eyeball (Line of Sight) Method

This method requires a two-member crew, one vehicle, and a DMI. The procedure starts by crew members driving on the roadway and estimating where the no-passing zone should begin due to approaching sight distance restrictions. The vehicle stops at this

point, and the crew members zero out the DMI. Then, the vehicle resumes moving forward to the point where the approaching vehicle would appear. A crew member reads the DMI at this point. The procedure should be repeated several times until the best location for the no-passing zone is determined.

Laser Rangefinder Method, Optical Rangefinder Method

These methods are similar to the eyeball method except a laser or optical rangefinder is used instead of a DMI.

Remote-Control Vehicle Method

This method employs a two-member crew, one vehicle, and one remote-control vehicle. The procedure begins from the estimated eyeball point (the estimated location where the no-passing zone should begin due to approaching sight distance restrictions). The crew members send the remote-control vehicle forward toward the approaching horizontal or vertical curve, stop the vehicle just as it disappears from view, and measure the distance to the point using the rangefinder. This procedure should be repeated several times until the best location for the no-passing zone is determined.

Speed and Distance Method

The method is similar to the eyeball method but instead of applying a DMI, the crew members record both the average speed of a passing vehicle and the travel time of the vehicle from the estimated eyeball point until it disappears. The distance traveled by the

vehicle is determined by speed multiplied by the time traveled. This procedure should be repeated several times until the best location for the no-passing zone is determined.

Videolog Method, Photolog Method

The videolog and photolog methods use a specialized data collection vehicle equipped with a camera. The vehicle travels on the highway while the camera records the video or image of the actual highway scene at defined intervals. The videos or images are integrated with the geographical references and the sight distances are measured from videologs or photologs of the highway.

The names of the two-vehicle, distance measuring equipment, rope, and towed-target methods have been used in the literature interchangeably. Brown and Hummer (*19*, *20*) conducted a telephone survey and asked engineers in 13 state departments of transportation (DOTs) and also all 14 divisions of the North Carolina DOT about the methods they used/had used before. Table 7 lists the result of the survey. Furthermore, they compared some of the current methods at 20 horizontal curve sites and 20 hill sites. They evaluated the time required to perform each method, equipment costs, training needs, and accuracy. Based on their study, they suggested that the highway agencies use the one-vehicle method.

Table 7. Survey results of no-passing zone location methods

Method	DOT
Cone Method	New Jersey (used to)
Two-Person Walking Method	North Carolina (used to) Iowa
One-Vehicle Method	North Carolina (5 districts)
Two-Vehicle Method	North Carolina (9 districts) Pennsylvania New Jersey Texas Michigan California Colorado Kentucky (some districts)
Videolog Method	Virginia Wisconsin Arizona New York
Photolog Method	Connecticut

Source: Reference (*20*)

Although there are several methods for identifying no-passing zones, each one has a setback because of the time required, accuracy obtained, and related safety issues presented. Some of the methods locate no-passing zones based on measuring passing sight distance along the chord of the curve (not along the curve itself), so the results wouldn't be accurate for locating no-passing zones particularly on horizontal curves. Additionally, the current methods rely on judgment in determining the beginning and ending of no-passing zones. However, by using GPS, crews may be able to obtain the location of no-passing zones more quickly, accurately, and safely, and for a relatively low cost.

GLOBAL POSITIONING SYSTEM

GPS was initiated in 1973 to create a Defense Navigation Satellite System (DNSS). Later that year, the DNSS program was named Navstar. In 1978, the first satellite in the system, Navstar 1, was launched. Following the United States, Russia launched a system in 1982 called the Global Navigation Satellite System (GLONASS). GPS provides continuous (24-hour) reliable location information where there is an unobstructed line of sight to four or more GPS satellites. The system provides spatial coordinate triplets of longitude, latitude, and altitude for every position on Earth based on the observations made on electromagnetic signals transmitted from a satellite constellation. Until May 1, 2000, the government intentionally degraded the position accuracy of GPS signals for nonmilitary users, a practice known as selective availability.

GPS consists of three parts: the space segment, the control segment, and the user segment. The space segment is composed of 24 satellites, each of which is circling the Earth in a precisely known orbit. Four additional satellites are held in reserve as spares. The space segment also includes the boosters required to launch the satellites into orbit. The control segment is composed of a master and alternate control, and a host of ground antennas and monitor stations. The user segment is composed of users of the Standard Positioning Service. Each satellite contains four precise atomic clocks operating on a level of 1 sec of error in 3 million years to control the timing of the signals they transmit. The satellites are at known locations at all times and transmit three L-band carrier signals: L1, L2, and L5 (L5 is a new signal for civilian use). A GPS receiver analyzes the coarse acquisition (C/A) code broadcast over the carrier signals and measures the

time the signal was sent from the satellite and received by the receiver. The time is multiplied by the signal speed, and a distance (range) is determined. Using ranging code from four satellites, the receiver can calculate its own position in three-dimensional space. By logging position and time data, other kinematic parameters such as velocity and acceleration can be derived. Most GPS receivers output data in National Marine Electronics Association (NMEA)-0183 format.

GPS can provide a wide range of accuracies. In general, the higher the accuracy required, the higher the cost and the greater the complexity of using GPS. There are factors that can degrade the GPS signal and thus affect the accuracy of GPS. The factors include ionosphere and troposphere delays, signal multipath, receiver clock errors, orbital errors, and number of satellites visible. Other factor that affects the accuracy of GPS is the geometry and arrangement of satellites in the sky. Satellites that are located farther apart in the sky provide a more accurate position solution than ones close together (Figure 7). GPS receivers usually report the quality of satellite geometry in terms of Position Dilution of Precision (PDOP). A low PDOP indicates a higher probability of accuracy, and a high PDOP indicates a lower probability of accuracy. A dilution of precision value of 3 or less is excellent, a value between 4 and 6 is good, and a value of 9 and greater represents a low confidence level.

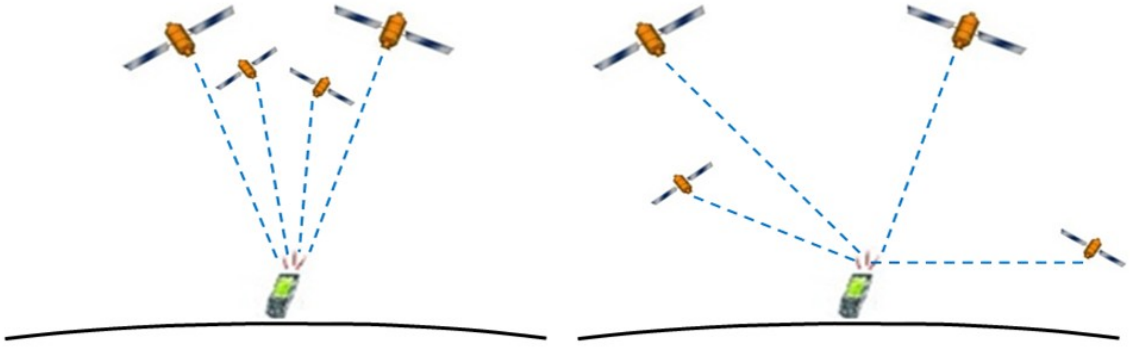

(a) **(b)**

Figure 7. Position Dilution of Precision (PDOP): (a) low PDOP, and (b) high PDOP

High-end GPS receivers, compared to autonomous receivers, reduce GPS errors and provide more accurate and reliable readings by using a differential signal broadcast from either known locations (reference stations) on Earth or other sources (commercial or non-commercial satellite networks). A reference station tracks the GPS satellites and has a true range to each satellite (the exact number of wavelengths between itself and the satellite). This information, along with its known location, is sent to the receiver (see Figure 8). High-end GPS devices are usually divided into four categories based on accuracy levels: Wide Area Augmentation System (WAAS), sub-meter, decimeter, and centimeter. Many vendors are highly optimistic about claimed accuracy, and most accuracies are based on pass-to-pass accuracy and not repeatability (*21*). Repeatability is the ability to return to the exact same location at any time.

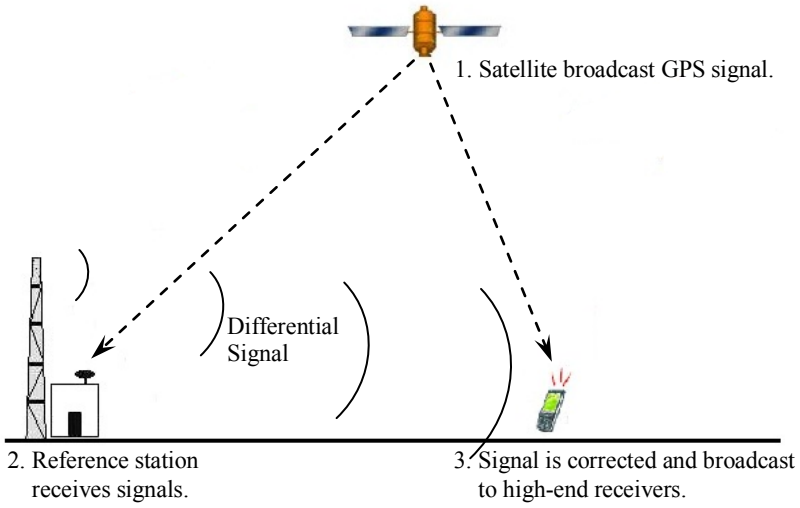

Figure 8. GPS signal correction

Differential Global Positioning System

The differential global positioning system (DGPS) is an extension of the GPS system and requires a differential signal from either a free service, such as WAAS or the Coast Guard Beacon system, or a commercial service such as OmniStar or John Deere's StarFire.

WAAS is the United States' implementation of Satellite-Based Augmentation Systems (SBAS). SBASs are designed to dramatically improve GPS performance. Many nations are making plans for SBAS service that appear under a variety of names (for example Euro Geostationary Navigation Overlay Service (EGNOS) in Europe, Multi-functional Satellite Augmentation System (MSAS) in Japan, GPS Aided GEO Augmented Navigation (GAGAN) in India) A WAAS-capable receiver can provide a position accuracy of better than 10 ft 95 percent of the time. WAAS consists of approximately 25 ground reference stations positioned across the United States that

monitor GPS satellite data. Two master stations, located on either coast, collect data from the reference stations and create a GPS correction message. The corrected differential message is then broadcast through one of two geostationary satellites, or satellites with a fixed position over the equator. The information is compatible with the basic GPS signal structure, which means any WAAS-enabled GPS receiver can read the signal. For some users in the U.S., the position of the satellites over the equator makes it difficult to receive the signals when trees or mountains obstruct the view of the horizon. WAAS signal reception is ideal for open land and marine applications. WAAS provides extended coverage both inland and offshore compared to the land-based DGPS system (*22*).

The Coast Guard Beacon System is a land-based augmentation system (LBAS) consisting of a network of towers that receive GPS signals and transmit a corrected signal by beacon transmitters. In order to get the corrected signal, users must have a differential beacon receiver and beacon antenna in addition to their GPS receiver.

Unlike WAAS and the Coast Guard beacon system, commercial services need subscriptions, and the cost of the subscription varies. OmniStar Virtual Base Station (VBS) costs $800 per year and requires only a single channel receiver. OmniStar High Performance (HP) costs $2500 per year and requires a dual-channel receiver. The StarFire I has a free signal for those who buy the hardware. The StarFire II costs $800 per year and requires a dual-channel receiver like OmniStar HP (*21*).

Real Time Kinematic System

Real Time Kinematic (RTK) is not only the most accurate of all GPS systems, but is the only system that can achieve complete repeatability, allowing a user to return to the most accurate location, indefinitely. RTK usually provides centimeter-level accuracy. The system utilizes two receivers: a static ground base station and one or more roving receivers. The base station receives measurements from satellites and communicates with the roving receiver(s) through a radio link. The roving receiver processes data in real time to produce an accurate position relative to the base station. All of this produces measurements with an immediate accuracy to within 1 to 2 inches. The total cost of a full RTK system with base station, receiver, data logger, and software is usually around $40,000 (*21*). In addition to the high cost of the system, there are some issues related to applying the RTK system. For example, there always needs to be line of sight between the ground station of the RTK and the roving receiver, and the distance between them should always be within 6 to 10 mi. The receiver must also simultaneously track five satellites to become initialized and then continue to track four satellites to remain initialized. However, Post Processing Kinematic (PPK) or "RTK with Infill" can solve the need to continuously track. Furthermore, RTK needs up to 30 min before it begins initialization (*21*). Table 8 compares different GPS devices.

Table 8. Comparison of different GPS devices

	Autonomous (Standalone) GPS	High-End GPS Devices			
		WAAS	Sub-meter	Decimeter	Centimeter
Price Range	< $100	$100-$500	$500-$2500	$2500-$7500	$15,000-$50,000
Source of Signal Correction	-	WAAS	US Coast Guard, OmniStar VBS, StarFire I, local differential services	OmniStar HP, StarFire II (requires dual-channel receiver)	RTK system (requires a base station within 6-10 mi)
Accuracy[1]	10-100 ft	3-10 ft	1-3 ft	3-12 inches	< 1-2 inches
Advantage	lowest cost, small handheld unit, no additional equipment or service fees are required	low cost, good accuracy, small handheld unit, no additional equipment or service fees are required	better accuracy	best accuracy without using RTK	highest accuracy, repeatability[2]

[1] Accuracy in horizontal position
[2] Repeatability is the ability to return to the exact same location at any time.

GPS DATA ACCURACY

The relative accuracy of a GPS run is generally good, and the absolute accuracy can be achieved through combining multiple GPS data sets collected over a period of time. Young and Miller (*23*) showed that the spatial error from successive GPS data is highly correlated. Even though the GPS error is widely published to be in the range of 1 to 5 m, the relative accuracy of sequential GPS data is much greater. If successive GPS data points use the same constellation of satellites, the relative error between the two data points is minimal. Assuming absolute errors of 2 m and 5 m, respectively, for horizontal and vertical error, the relative error between successive readings is easily sub-meter in both dimensions. The error correlation between successive GPS data was estimated

between the 0.99- and 0.999-level in the work performed by Young and Miller. They showed that the absolute position error of their three-dimensional model was reduced as a function of the number of observations. Figure 9 shows the hypothetical reduction in the absolute position error of the three-dimensional model as a function of the number of observations, assuming 2 m and 5 m random errors, respectively, for horizontal and vertical positions.

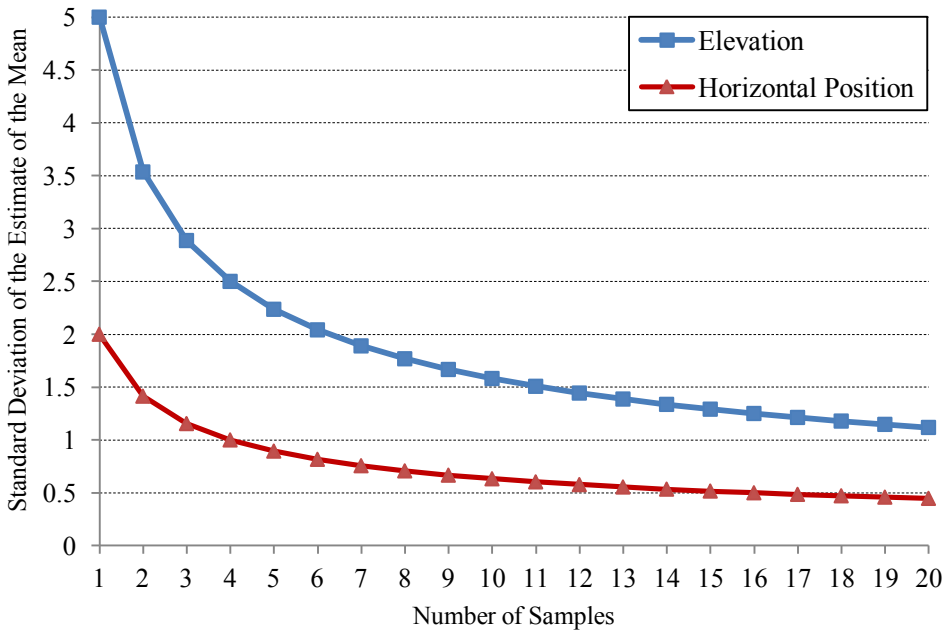

Figure 9. Hypothetical reduction in the absolute position error of the three-dimensional model as a function of the number of observations (*23*)

Young and Miller believed that the high correlation of GPS data error provides in essence a high quality estimate of heading in the horizontal plane and grade in the vertical plane. Additional error reduction arises because successive estimates of slope are highly independent, unlike position estimates. Figure 10 indicates that the relative

shape of the roadway is consistently captured in the GPS data, despite the differences in absolute elevation. Since the researchers did not collect the GPS data in the field but used GPS data from previous roadway inventory, the figures suggest that possibly several different GPS receivers, each with a different bias, were used to collect the elevation data.

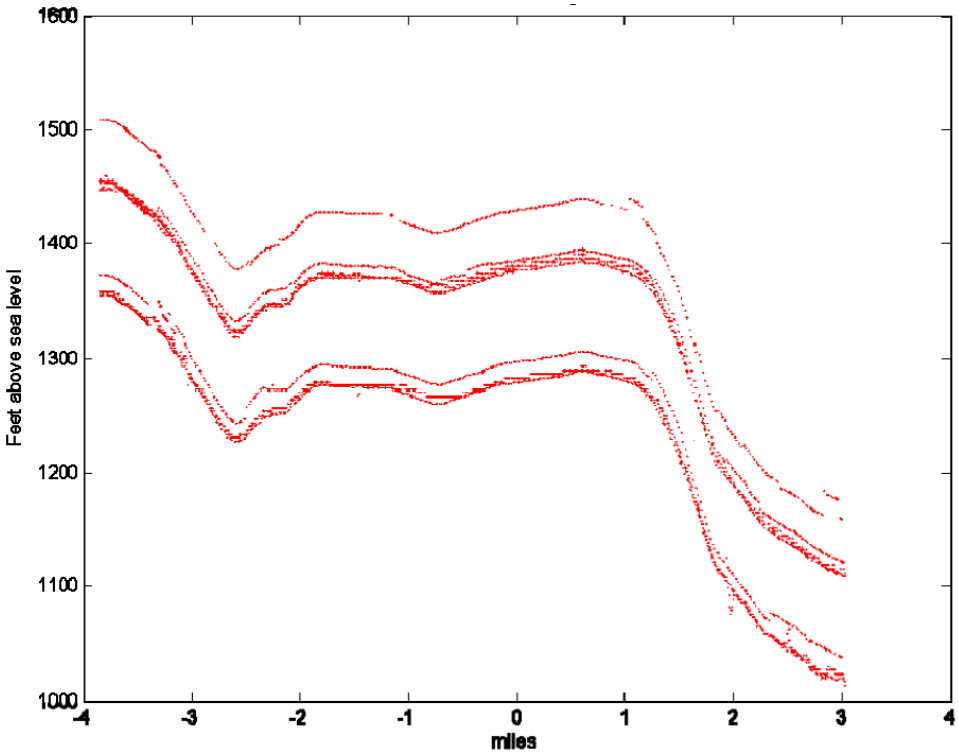

Figure 10. GPS elevation for a Kansas highway section, K-177 (*23*)

Based on the above discussion, to model the geometry of a roadway alignment, it is not necessary to have the exact location (coordination) of each individual data point collected with a GPS receiver. Rather, if the relative positions of the sequential GPS data are accurate, the geometry of the roadway alignment can be determined. However,

the absolute position might be useful to have recorded in the long-run as GPS reveivers become less expensive and more easy to use.

GPS APPLICATION IN HIGHWAY ENGINEERING

GPS has been used extensively in research projects related to transportation engineering. In highway engineering, some researchers have applied GPS technology to their studies. Awuah-Baffour et al. (*24*) combined GPS technology with kinematic vehicle operations to collect roadway alignment, grade, and cross-slope data simultaneously. Also, in another research effort, Awuah-Baffour investigated the use of a multi-antenna, single-receiver configuration of GPS to determine roadway cross slope (*25*). Roh et al. (*26*) determined road alignments based on collected GPS data using an RTK DGPS/GLONASS combination and compared their positioning accuracy to the values of the existing design drawings. Young and Miller (*23*) developed methods to process over 11 million GPS data points collected by the Kansas Department of Transportation, resulting in a geometric model of the state highway system.

CHAPTER III

THEORETICAL APPROACH

The goal of this research was to develop new analytical algorithms to address the horizontal and vertical alignment concepts and determine the availability of passing sight distances in order to establish a method for automating the process of locating no-passing zones. This chapter first presents a method for converting GPS data to be used in the developed algorithms. Then it describes a method for smoothing the GPS data, and also an algorithm for geometric modeling of highways is developed. Finally, it outlines the development of new algorithms for evaluating sight distances. The three main algorithms deal with the vertical sight distance, horizontal sight distance, and three-dimensional sight distance. Furthermore, developing the automated method for locating no-passing zones requires having the geometric definition of the roadway alignments. The road geometry obtained using GPS data is represented as a curve (center of travel lane) rather than as a surface. Two other new algorithms to be used in the main algorithms are also presented in this chapter: one for converting the center of the travel lane to the roadway center line, and the other for modeling the right and the left visual clear zone boundaries. Finally, the chapter explains how the developed algorithms can be incorporated into a computer model to locate no-passing zones on two-lane highways.

GLOBAL POSITIONING SYSTEM DATA CONVERSION

Every position on Earth is uniquely defined by GPS data in the format of longitude λ, latitude φ, and altitude above or below sea level. Longitude and latitude are angles measured from the Earth's center to a point on the Earth's surface (Figure 11). Latitude is the angular distance North or South of the equator from the center of the Earth (up to 90 degrees N/S). Longitude is the angular distance East or West of a point on the Earth, measured from the center of the Earth (up to 360 degrees E/W). The angles are measured in degrees or in grads.

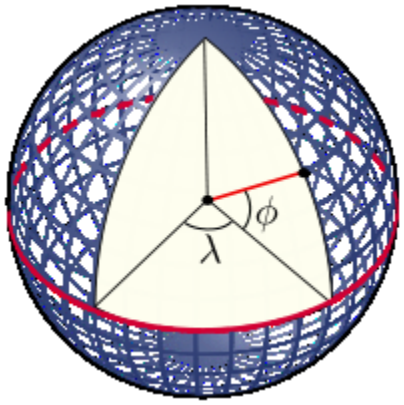

Figure 11. Definition of longitude and latitude of a position on Earth

The true shape of the Earth is not spherical due to the existing mountains, valleys, oceans, and other physical features on the Earth. The topographic surface of the Earth undulates, and it has abrupt elevation changes (see Figure 12). Geoid is an imaginary surface of the Earth, also known as the surface of equal gravitational attraction, that coincides with the mean sea surface of the Earth. This surface is perpendicular to the direction of gravitational force and is shown in red in Figure 12.

Ellipsoid, shown by the dashed line in the figure, is a mathematical surface that generally approximates the geoid.

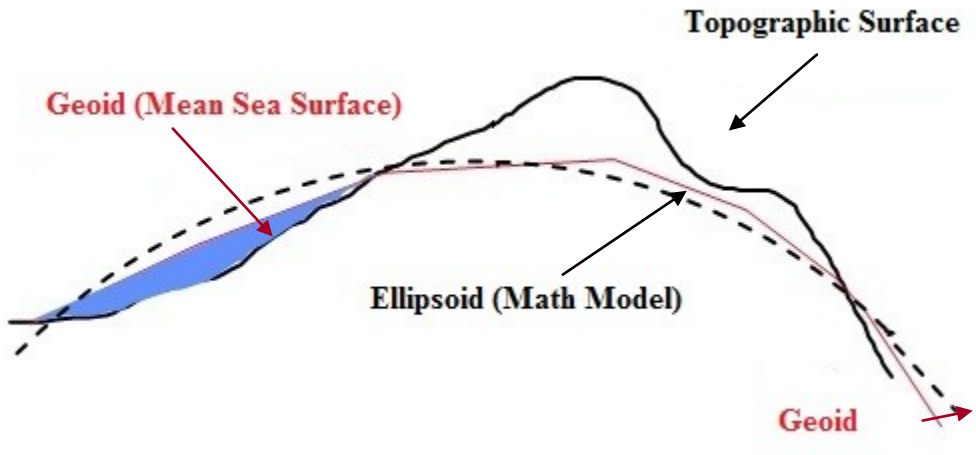

Figure 12. Topographic surface, geoid, and ellipsoid

There are many defined ellipsoids that approximate the Earth. For instance, the Clarke ellipsoid of 1866 was used for the North American Datum of 1927 in the United States. Currently, the Geodetic Reference System (GRS80) and the World Geodetic System of 1984 (WGS84) are commonly used. Semiaxis *a*, semiaxis *b*, and flattening *f* are the three defining parameters, but only two of them are used to define sizes and shapes of each ellipsoid. The relationship between the three parameters is:

$$f = 1 - \frac{b}{a} \tag{5}$$

For the Clarke 1866 ellipsoid, the defining parameters are semiaxes *a* and *b*. For the GRS80 and WGS84 ellipsoids, the defining parameters are semiaxis *a* and flattening *f*. Table 9 lists the parameters for these three ellipsoids (*27*).

Table 9. Defining ellipsoidal parameters (*27*)

Ellipsoid	Semiaxis, *a* (m)	Semiaxis, *b* (m)	Flatenning, *f*
Clarke, 1866	6,378,206.4*	6,356,583.8*	1/294.978698214
GRS80	6,378,137.0*	6,356,752.3	1/298.257222101*
WGS84	6,378,137.0*	6,356,752.3	1/298.257223563*

*Defining parameters for the ellipsoids.
Source: Reference (*27*)

Once the GPS raw data are collected in the format of longitudes, latitudes, and altitudes, a suitable map projection should be selected to transform the terrestrial coordinates on the curved surface of the Earth to a planar Cartesian coordinate system. In other words, the longitudes and latitudes (λ and φ) must be converted into easting and northing coordinates (x and y, where x corresponds to the east-west dimension and y to the north-south). A map projection is a mathematical algorithm to transform locations defined on the curved surface of the Earth into locations defined on the flat surface of a map. The conversion of the curved surface to the planar surface is always accompanied by some type of distortion, due to the spheroidal/ellipsoidal figure of the Earth. However, map projections can preserve one or several characteristics of the surface at the cost of distorting other features. Therefore, selection of the most suitable map projection technique is an important task in this research.

The Texas Legislature has legislatively defined some Geographic Information Standards, including specifying the North American Datum of 1983 (NAD83) and two map projections (Lambert Conformal and Albers Equal Area) for statewide use (*28*).

The properties that are unique for the Texas Conformal projection and required for the conversion process in this research are presented in Table 10.

Table 10. Properties of Texas Conformal projection

Properties	Description/Value
Mapping System Name	Texas Centric Mapping System/Lambert Conformal
Abbreviation	TCMS/LC
Projection	Lambert Conformal Conic
Latitude Grid Origin (ϕ_0)	18° N
Longitude Grid Origin (λ_0)	100° W
Northern Standard Parallel (ϕ_N)	35° N
Southern Standard Parallel (ϕ_S)	27.5° N
False Easting (E_0)	1,500,000 m
False Northing (N_b)	5,000,000 m
Datum	NAD83
Unit	Meter

The datum recommended by the Texas Administrative Code is NAD83. A datum is a set of reference points on the Earth's surface against which position measurements are made, along with an associated model of the shape of the Earth (reference ellipsoid) to define a geographic coordinate system. NAD83 uses GRS80 ellipsoid. The GRS80 was originally adopted as one of the standard measurements of the Earth's shape and size by the International Union of Geodesy and Geophysics (IUGG) in 1979.

Zone Constants in Lambert Conformal Conic

Four sets of parameters define a zone in the Lambert Conformal Conic map projection (*25*). The sets of parameters are:

1. The defining ellipsoidal parameters *a* (semiaxis) and *f* (flattening)
2. Latitude grid origin (ϕ_0) and longitude grid origin (λ_0)
3. Northern latitude parallel (ϕ_N) and southern latitude parallel (ϕ_S)
4. False easting (E_0) and north easting (N_b)

The map projection uses the following common functions:

$$W(\phi) = \sqrt{1 - e^2 \sin^2 \phi} \tag{6}$$

$$M(\phi) = \frac{\cos \phi}{W(\phi)} \tag{7}$$

$$T(\phi) = \sqrt{\left(\frac{1 - \sin \phi}{1 + \sin \phi}\right)\left(\frac{1 + e \sin \phi}{1 - e \sin \phi}\right)^e} \tag{8}$$

In Equation (6), *e* is the first eccentricity of the ellipse as defined by the following equation:

$$e = \frac{\sqrt{a^2 - b^2}}{a} = \sqrt{2f - f^2} \tag{9}$$

where *a* and *b* are semiaxes and *f* is flattening of the ellipsoid.

The first eccentricity of the GRS80 ellipsoid is calculated as:

$$e = \sqrt{2f - f^2} = \sqrt{2\left(\frac{1}{298.257222101}\right) - \left(\frac{1}{298.257222101}\right)^2} = 0.081819191$$

The defining zone constants for a Lambert Conformal Conic map projection are:

$$w_1 = W(\phi_S) \tag{10}$$

$$w_2 = W(\phi_N) \tag{11}$$

$$m_1 = M(\phi_S) \tag{12}$$

$$m_2 = M(\phi_N) \tag{13}$$

$$t_0 = T(\phi_0) \tag{14}$$

$$t_1 = T(\phi_S) \tag{15}$$

$$t_2 = T(\phi_N) \tag{16}$$

$$n = \sin \phi_0 = \frac{\ln (m_1) - \ln (m_2)}{\ln (t_1) - \ln (t_2)} \tag{17}$$

$$F = \frac{m_1}{n \cdot t_1^n} \tag{18}$$

$$R_b = a\, F\, t_0^n \tag{19}$$

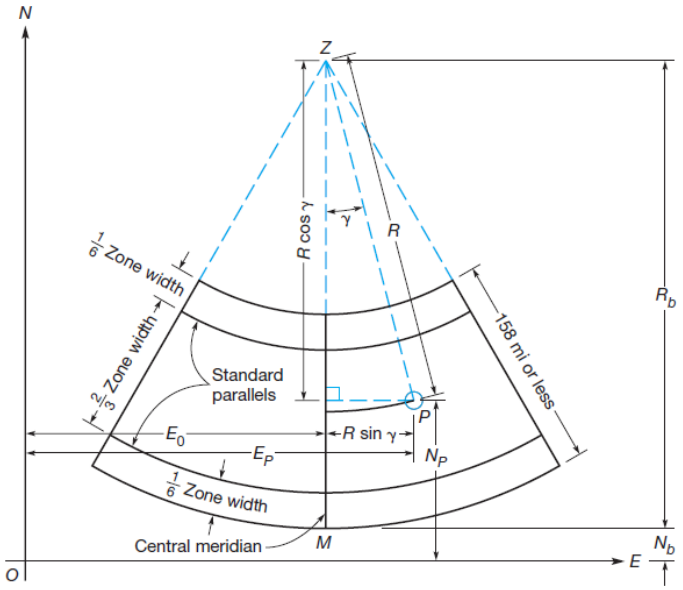

Figure 13. Lambert Conformal Conic projection (*27*)

From Figure 13, the following equations can be constructed for calculating the easting and northing coordinates of point P (Cartesian coordinates of point P):

$$E_P = R \sin\gamma + E_0 \tag{20}$$

$$N_P = R_b - R\cos\gamma + N_b \tag{21}$$

where:

$$\gamma = (\lambda_0 - \lambda_P)\, n \tag{22}$$

$$R = a\, F\, t^n \tag{23}$$

$$t = T(\phi_P) \tag{24}$$

Therefore, the equations for converting the GPS longitude and latitude values into easting and northing values are written in the form:

$$m_1 = \frac{\cos\phi_S}{\sqrt{1 - e^2 \sin^2\phi_S}} \tag{25}$$

$$m_2 = \frac{\cos\phi_N}{\sqrt{1 - e^2 \sin^2\phi_N}} \tag{26}$$

$$t_1 = \left(\frac{1 - \sin\phi_S}{1 + \sin\phi_S}\right)^{0.5} \left(\frac{1 + e\sin\phi_S}{1 - e\sin\phi_S}\right)^{0.5e} \tag{27}$$

$$t_2 = \left(\frac{1 - \sin\phi_N}{1 + \sin\phi_N}\right)^{0.5} \left(\frac{1 + e\sin\phi_N}{1 - e\sin\phi_N}\right)^{0.5e} \tag{28}$$

$$n = \frac{\ln(m_1) - \ln(m_2)}{\ln(t_1) - \ln(t_2)} \tag{29}$$

$$R_b = a\left(\frac{m_1}{n\, t_1^{\,n}}\right)\left(\frac{1 - \sin\phi_0}{1 + \sin\phi_0}\right)^{0.5n} \left(\frac{1 + e\sin\phi_0}{1 - e\sin\phi_0}\right)^{0.5en} \tag{30}$$

$$R = a\left(\frac{m_1}{n\, t_1^{\,n}}\right)\left(\frac{1 - \sin\phi_P}{1 + \sin\phi_P}\right)^{0.5n} \left(\frac{1 + e\sin\phi_P}{1 - e\sin\phi_P}\right)^{0.5en} \tag{31}$$

$$E_P = R \sin [(\lambda_0 - \lambda_P) n] + E_0 \quad (32)$$

$$N_P = R_b - R \cos [(\lambda_0 - \lambda_P) n] + N_b \quad (33)$$

ϕ_P and λ_P are terrestrial coordinates of point P that represent latitude and longitude in degrees, and E_P and N_P are Cartesian coordinates of point P (easting and northing values of the point) in meters. For inclusion in the algorithms developed in this research, all the GPS points had to be converted into northing and easting values in English units. Therefore, an algorithm was created to perform the conversion. The input of the algorithm was longitude, latitude, and altitude of GPS data points, and the output included easting, northing, and elevation of each point (x, y, and z).

GEOMETRIC MODELING OF HIGHWAY

Developing the automated method for locating no-passing zones using GPS data requires having the geometric definition of the roadway alignments. Roadway profiles, especially long segments, are unique in that they consist of multiple combinations of tangents and parabolic curves. Furthermore, roadway surfaces are continuous and the change in grade over a few feet is usually small. However, the accuracy of GPS data, especially when collected from a moving vehicle, can vary drastically due to the satellite positions, and smooth profiles cannot be taken directly from a single GPS data collection run. Furthermore, multiple data collection runs have unnecessary repetitions in data, and they may not necessarily provide the accurate data. Therefore, it is necessary to smooth the GPS data points to obtain the best curve representing the geometry of two-lane

highways. In mathematics, curve fitting models are generally used for different purposes such as parameter estimation, functional representation, data smoothing, or data reduction. The objective of this research was to perform a curve fitting process on the set of data points for the purpose of data smoothing.

Various mathematical curve fitting and data smoothing techniques have been used in previous studies to define the best presentation of roadways based on the observation data points. Since it is not possible in highway engineering to define a global function to fit the roadway data profile, other researchers have suggested using parametric curves defined with piecewise polynomials such as spline curves to obtain the geometric definition of highways (*6, 8, 29-31*).

The word *spline* is adapted from the ship building industry, where it describes the thin, flexible strips of woods used by draftsmen and shipbuilders to thread between the metal weights. A spline curve is a sequence of curve segments that are connected (piecewise parametric polynomials) and form a single continuous curve. Splines are defined mathematically by two or more control points. Control points are data points that affect the shape of the curve. The curve may pass near or through some of the control points. The control points that lie on the curve are called knots. Basic spline (B-spline) is a function that has minimal support with respect to a given degree, smoothness, and domain partition. B-spline does not interpolate the control points (i.e. the curve does not pass through the control points).

In this research, a cubic B-spline curve was chosen as the three-dimensional representation of highway alignments. Suppose the total number of control points is *n* (*n* defines the total number of collected GPS data points along the highway):

$P_1, P_2, P_3, P_4, \ldots, P_n$

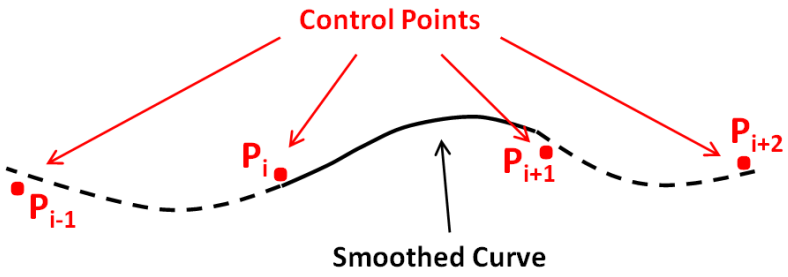

Figure 14. Cubic B-spline curve

The cubic B-spine is defined as follows:

$$[x(t), y(t), z(t)] = \sum B_{i,4}(t)\, P_i \qquad (34)$$

where $B_{i,4}(t)$ are the B-spline blending functions of degree 3, and P_i are the control points. The blending functions sum to 1 and are positive everywhere. They describe how to blend the control points to make the curve. Each $B_{i,4}(t)$ is only non-zero for a small range of t values, so the curve has local control.

Points P_i and P_{i+1} are calculated as:

$$P_i = \begin{pmatrix} x_i \\ y_i \\ z_i \end{pmatrix}$$

and

$$P_{i+1} = \begin{pmatrix} x_{i+1} \\ y_{i+1} \\ z_{i+1} \end{pmatrix}$$

The smoothed curve between points P_i and P_{i+1} (see Figure 14) can be calculated with a moving window of four points at a time ($2 \leq i \leq n-2$):

$$[x(t), y(t), z(t)] = \sum B_{i,4}(t)\, P_i$$

$$= \frac{1}{6}\left(-t^3 + 3t^2 - 3t + 1\right)P_{i-1} + \frac{1}{6}\left(3t^3 - 6t^2 + 4\right)P_i + \frac{1}{6}\left(-3t^3 + 3t^2 + 3t + 1\right)P_{i+1}$$

$$+ \frac{1}{6}(t^3)P_{i+2}$$

There is also the matrix form for the curve:

$$[x(t), y(t), z(t)] = \frac{1}{6}\ [t^3\ t^2\ t\ \ 1] \begin{bmatrix} -1 & 3 & -3 & 1 \\ 3 & -6 & 3 & 0 \\ -3 & 0 & 3 & 0 \\ 1 & 4 & 1 & 0 \end{bmatrix} \begin{bmatrix} x_{i-1} & y_{i-1} & z_{i-1} \\ x_i & y_i & z_i \\ x_{i+1} & y_{j+1} & z_{i+1} \\ x_{i+2} & y_{i+2} & z_{i+2} \end{bmatrix} \qquad (35)$$

where t is a parameter greater than or equal to 0 and less than or equal to 1. The x, y, and z values of each point located on the curve between P_j and P_{j+1} can be generated through changing the value of t from 0 to 1. The number of the generated points (belonging to the smoothed curve) would be more than the number of the original points, depending on the values selected for the parameter t. If the parameter t varies by σ, the number of the generated points is $(n-3)/\sigma$, where n is the number of the original points.

An algorithm was developed, by applying the cubic B-spline method, to smooth the data that had been previously converted. The input of the algorithm was the Cartesian coordinates (x, y, and z) of data points and the output included the smoothed curve in the form of points (Cartesian coordinates). For the algorithm, σ was selected to be 0.05 (i.e. t varied by 0.05). Therefore, 20 points were generated for each moving window, resulting in the total number of the points being equal to:

$$\frac{n - 3}{0.05}$$

where *n* is the number of the original points. Figure 15 shows the flowchart of geometric modeling of highway applying cubic B-spline method. The algorithm will be a part of the NPZ computer model that will be discussed at the end of chapter 3.

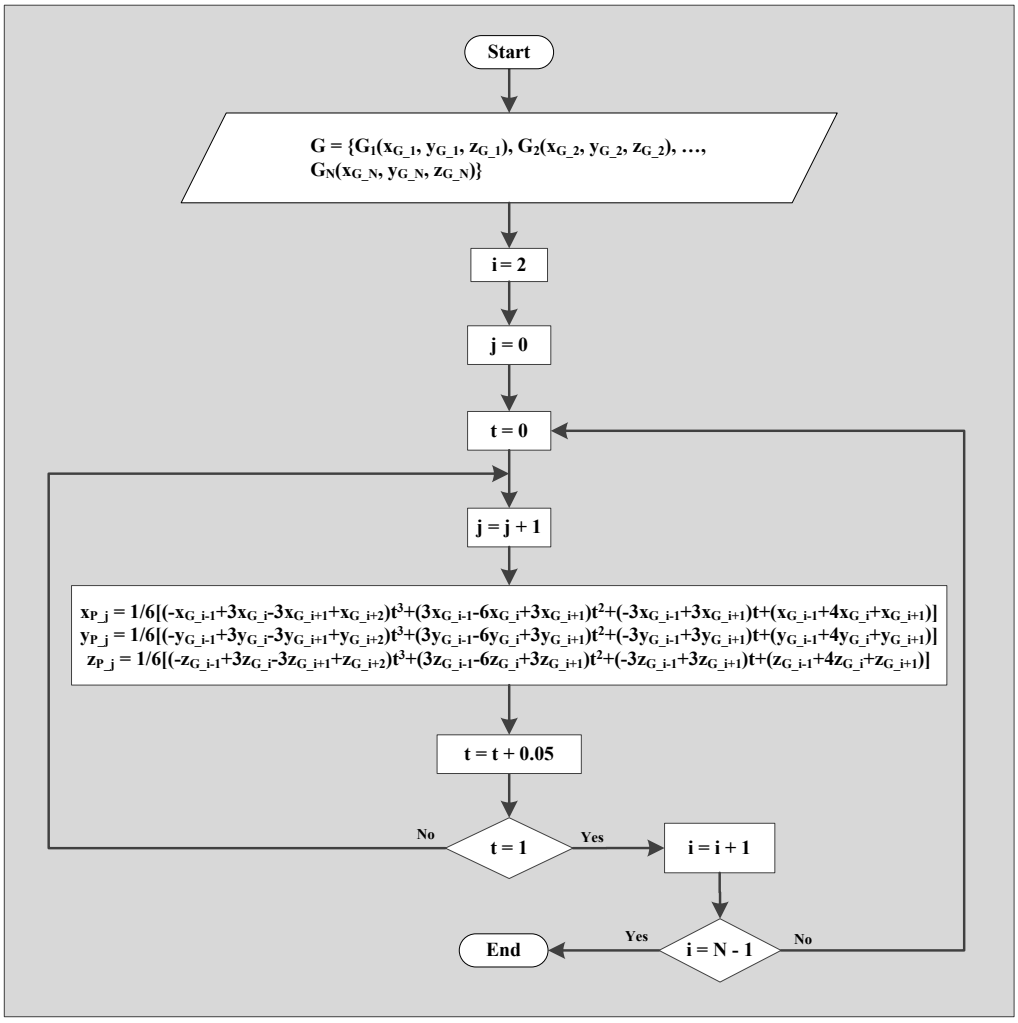

Figure 15. Flowchart for data smoothing and geometric modeling of highway

MODELING OF ROADWAY CENTER LINE

As it was discussed in Chapter 2, according to the MUTCD, the passing sight distance on a horizontal curve is the distance measured along the center line between two points on a line tangent to the embankment or other obstruction that cuts off the view on the inside of the curve (see Figure 4). The smoothed data, originally collected by using a GPS receiver, do not correspond with the roadway center line since the vehicle that collects the data travels in one direction of the roadway and does not go over the center line. Assuming the vehicle follows a path centered in its lane and the GPS antenna is mounted in the center of the vehicle, the geometric definition of the roadway represents the center of the travel lane. Therefore, it is necessary to convert this line (center of the lane) to a line that represents the center line of the road (the marked center line, not the geometric center of the pavement). The basic concept is to offset the consecutive points that represent the center of the lane to the left by one-half the lane width. While simple in concept, the mathematical formulation that will work in all situations is slightly complicated and is described below.

Assuming that $G_i \in \{G_1, G_2, G_3 \ldots\}$ are the smoothed data points collected originally with a GPS receiver, they represent the center of the travel lane. The objective is to define the geometry of the roadway center line. Let's consider G_i and G_{i+1} as two successive GPS data points defined in an *x*-*y* system of Cartesian coordinates, where:

$$G_i = \begin{pmatrix} x_{G_i} \\ y_{G_i} \end{pmatrix}$$

and

$G_{i+1} = \begin{pmatrix} x_{G_{i+1}} \\ y_{G_{i+1}} \end{pmatrix}$

and consider C_i as the projection of the point located on the roadway center line on the *x-y* plane and corresponding to G_i (see Figure 16). Relative positions of G_{i+1} and C_i from point G_i can be expressed by vectors $\overrightarrow{G_iG_{i+1}}$ and $\overrightarrow{G_iC_i}$, respectively. The dot (inner) product of two vectors is a scalar quantity equal to the product of the magnitudes of the two vectors times the cosine of the angle between them. The dot product is defined for the two vectors $\overrightarrow{G_iG_{i+1}}$ and $\overrightarrow{G_iC_i}$ by:

$$\langle \overrightarrow{G_iG_{i+1}}, \overrightarrow{G_iC_i} \rangle = \left\| \overrightarrow{G_iG_{i+1}} \right\| \left\| \overrightarrow{G_iC_i} \right\| \cos\theta \qquad (36)$$

where the notation $\langle . , . \rangle$ denotes the dot product; $\left\| \overrightarrow{G_iG_{i+1}} \right\|$ and $\left\| \overrightarrow{G_iC_i} \right\|$ denote the lengths (norms) of the vectors $\overrightarrow{G_iG_{i+1}}$ and $\overrightarrow{G_iC_i}$; and θ is the angle between the vectors.

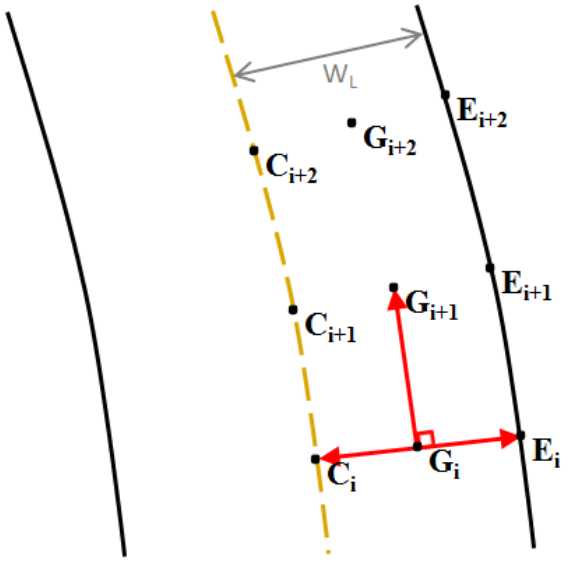

Figure 16. Modeling of the roadway center line

G_i and G_{i+1} are spaced close to each other so that $\overrightarrow{G_iG_{i+1}}$ and $\overrightarrow{G_iC_i}$ are perpendicular (orthogonal) and the angle between the vectors is 90 degrees:

$$\langle \overrightarrow{G_iG_{i+1}} , \overrightarrow{G_iC_i} \rangle = \left\| \overrightarrow{G_iG_{i+1}} \right\| \left\| \overrightarrow{G_iC_i} \right\| \cos 90° \tag{37}$$

Since the cosine of 90 is zero:

$$\langle \overrightarrow{G_iG_{i+1}} , \overrightarrow{G_iC_i} \rangle = 0 \tag{38}$$

In Cartesian coordinates, the dot product is numerically equal to the sum of the products of the vector components. If the vectors are expressed in terms of unit vectors $\hat{i}$ and $\hat{j}$ along the *x* and *y* directions, the dot product of the vectors can be expressed in the following form (assuming that $\overrightarrow{G_iG_{i+1}}$ and $\overrightarrow{G_iC_i}$ are in the *x*-*y* plane):

$$\langle \overrightarrow{G_iG_{i+1}} , \overrightarrow{G_iC_i} \rangle = (x_{G_{i+1}} - x_{G_i})(X - x_{G_i}) + (y_{G_{i+1}} - y_{G_i})(Y - y_{G_i}) \tag{39}$$

where X and Y represent the coordinates of C_i and:

$$\overrightarrow{G_iG_{i+1}} = (x_{G_{i+1}} - x_{G_i})\,\hat{i} + (y_{G_{i+1}} - y_{G_i})\,\hat{j} \tag{40}$$

$$\overrightarrow{G_iC_i} = (X - x_{G_i})\,\hat{i} + (Y - y_{G_i})\,\hat{j} \tag{41}$$

It can be inferred from Equation (38) that:

$$(x_{G_{i+1}} - x_{G_i})(X - x_{G_i}) + (y_{G_{i+1}} - y_{G_i})(Y - y_{G_i}) = 0 \tag{42}$$

Equation (42) contains six parameters: X, x_{G_i}, $x_{G_{i+1}}$, Y, y_{G_i}, and $y_{G_{i+1}}$. Since two of these parameters (i.e., X and Y) are unknown, another equation should be constructed in order to solve for unknown parameters. The GPS data points represent the center of the travel lane. Therefore:

$$\left\| \overrightarrow{G_iC_i} \right\| = 0.5\ W_L \tag{43}$$

$\left\|\overrightarrow{G_iC_i}\right\|$ denotes the length of the vector $\overrightarrow{G_iC_i}$, and W_L denotes the width of the travel lane, which is a user-defined parameter (assuming the highway is homogeneous in the lane geometry along its length). According to the Pythagorean Theorem, length of the vector $\vec{u} = (u_1, u_2)$ is given by $\|\vec{u}\| = (u_1^2 + u_2^2)^{0.5}$, so that:

$$\left\|\overrightarrow{G_iC_i}\right\| = ((X - x_{G_i})^2 + (Y - y_{G_i})^2)^{0.5} \quad (44)$$

Substituting for $\left\|\overrightarrow{G_iC_i}\right\|$ from Equation (44) in Equation (43), the following relationship is obtained:

$$((X - x_{G_i})^2 + (Y - y_{G_i})^2)^{0.5} = 0.5W_L \quad (45)$$

Since Equation (42) is a linear equation, the simultaneous set of Equations (42) and (45) can be easily solved by method of substitution. First, Equation (42) is solved for X in terms of Y:

$$X = x_{G_i} + [(y_{G_i} - y_{G_{i+1}})(Y - y_{G_i})/(x_{G_{i+1}} - x_{G_i})] \quad (46)$$

Then, it is substituted for X in Equation (45), and Y is solved. There are two possible solutions for Y:

$$Y = y_{G_i} \pm \{0.25W_L^2 (x_{G_{i+1}} - x_{G_i})^2 / [(y_{G_i} - y_{G_{i+1}})^2 + (x_{G_{i+1}} - x_{G_i})^2]\}^{0.5} \quad (47)$$

To find their corresponding X values, the values for Y are substituted into Equation (46) and X is solved. For the special case where $x_{G_{i+1}} = x_{G_i}$, the value of the denominator in Equation (46) is zero. In such a case, X and Y are determined from the following equations:

$$X = y_{G_i} \pm 0.5W_L \quad (48)$$

and

$$Y = y_{G_i} \tag{49}$$

As was discussed previously, by solving the two variables X and Y within simultaneous sets of equations, two sets of possible solutions can be found. One of the solutions represents the coordinates of C_i, while the other represents E_i, the projection of the point corresponding to the edge of the travel lane on the *x*-*y* plane (see Figure 16). The next step is to determine exactly which of the two solutions corresponds to C_i. In mathematics, the cross (vector) product is a binary operation on two vectors in three-dimensional space. It results in a vector that is perpendicular to both of the vectors being multiplied and normal to the plane containing them. Given two vectors, $\vec{u} = (u_1, u_2, u_3)$ and $\vec{v} = (v_1, v_2, v_3)$, in Cartesian coordinates, the cross product in the form of a determinant is:

$$[\,\vec{u}\,,\vec{v}\,] = \begin{vmatrix} \hat{i} & \hat{j} & \hat{k} \\ u_1 & u_2 & u_3 \\ v_1 & v_2 & v_3 \end{vmatrix} = (u_2v_3 - u_3v_2)\,\hat{i} - (u_1v_3 - u_3v_1)\,\hat{j} + (u_1v_2 - u_2v_1)\,\hat{k} \tag{50}$$

where the notation [., .] denotes the cross product.

The direction of $[\,\vec{u}\,,\vec{v}\,]$ is given by the right-hand rule: if the fingers of the right hand curl in the direction of rotation (through an angle less than 180 degrees) from $\vec{u}$ to $\vec{v}$, then the thumb points in the direction of $[\,\vec{u}\,,\vec{v}\,]$ (see Figure 17).

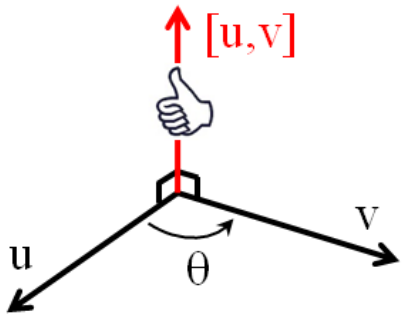

Figure 17. Cross product of two vectors in respect to a right-handed coordinate system

Let's assume the first set of X and Y corresponds to C_i. Since $\overrightarrow{G_iG_{i+1}}$ and $\overrightarrow{G_iC_i}$ are in the same *x*-*y* plane, the resulting vector of $\left[\overrightarrow{G_iG_{i+1}}, \overrightarrow{G_iC_i}\right]$ should point purely in the *z*-direction and lie along the positive *z*-axis (based on the cross product definition; Figure 17):

$$\left[\overrightarrow{G_iG_{i+1}}, \overrightarrow{G_iC_i}\right] = \begin{vmatrix} \hat{i} & \hat{j} & \hat{k} \\ x_{G_{i+1}} - x_{G_i} & y_{G_{i+1}} - y_{G_i} & 0 \\ X - x_{G_i} & Y - y_{G_i} & 0 \end{vmatrix}$$

$$= ((x_{G_{i+1}} - x_{G_i})(Y - y_{G_i}) - (y_{G_{i+1}} - y_{G_i})(X - x_{G_i}))\,\hat{k}$$

$$= \alpha\,\hat{k} \tag{51}$$

where $\hat{k}$ is the unit vector in the direction of the *z*-axis and

$$\alpha = (x_{G_{i+1}} - x_{G_i})(Y - y_{G_i}) - (y_{G_{i+1}} - y_{G_i})(X - x_{G_i}) \tag{52}$$

Trying the first set of X and Y (X_1 and Y_1) in α, if $\alpha > 0$, then the vector $\left[\overrightarrow{G_iG_{i+1}}, \overrightarrow{G_iC_i}\right]$ lies along the positive *z*-axis and the assumption is correct (i.e., X_1 and Y_1 correspond to C_i). Otherwise, they correspond to E_i, while X_2 and Y_2 correspond to C_i.

Similar methods are applied to determine the remaining $\{C_i\}$ from $\{G_i\}$. For example, by using G_1 and G_2 and applying a similar method, the coordinates of C_1 (the *x*-*y* projection of the point located on the roadway center line corresponding to G_1) can be determined. Figure 18 shows the flowchart for modeling of roadway center line, and Algorithm 1 summarizes the proposed procedure.

The result of the process is a series of points that represent the center line of the roadway. The center line definition then serves as the starting point for each of the next two steps: defining the visual clear zone and defining the sight line for the passing sight distance.

MODELING OF VISUAL CLEAR ZONE BOUNDARIES

In horizontal curves, a no-passing zone should be provided if the sight line intersects the outer edge of the visual clear zones on either side of the roadway. The sight line is defined as a line that begins on the center line corresponding to a point where a vehicle is located and ends at the point located on the center line where the length of the center line between two points is equal to the passing sight distance defined by the MUTCD. As defined for this effort, visual clear zones are corridors of unobstructed vision immediately adjacent to both sides of two-lane highways (including shoulders, if they exist, and areas beyond the shoulders), permitting vehicle drivers to see approaching vehicles. There can be no sight distance obstructions in the area between the center line and the visual clear zone boundaries on each side of the road. Only a few methods have been developed to determine the appropriate clear zone for the purpose of providing

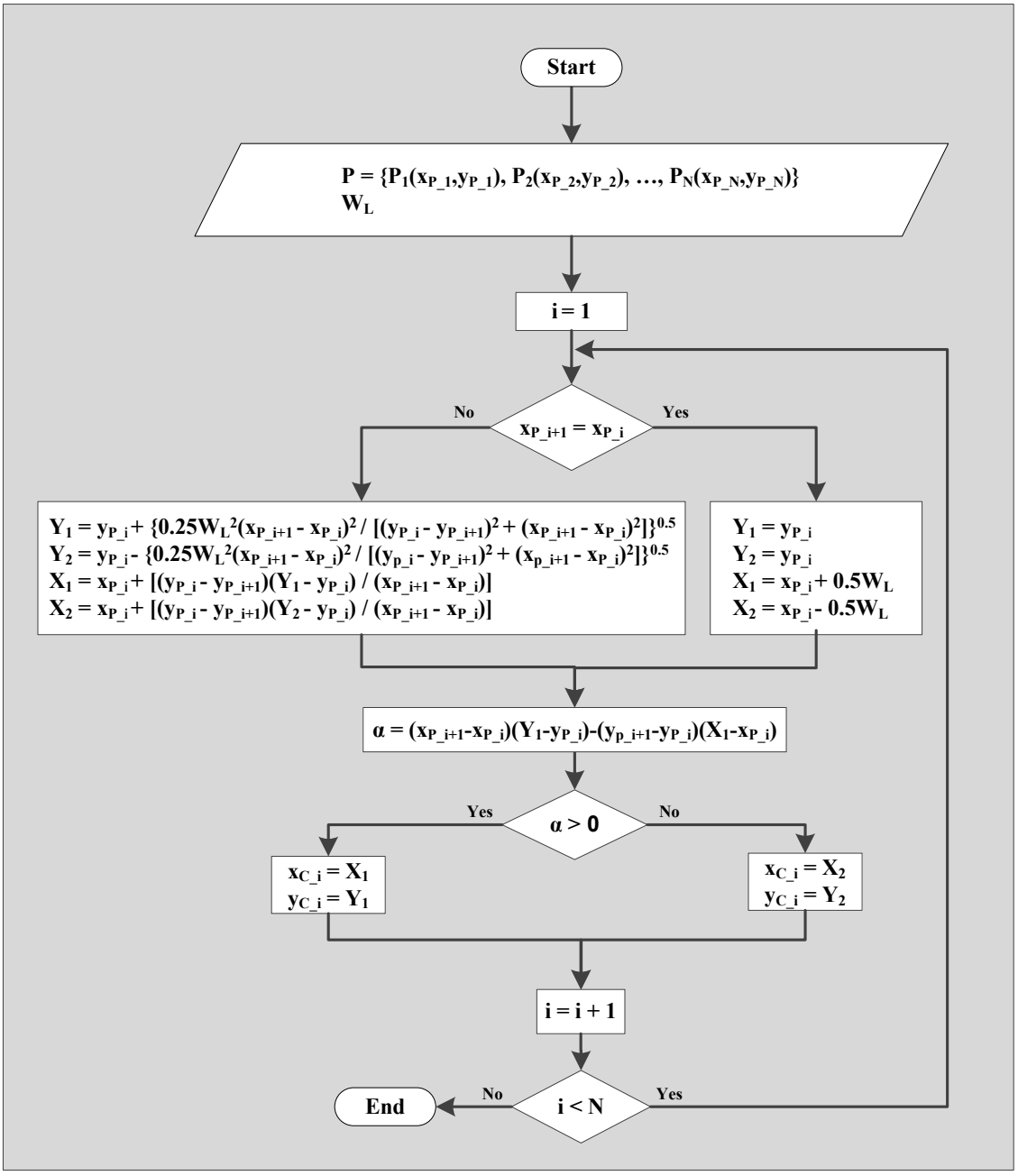

Figure 18. Flowchart for modeling of roadway center line

Algorithm 1. Modeling of roadway center line

Input $G = \{G_1(x_{G_1}, y_{G_1}), G_2(x_{G_2}, y_{G_2}), \ldots, G_N(x_{G_N}, y_{G_N})\}$
Input W_L
$i \leftarrow 1$
repeat
  if $x_{G_{i+1}} = x_{G_i}$ **then**
  $Y_1 = y_{G_i}$
  $Y_2 = y_{G_i}$
  $X_1 = y_{G_i} + 0.5W_L$
  $X_2 = y_{G_i} - 0.5W_L$
  else
  $Y_1 = y_{G_i} + \{0.25W_L^2 (x_{G_{i+1}} - x_{G_i})^2 / [(y_{G_i} - y_{G_{i+1}})^2 + (x_{G_{i+1}} - x_{G_i})^2]\}^{0.5}$
  $Y_2 = y_{G_i} - \{0.25W_L^2 (x_{G_{i+1}} - x_{G_i})^2 / [(y_{G_i} - y_{G_{i+1}})^2 + (x_{G_{i+1}} - x_{G_i})^2]\}^{0.5}$
  $X_1 = x_{G_i} + [(y_{G_i} - y_{G_{i+1}})(Y_1 - y_{G_i})/(x_{G_{i+1}} - x_{G_i})]$
  $X_2 = x_{G_i} + [(y_{G_i} - y_{G_{i+1}})(Y_2 - y_{G_i})/(x_{G_{i+1}} - x_{G_i})]$
  end if
  $\alpha = (x_{G_{i+1}} - x_{G_i})(Y_1 - y_{G_i}) - (y_{G_{i+1}} - y_{G_i})(X_1 - x_{G_i})$
  if $\alpha > 0$ **then**
    $x_{C_i} = X_1$
    $y_{C_i} = Y_1$
  else
    $x_{C_i} = X_2$
    $y_{C_i} = Y_2$
  end if
  $i \leftarrow i + 1$
until $i = N$
return
$\{C = \{C_1(x_{C_1}, y_{C_1}), C_2(x_{C_2}, y_{C_2}), \ldots, C_{N-1}(x_{C_{N-1}}, y_{C_{N-1}})\}\}$

adequate sight distance (*32-34*). Those methods involve the approximation of the *required* boundary of the clear zone based on the horizontal sight distance considerations. However, the method being presented in this research is appropriate for constructing the minimum boundary of the visual clear zone in order to calculate the *available* horizontal sight distance. The difference in determining required versus

available sight distance is important when developing a model that will calculate the location of no-passing zones. For this research, it was assumed that the visual clear zones had uniform lateral clearance along the alignment, and the visual clear zone boundaries were offset from the roadway center line by a fixed specific distance. For cases where the width of the visual clear zone changes the user can divide the roadway into distinct segments for analysis. This section of the research describes a method for defining the geometry of visual clear zone boundaries of the roadway.

The approach is similar to that used to define the center line except that the visual clear zone boundaries must be defined on both the right and left side of the roadway. $\{C_i\}$ involves the *x-y* projections of the points located on the center line of the roadway, as generated in the previous section. Let's consider C_i and C_{i+1} as the *x-y* projections of two successive points on the roadway center line, and R_i as the *x-y* projection of the point located on the right clear zone boundary corresponding to C_i (see Figure 19). The dot product can be defined for the two vectors of $\overrightarrow{C_iC_{i+1}}$ and $\overrightarrow{C_iR_i}$ by the following ($\overrightarrow{C_iC_{i+1}}$ and $\overrightarrow{C_iR_i}$ are in the same plane):

$$\langle \overrightarrow{C_iC_{i+1}} , \overrightarrow{C_iR_i} \rangle = (x_{C_{i+1}} - x_{C_i})(X' - x_{C_i}) + (y_{C_{i+1}} - y_{C_i})(Y' - y_{C_i}) \quad (53)$$

where X' and Y' represent the coordinates of R_i and:

$$\overrightarrow{C_iC_{i+1}} = (x_{C_{i+1}} - x_{C_i})\,\hat{i} + (y_{C_{i+1}} - y_{C_i})\,\hat{j} \quad (54)$$

$$\overrightarrow{C_iR_i} = (X' - x_{C_i})\,\hat{i} + (Y' - y_{C_i})\,\hat{j} \quad (55)$$

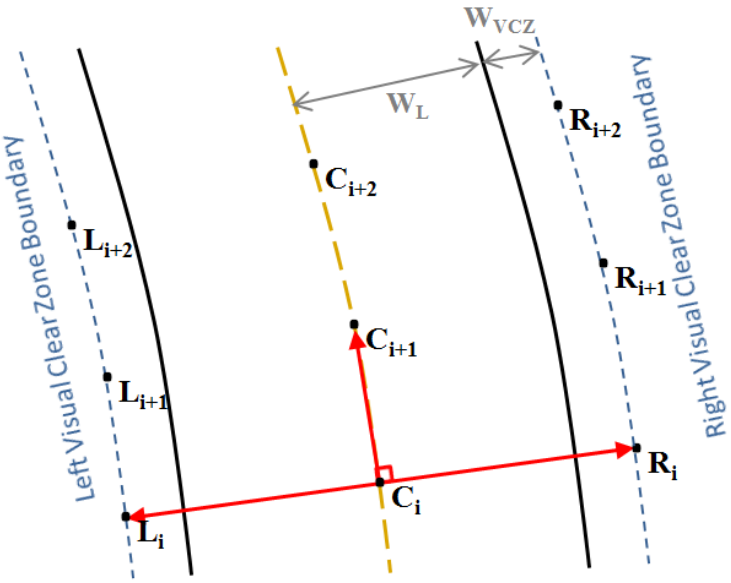

Figure 19. Modeling of the visual clear zone boundaries

Since C_i and C_{i+1} are close to each other, the vectors are perpendicular (orthogonal):

$$(x_{C_{i+1}} - x_{C_i})(X' - x_{C_i}) + (y_{C_{i+1}} - y_{C_i})(Y' - y_{C_i}) = 0 \quad (56)$$

Equation (56) contains six parameters x_{C_i}, $x_{C_{i+1}}$, X', y_{C_i}, $y_{C_{i+1}}$, and Y'. Since two of these parameters (i.e., X' and Y') are unknown, another equation should be constructed in order to solve for unknown parameters. Point C_i represents the *x*-*y* projection of the center line of the roadway:

$$\left\|\overrightarrow{C_iR_i}\right\| = W_L + W_{VCZ} \quad (57)$$

$\left\|\overrightarrow{C_iR_i}\right\|$ denotes the length of the vector $\overrightarrow{C_iR_i}$, and W_L and W_{VCZ} denote the width of the travel lane and the width of the visual clear zone on each side of the roadway, respectively (user-defined parameters, assuming the highway is homogeneous in the lane

geometry along its length). According to the Pythagorean Theorem, $\left\|\overrightarrow{C_iR_i}\right\| =$ $((X' - x_{C_i})^2+(Y' - y_{C_i})^2)^{0.5}$. Therefore:

$$((X' - x_{C_i})^2 + (Y' - y_{C_i})^2)^{0.5} = W_L + W_{VCZ} \quad (58)$$

Since Equation (56) is a linear equation, the simultaneous set of Equation (56) and (58) can be easily solved by method of substitution. First, Equation (56) is solved for X in terms of Y:

$$X' = x_{C_i} + [(y_{C_i} - y_{C_{i+1}})(Y' - y_{C_i})/(x_{C_{i+1}} - x_{C_i})] \quad (59)$$

Then, it is substituted for X' in Equation (58), and Y' is solved. There are two possible solutions for Y':

$$Y' = y_{C_i} \pm \{(W_L + W_{VCZ})^2 (x_{C_{i+1}} - x_{C_i})^2 / [(y_{C_i} - y_{C_{i+1}})^2 + (x_{C_{i+1}} - x_{C_i})^2]\}^{0.5} \quad (60)$$

To find their corresponding X' values, the values for Y' are substituted into Equation (59) and X' is solved. For the special case where $x_{C_{i+1}} = x_{C_i}$, the value of the denominator in Equation (59) is zero. In such a case, X' and Y' are determined from the following equations:

$$X' = y_{C_i} \pm (W_L + W_{VCZ}) \quad (61)$$

and

$$Y' = y_{C_i} \quad (62)$$

As was discussed previously, solving the simultaneous set of linear and quadratic equations in two variables, X' and Y', gives two pairs of solutions. The solutions should correspond to the points R_i and L_i (the *x-y* projections of the points corresponding to C_i, located on the outer edges of the right and left visual clear zones). Let's assume the first

pair of solutions corresponds to R_i. Since $\overrightarrow{C_iR_i}$ and $\overrightarrow{C_iC_{i+1}}$ are in the same *x*-*y* plane, the resulting vector of $\left[\overrightarrow{C_iR_i}, \overrightarrow{C_iC_{i+1}}\right]$ should point purely in the *z*-direction and lie along the positive *z*-axis (based on the cross product definition; Figure 17):

$$\left[\overrightarrow{C_iR_i}, \overrightarrow{C_iC_{i+1}}\right] = \begin{vmatrix} \hat{i} & \hat{j} & \hat{k} \\ X' - x_{C_i} & Y' - y_{C_i} & 0 \\ x_{C_{i+1}} - x_{C_i} & y_{C_{i+1}} - y_{C_i} & 0 \end{vmatrix}$$

$$= ((X' - x_{C_i})(y_{C_{i+1}} - y_{C_i}) - (Y' - y_{C_i})(x_{C_{i+1}} - x_{C_i}))\,\hat{k}$$

$$= \beta\,\hat{k} \tag{63}$$

where $\hat{k}$ is the unit vector in the direction of the *z*-axis and:

$$\beta = (X' - x_{C_i})(y_{C_{i+1}} - y_{C_i}) - (Y' - y_{C_i})(x_{C_{i+1}} - x_{C_i}) \tag{64}$$

Trying the first pair of solutions (X'_1 and Y'_1) in β, if $\beta > 0$, the vector $\left[\overrightarrow{C_iR_i}, \overrightarrow{C_iC_{i+1}}\right]$ lies along the positive *z*-axis and the assumption is correct (i.e., X'_1 and Y'_1 correspond to R_i). Otherwise the set of X'_1 and Y'_1 corresponds to L_i, while X'_2 and Y'_2 correspond to R_i.

Similar methods are applied to determine the remaining $\{R_i\}$ and $\{L_i\}$ from $\{C_i\}$. For example, by using C_1 and C_2 and applying a similar method, R_1 and L_1 (the *x*-*y* projections of the points corresponding to C_1, located on the outer edges of the right and left visual clear zones) can be determined. Algorithm 2 represents the modeling of visual clear zone boundaries.

Algorithm 2. Modeling of visual clear zone boundaries

Input $C = \{C_1(x_{C_1}, y_{C_1}), C_2(x_{C_2}, y_{C_2}), \ldots, C_N(x_{C_N}, y_{C_N})\}$
Input W_L
Input W_{VCZ}
$i \leftarrow 1$
repeat
  if $x_{C_{i+1}} = x_{C_i}$ **then**
  $Y'_1 = y_{C_i}$
  $Y'_2 = y_{C_i}$
  $X'_1 = y_{C_i} + (W_L + W_{VCZ})$
  $X'_2 = y_{C_i} - (W_L + W_{VCZ})$
  else
  $Y'_1 = y_{C_i} + \{(W_L + W_{VCZ})^2 (x_{C_{i+1}} - x_{C_i})^2 / [(y_{C_i} - y_{C_{i+1}})^2 + (x_{C_{i+1}} - x_{C_i})^2]\}^{0.5}$
  $Y'_2 = y_{C_i} - \{(W_L + W_{VCZ})^2 (x_{C_{i+1}} - x_{C_i})^2 / [(y_{C_i} - y_{C_{i+1}})^2 + (x_{C_{i+1}} - x_{C_i})^2]\}^{0.5}$
  $X'_1 = x_{C_i} + [(y_{C_i} - y_{C_{i+1}})(Y'_1 - y_{C_i})/(x_{C_{i+1}} - x_{C_i})]$
  $X'_2 = x_{C_i} + [(y_{C_i} - y_{C_{i+1}})(Y'_2 - y_{C_i})/(x_{C_{i+1}} - x_{C_i})]$
  end if
  $\beta = (X'_1 - x_{C_i})(y_{C_{i+1}} - y_{C_i}) - (Y'_1 - y_{C_i})(x_{C_{i+1}} - x_{C_i})$
  if $\beta > 0$ **then**
    $x_{R_i} = X'_1$
    $y_{R_i} = Y'_1$
    $x_{L_i} = X'_2$
    $y_{L_i} = Y'_2$
  else
    $x_{R_i} = X'_2$
    $y_{R_i} = Y'_2$
    $x_{L_i} = X'_1$
    $y_{L_i} = Y'_1$
  end if
  $i \leftarrow i + 1$
until $i = N$
return
$\{R = \{R_1(x_{R_1}, y_{R_1}), R_2(x_{R_2}, y_{R_2}), \ldots, R_{N-1}(x_{R_{N-1}}, y_{R_{N-1}})\},$
$L = \{L_1(x_{L_1}, y_{L_1}), L_2(x_{L_2}, y_{L_2}), \ldots, L_{N-1}(x_{L_{N-1}}, y_{L_{N-1}})\}\}$

The procedure described above is for the case when the widths of the visual clear zones on the right and the left sides of the road are equal. When the widths of the right and the left visual clear zones are not equal, Equation (58) will be in the form of:

$$((X' - x_{C_i})^2 + (Y' - y_{C_i})^2)^{0.5} = W_L + W_{RVCZ} \quad (65)$$

where W_{RVCZ} denotes the width of the visual clear zone on the right side of the roadway. By solving the two variables X' and Y' within a simultaneous set of Equations (56) and (65), two pairs of solutions can be found:

$$X' = x_{C_i} + [(y_{G_i} - y_{C_{i+1}})(Y' - y_{C_i})/(x_{C_{i+1}} - x_{C_i})] \quad (66)$$

$$Y' = y_{C_i} \pm \{(W_L + W_{RVCZ})^2 (x_{C_{i+1}} - x_{C_i})^2 / [(y_{C_i} - y_{C_{i+1}})^2 + (x_{C_{i+1}} - x_{C_i})^2]\}^{0.5} \quad (67)$$

For the special case where $x_{C_{i+1}} = x_{C_i}$, X' and Y' are determined from the following equations:

$$X' = y_{C_i} \pm (W_L + W_{RVCZ}) \quad (68)$$

and

$$Y' = y_{C_i} \quad (69)$$

Only the point corresponding to R_i would be acceptable since Equation (65) was constructed based on point R_i. Trying both pairs of solutions in β, the pair (X' and Y') that makes β positive corresponds to R_i would be acceptable, and the other pair is rejected.

In order to find the coordinates of L_i, all the previous equations are rewritten with respect to L_i, the point located on the left clear zone boundary. For example, Equation (65) is rewritten as:

$$((X' - x_{C_i})^2 + (Y' - y_{C_i})^2)^{0.5} = W_L + W_{LVCZ} \quad (70)$$

Two pairs of solutions are found when solving the two variables X' and Y' within a simultaneous set of Equations (56) and (70):

$$X' = x_{C_i} + [(y_{G_i} - y_{C_{i+1}})(Y' - y_{C_i})/(x_{C_{i+1}} - x_{C_i})] \quad (71)$$

$$Y' = y_{C_i} \pm \{(W_L + W_{LVCZ})^2 (x_{C_{i+1}} - x_{C_i})^2 / [(y_{C_i} - y_{C_{i+1}})^2 + (x_{C_{i+1}} - x_{C_i})^2]\}^{0.5} \quad (72)$$

For the special case where $x_{C_{i+1}} = x_{C_i}$, X' and Y' are determined from the following equations:

$$X' = y_{C_i} \pm (W_L + W_{LVCZ}) \quad (73)$$

and

$$Y' = y_{C_i} \quad (74)$$

In this case, since Equation (70) was constructed based on point L_i, only the pair corresponding to L_i would be acceptable. Trying both pairs of solutions in β, the pair (X' and Y') that makes β negative corresponds to L_i would be acceptable, and the other pair is rejected.

Figure 20 shows the flowchart for modeling of visual clear zone boundaries. At the completion of this step, the result is a definition of two boundary lines on each side of the roadway. The area between these two lines does not contain any sight distance obstructions. The visual clear zone boundaries serve as the threshold criteria that the sight line is compared to in the Horizontal Sight Distance Algorithm.

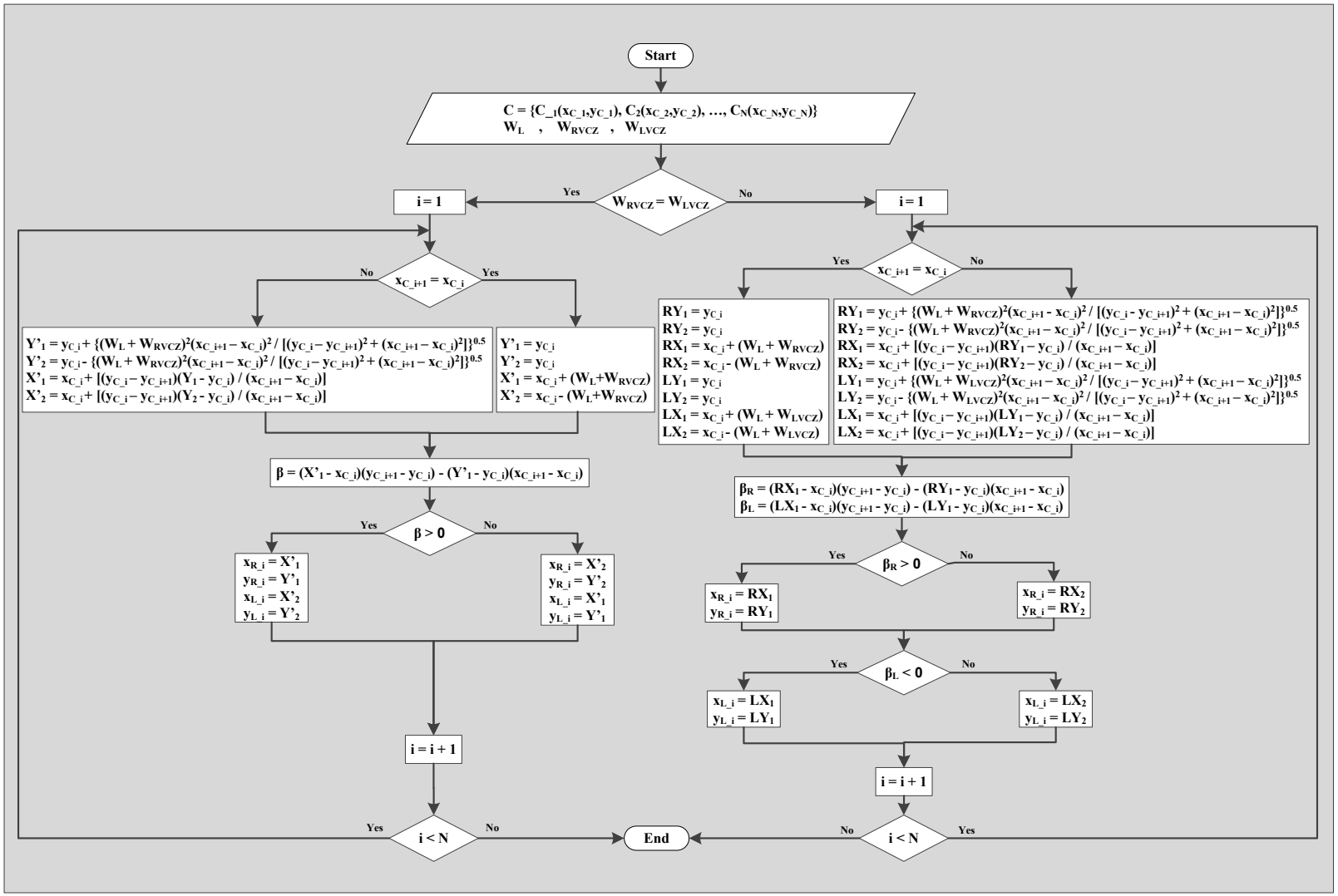

Figure 20. Flowchart for modeling visual clear zone boundaries

VERTICAL SIGHT DISTANCE ALGORITHM

According to the MUTCD (*2*), "*the passing sight distance on a vertical curve is the distance at which an object 3.5 feet above the pavement surface can be seen from a point 3.5 feet above the pavement*" (see Figure 3).

In vertical curves, there is not adequate sight distance anytime the pavement surface restricts the sight line. The sight line is defined as a line that begins 3.5 ft above the pavement surface corresponding to a point where a vehicle is located and ends at the point located 3.5 ft above the pavement surface where the object is located. Previous research efforts (*6, 8*) have been conducted and passing sight distance algorithms have been developed in such a way that examines the intersection of the sight line that originated from the points located 3.5 ft above the roadway center line and the pavement surface. Based on the previous studies, an iterative process is used in the algorithm to measure the availability of vertical passing sight distances, as explained in the following paragraphs.

In order to evaluate the available passing sight distance between an observation point and a target point, not only the visibility of the target point but all the points located between the two points must be checked. The procedure is required to examine probable sight-hidden dips (in vertical curves) or blind spots (in horizontal curves). Otherwise, it is possible for vehicles positioned in between the study vehicles, in observation and target points, to become lost in depressions or blind spots, even though the vehicles in observation and target points are spaced the minimum passing sight distance apart and the drivers may see each other (see Figure 21).

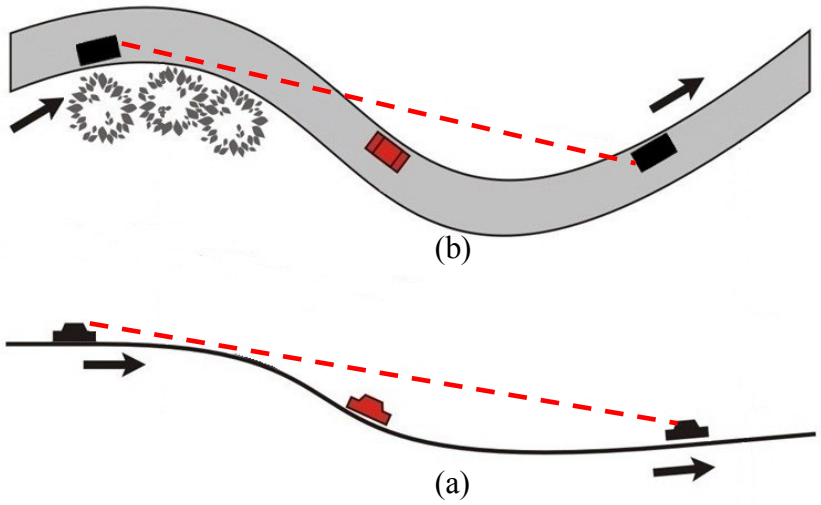

Figure 21. Lost vehicle in: (a) a vertical curve, and (b) a horizontal curve

To evaluate the available vertical passing sight distance between points O_i and T_s, located along a straight segment of a roadway, iterative locations downstream of O_i are tested (see Figure 22). A target point, referred to as $T_{i,j}$, is selected at a defined distance from the observation point. The interval between point O_i and point $T_{i,j}$ is tested for sight distance restriction. If a sight restriction is not found, then $T_{i,j+1}$ is tested for sight restrictions. Assuming no sight restrictions are found in each successive interval from O_i to the increasing points T_j, the process is repeated until a distance equal to the minimum required passing sight distance as set by the MUTCD (Table 6) is reached (point T_s).

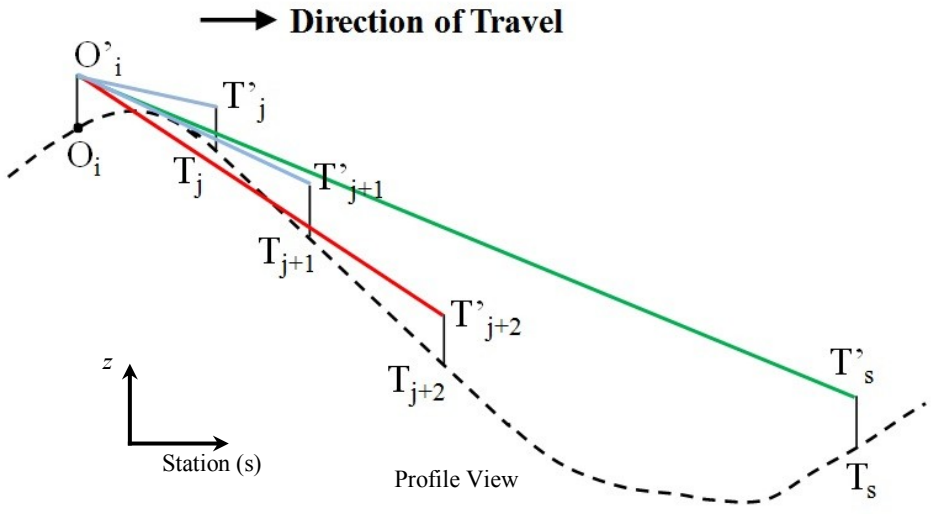

Figure 22. Passing sight distance evaluation for observation point O_i along a vertical alignment

In general terms, the determination of the theoretical sight line that is calculated for each interval from point O_i to the points farther down is as follows. First, 3.5 ft is added to the roadway elevations at point O_i and point T_{j+1}:

$$z_{O'_i} = z_{O_i} + 3.5 \tag{75}$$

$$z_{T'_{j+1}} = z_{T_{j+1}} + 3.5 \tag{76}$$

The line between these two points that are 3.5 ft above the pavement surface is the theoretical sight line. Next, the equation of the line between these two points is written as follows where stationing is the independent variable and elevation is the dependent variable. Knowing the two points O'_i and T'_{j+1} on the line, the slope of the line can be calculated:

$$m = \frac{z_{O'_i} - z_{T'_{j+1}}}{s_{O'_i} - s_{T'_{j+1}}} \tag{77}$$

where $s_{O'_i}$ and $s_{T'_{j+1}}$ represent the station values of points O'_i and T'_{j+1}, respectively. The stationing values are determined for points along a straight segment of a roadway by calculating the incremental distances between two consecutive points via the following equation:

$$\Delta_s = ((x_{p+1} - x_p)^2 + (y_{p+1} - y_p)^2)^{0.5} \tag{78}$$

The general form of the equation of a straight line is:

$$z = ms + b \tag{79}$$

where *m* is the slope of the line and *b* is the *z*-intercept.

The two points O'_i and T'_{j+1} are on the line. Therefore, by substituting the slope and one of the points in Equation (76), the *z*-intercept can be found:

$$z = ms + b$$

$$z_{O'_i} = \left(\frac{z_{O'_i} - z_{T'_{j+1}}}{s_{O'_i} - s_{T'_{j+1}}}\right) s_{O'_i} + b$$

$$b = z_{O'_i} - \left(\frac{z_{O'_i} - z_{T'_{j+1}}}{s_{O'_i} - s_{T'_{j+1}}}\right) s_{O'_i} \tag{80}$$

After calculating the slope and the *z*-intercept, the equation of the line can be determined:

$$z = \left(\frac{z_{O'_i} - z_{T'_{j+1}}}{s_{O'_i} - s_{T'_{j+1}}}\right) s + z_{O'_i} - \left(\frac{z_{O'_i} - z_{T'_{j+1}}}{s_{O'_i} - s_{T'_{j+1}}}\right) s_{O'_i}$$

$$z = \left(\frac{z_{O'_i} - z_{T'_{j+1}}}{s_{O'_i} - s_{T'_{j+1}}}\right)(s - s_{O'_i}) + z_{O'_i}$$

$$z = \left(\frac{(z_{O_i} + 3.5) - (z_{T_{j+1}} + 3.5)}{s_{O'_i} - s_{T'_{j+1}}}\right)(s - s_{O'_i}) + (z_{O_i} + 3.5)$$

$$z = \left(\frac{z_{O_i} - z_{T_{j+1}}}{s_{O'_i} - s_{T'_{j+1}}}\right)(s - s_{O'_i}) + (z_{O_i} + 3.5) \quad (81)$$

After determining the equation of the line, the points (midpoints) can be identified between point O_i and the ending station of the theoretical sight line (there will be only one point, T_j, for the case of the sight line between points O_i and T_{j+1}). Elevations of the points (located on the sight line) corresponding to each of the midpoints can be found (by substituting the station value of the midpoints in the equation of the line) and compared to the corresponding roadway elevations at those midpoints (i.e., the elevations of the midpoints themselves). There are no sight restrictions in a given iteration if the sight line elevations are greater than the roadway profile. However, if at any station a roadway pavement elevation is greater than its corresponding sight line elevation, there is not adequate passing sight distance. If this occurs, the loop of checking O_i and farther points is broken. The vertical sight distance evaluation procedure is described in Algorithm 3.

Algorithm 3. Vertical sight distance evaluation between O_i and T_s

Input i
Input s
Initiate $\{O_i(x_{O_i}, z_{O_i}), T_j(x_{T_j}, z_{T_j}), T_{j+1}(x_{T_{j+1}}, z_{T_{j+1}}), \ldots, T_s(x_{T_s}, z_{T_s})\}$
Generate $\{O_i'(x_{O_i}, z_{O_i}+3.5), T_j'(x_{T_j}, z_{T_j}+3.5), T_{j+1}'(x_{T_{j+1}}, z_{T_{j+1}}+3.5), \ldots, T_s'(x_{T_s}, z_{T_s}+3.5)\}$
Flag_problem ← false
j ← i + 1
    repeat
    Connect O_i' to T_j'
    k ← j
    repeat
        if $z_{O_i'T_{j+1}'} > z_{T_k}$ **then**
            k ← k +1
        else
        Flag_problem ← true
        Break
        end if
    until $T_k = T_{j+1}$
    if Flag_problem = true
        Break
    else
    j ← j + 1
until $j > s$
if $j > s$ **then**
    return "There is adequate vertical sight distance between O_i and T_s."
else
    return "There is NOT adequate vertical sight distance between O_i and T_s."
end if

HORIZONTAL SIGHT DISTANCE ALGORITHM

To evaluate the available horizontal sight distance between two points, the sight line must be checked to determine whether it stays within the limits of the visual clear zones (in other words, the sight line should not cross the visual clear zone boundaries). The sight distance algorithm should examine the intersection of the sight line that originated

from the points located on the roadway center line as well as the visual clear zone boundaries. The intersection should be examined for the visual clear zone boundaries on both sides of the roadway in order to consider any probable changes in alignment (left curve or right curve) in that specific segment. An iterative process will be used in the algorithm to measure the availability of passing sight distances in horizontal alignments.

In order to evaluate the available horizontal sight distance between points C_i and C_s, located along an arbitrary segment of the roadway alignment, the following cross product operations can be used:

$$\left[\overrightarrow{C_iC_s}\,,\,\overrightarrow{C_iR_j}\right] = \begin{vmatrix} \hat{i} & \hat{j} & \hat{k} \\ x_{C_s} - x_{C_i} & y_{C_s} - y_{C_i} & 0 \\ x_{R_j} - x_{C_i} & y_{R_j} - y_{C_i} & 0 \end{vmatrix}$$

$$= ((x_{C_s} - x_{C_i})(y_{R_j} - y_{C_i}) - (y_{C_s} - y_{C_i})(x_{R_j} - x_{C_i}))\,\hat{k}$$

$$= \gamma\,\hat{k} \quad ; \qquad j = \text{i to s} \tag{82}$$

and

$$\left[\overrightarrow{C_iC_s}\,,\,\overrightarrow{C_iL_j}\right] = \begin{vmatrix} \hat{i} & \hat{j} & \hat{k} \\ x_{C_s} - x_{C_i} & y_{C_s} - y_{C_i} & 0 \\ x_{L_j} - x_{C_i} & y_{L_j} - y_{C_i} & 0 \end{vmatrix}$$

$$= ((x_{C_s} - x_{C_i})(y_{L_j} - y_{C_i}) - (y_{C_s} - y_{C_i})(x_{L_j} - x_{C_i}))\,\hat{k}$$

$$= \delta\,\hat{k} \quad ; \qquad j = \text{i to s} \tag{83}$$

where $\hat{k}$ is the unit vector in the direction of the *z*-axis and:

$$\gamma = (x_{C_s} - x_{C_i})(y_{R_j} - y_{C_i}) - (y_{C_s} - y_{C_i})(x_{R_j} - x_{C_i}) \quad ; \quad j = \text{i to s} \tag{84}$$

$$\delta = (x_{C_s} - x_{C_i})(y_{L_j} - y_{C_i}) - (y_{C_s} - y_{C_i})(x_{L_j} - x_{C_i}) \quad ; \quad j = \text{i to s} \tag{85}$$

C_i is the projection of the point located on the roadway center line on the *x-y* plane that corresponds to the passing vehicle location. C_s is the projection of the point located on the roadway center line on the *x-y* plane with the minimum required sight distance from C_i and is determined by adding the discrete sections of C_iC_{i+1}:

$$\overline{C_iC_s} = \overline{C_iC_{i+1}} + \overline{C_{i+1}C_{i+2}} + \ldots + \overline{C_{s-1}C_s} \quad (86)$$

where $\overline{C_iC_{i+1}}$ is the length of the roadway center line between C_i and C_{i+1}.

The length of the roadway center line between C_i and C_s is equal to the required passing sight distance from the MUTCD (Table 6). R_j and L_j are the *x-y* projections of the points located on the right and left clear zone boundaries, respectively, downstream of point C_i (see Figure 23):

$$R_j \in \{R_i, R_{i+1}, R_{i+2} \ldots, R_S\} \quad (87)$$

$$L_j \in \{L_i, L_{i+1}, L_{i+2} \ldots, L_S\} \quad (88)$$

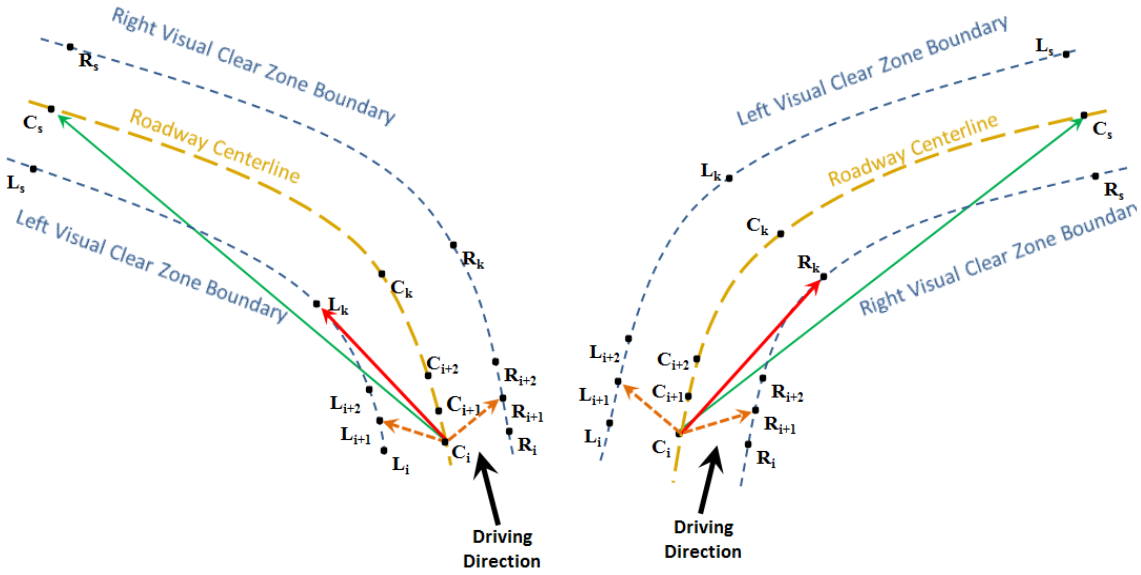

Left Curve **Right Curve**

Figure 23. Passing sight distance evaluation in right and left curves along horizontal alignments

In order to have adequate horizontal sight distance between C_i and C_s, vectors $\overrightarrow{C_iR_j}$ and $\overrightarrow{C_iL_j}$ should always be in both sides of the vector $\overrightarrow{C_iC_s}$, respectively (see Figure 23). In other words, γ and δ should be negative and positive, respectively, for all values of j. On the other hand, if there is any point on the right (left) visual clear zone boundary, such as R_k (L_k), that makes γ positive (δ negative), there is not enough horizontal sight distance in that segment of the roadway. The horizontal sight distance evaluation procedure is described in Algorithm 4.

Algorithm 4. Horizontal sight distance evaluation between C_i and C_s

Input i
Input s
Input $C = \{C_i(x_{C_i}, y_{C_i}), C_{i+1}(x_{C_{i+1}}, y_{C_{i+1}}), \ldots, C_s(x_{C_s}, y_{C_s})\}$
Input $R = \{R_i(x_{R_i}, y_{R_i}), R_{i+1}(x_{R_{i+1}}, y_{R_{i+1}}), \ldots, R_s(x_{R_s}, y_{R_s})\}$
Input $L = \{L_i(x_{L_i}, y_{L_i}), L_{i+1}(x_{L_{i+1}}, y_{L_{i+1}}), \ldots, L_s(x_{L_s}, y_{L_s})\}$
j ← i
repeat
  $\gamma = (x_{C_s} - x_{C_i})(y_{R_j} - y_{C_i}) - (y_{C_s} - y_{C_i})(x_{R_j} - x_{C_i})$
  $\delta = (x_{C_s} - x_{C_i})(y_{L_j} - y_{C_i}) - (y_{C_s} - y_{C_i})(x_{L_j} - x_{C_i})$
  if $\gamma < 0$ AND $\delta > 0$ **then**
    j ← j +1
  else
    Break
  end if
until $j > s$
if $j > s$ **then**
  return {"There is adequate horizontal sight distance between C_i and C_s."}
else
  return {"There is NOT adequate horizontal sight distance between C_i and C_s."}
end if

While Figure 23 illustrates the case where the sight line began and ended on the same curve, it should be noted that the algorithm evaluates the sight distance not only for simple horizontal curves but also for any arbitrary horizontal alignment such as tangent sections and reverse curves. Figure 24 illustrates the case of a reverse curve where the sight line must be checked against the visual clear zone boundaries on both the right and left sides. In this figure, lines AX, BY, and CZ represent vector $\overrightarrow{C_iC_s}$ at different points along the roadway. At each of these points (and at all intermediate points), the algorithm checks to see if the sign for γ changes from negative to positive (indicating a sight distance obstruction) for the right side and if the sign for δ changes from positive to negative for the left side. As an example, the sign for γ at R_{i+n} is negative, but it is

positive at R_s, indicating that the sight line has crossed over the visual clear zone boundary between R_{i+n} and R_s. This would mean that there is not adequate sight distance between those points. At point B, the value of γ at R_p is negative and it stays negative for all points between B and Y, meaning that there are no sight distance obstructions at B. Point C illustrates a check of the left side visual clear zone boundary. The value of δ is positive at L_q but changes to negative at L_r, indicating a sight distance obstruction. Figure 24 also indicates how this algorithm works when checking sight distance for reverse curves or curves with multiple changes in alignment.

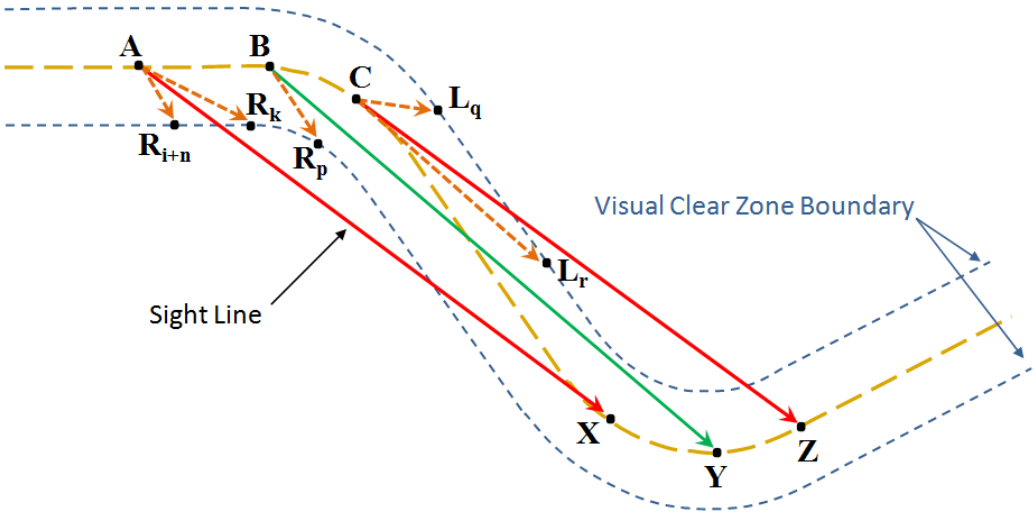

Figure 24. Application of algorithm to reverse curves

Figure 25 shows the flowchart for evaluating horizontal sight distance.

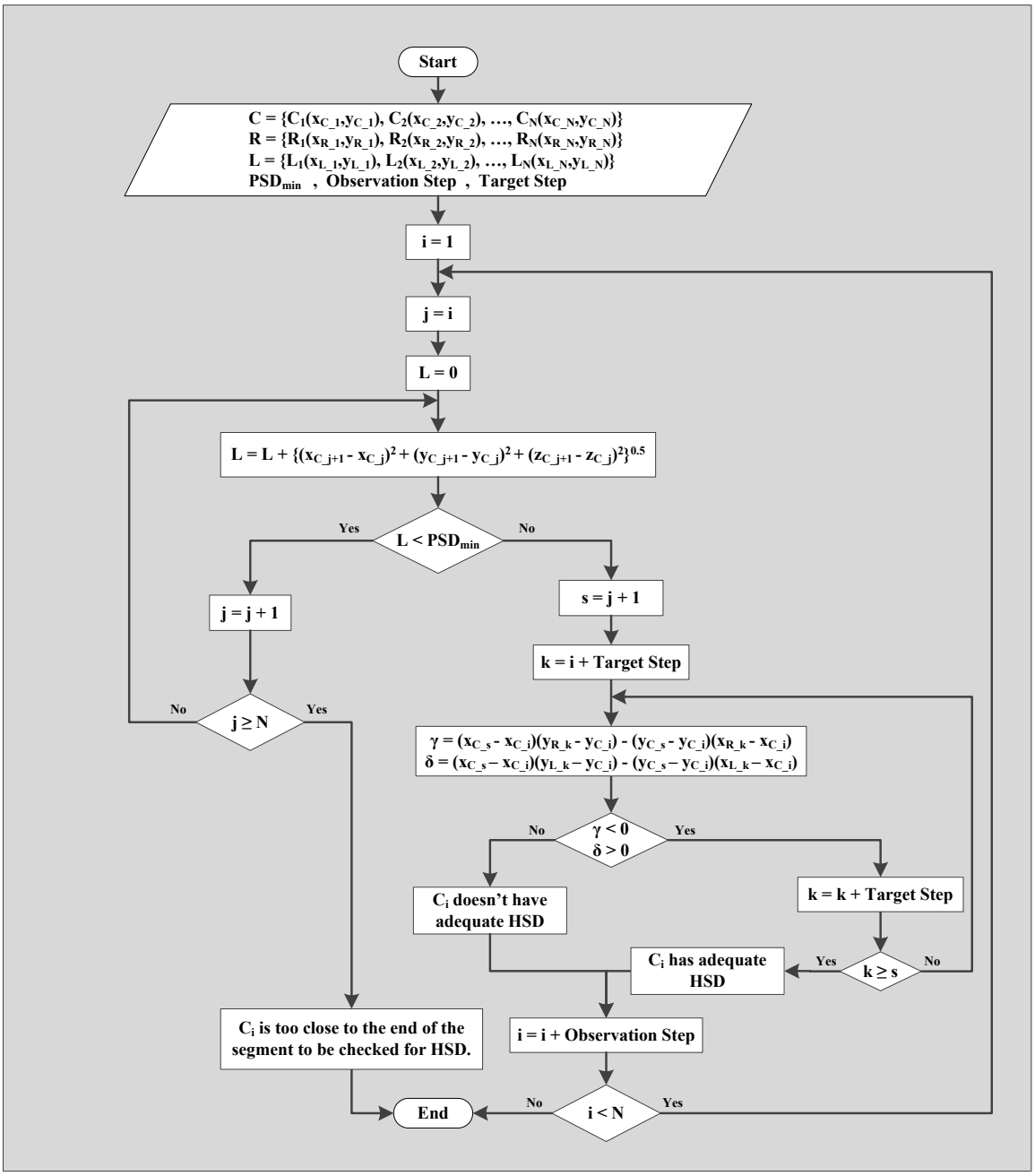

Figure 25. Flowchart for evaluating horizontal sight distance

THREE-DIMENSIONAL SIGHT DISTANCE ALGORITHM

On two-lane highways, sight distance may be obstructed by horizontal alignments, vertical alignments, or a combination of both. The vertical sight distance algorithm

presented previously in this chapter determines the availability of passing sight distance for any straight segment of two-lane highways. The horizontal sight distance algorithm presented in the previous section evaluates the passing sight distance for any arbitrary alignment of two-lane highways on level terrain.

Few research studies have examined cases where a vertical crest curve is overlapped on a horizontal curve. Some studies have suggested calculating sight distance at each point using projections on two-dimensional planes for vertical as well as horizontal alignments separately, and then taking the lower bound as the available sight distance at that point (*5, 7*). The lower bound has been defined as aggregated overlapping horizontal and vertical sight distances. However, it is not appropriate to judge the sight distance by looking at horizontal or vertical alignment separately because in horizontal alignment, the elevation information is not available, and in vertical alignment, the information related to the horizontal alignment of the road is not available. Therefore, this procedure is not accurate and does not consider the three-dimensional nature of the geometric design. Other researchers (*35-38*) developed three-dimensional sight distance models based on the curved parametric elements used in finite element methods or based on road surface idealization. However, those types of algorithms are only applicable to short, specific segments of newly designed highways. Generally, the majority of the existing roadways in the nation were designed and constructed a long time ago, and there is no design information related to those roadways/roadsides at the present time. Furthermore, the previous algorithms may not provide accurate results due to the approximation used in their numerical methods. This

section of the study presents a new analytical algorithm for evaluating the three-dimensional passing sight distance for any arbitrary alignment of two-lane highways. Using this technique, it is possible to address sight distance that cannot be identified through the separate processing of horizontal and vertical alignments.

Figure 26 shows a situation on a two-lane highway where a vertical crest curve is overlapped on a horizontal curve. The roadway is going uphill and at the same time turning around the hill. Therefore, the sight distance is restricted by the vertical crest as well as the horizontal curve formed due to the obstruction of the hill.

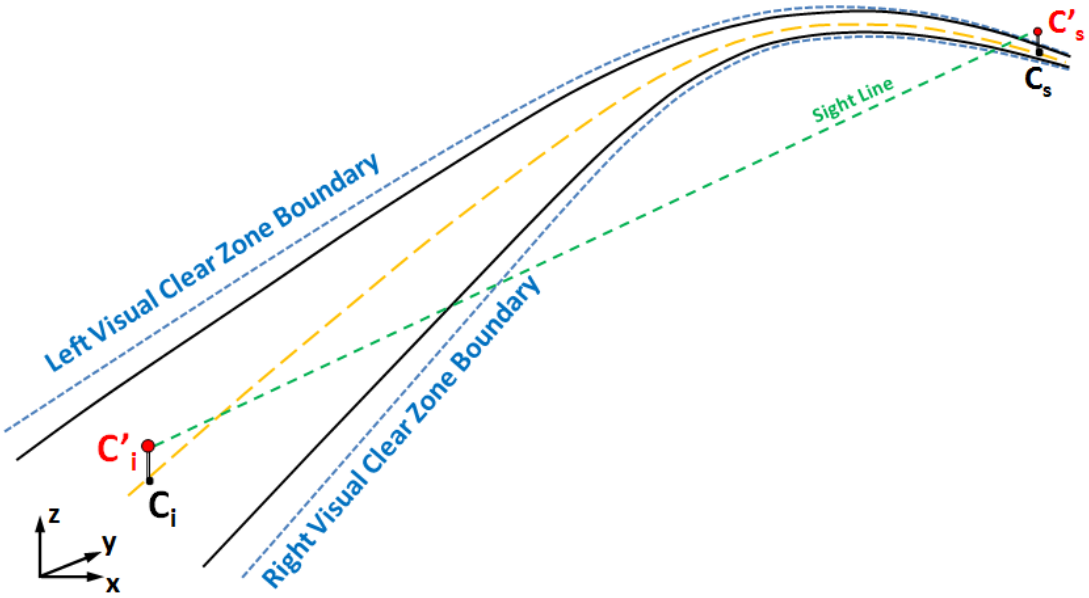

Figure 26. Overlapping a vertical curve on a horizontal curve in a two-lane highway

To evaluate the available horizontal sight distance between points C_i and C_s, spaced with the minimum passing sight distance apart, the sight line that begins 3.5 ft above C_i and ends at the point located 3.5 ft above C_s must be checked. If the sight line stays within

the limits of the visual clear zones (the blue dashed line in Figure 26) and does not go below the level of the pavement surface of the roadway, there would be adequate passing sight distance between the two points. C_i and C_s are defined in an *x-y-z* system of Cartesian coordinates as follows:

$$C_i = \begin{pmatrix} x_{C_i} \\ y_{C_i} \\ z_{C_i} \end{pmatrix}$$

and

$$C_s = \begin{pmatrix} x_{C_s} \\ y_{C_s} \\ z_{C_s} \end{pmatrix}$$

The equation of the straight line in three dimensions passing through C'_i and C'_s is defined by:

$$\frac{x - x_{C'_i}}{x_{C_s} - x_{C'_i}} = \frac{y - y_{C'_i}}{y_{C_s} - y_{C'_i}} = \frac{z - z_{C'_i}}{z_{C_s} - z_{C'_i}} = t \qquad (89)$$

where *t* is a parameter that can take any real value from $-\infty$ to $+\infty$.

C'_i and C'_s are the beginning and the end of the sight line and are located 3.5 ft above C_i and C_s. Therefore, the coordinates of C'_i and C'_s are as follows:

$$C'_i = \begin{pmatrix} x_{C_i} \\ y_{C_i} \\ z_{C_i} + 3.5 \end{pmatrix}$$

and

$$C'_s = \begin{pmatrix} x_{C_s} \\ y_{C_s} \\ z_{C_s} + 3.5 \end{pmatrix}$$

Substituting for the coordinates, the following equation is obtained:

$$\frac{x - x_{C_i}}{x_{C_s} - x_{C_i}} = \frac{y - y_{C_i}}{y_{C_s} - y_{C_i}} = \frac{z - (z_{C_i} + 3.5)}{(z_{C_s} + 3.5) - (z_{C_i} + 3.5)} = t \quad (90)$$

From Equation (90), the following parametric equations can be written:

$$x = (x_{C_s} - x_{C_i})\, t + x_{C_i} \quad (91)$$

$$y = (y_{C_s} - y_{C_i})\, t + y_{C_i} \quad (92)$$

$$z = (z_{C_s} - z_{C_i})\, t + z_{C_i} + 3.5 \quad (93)$$

To check whether the sight line goes below the level of the pavement surface, the method presented in the vertical sight distance algorithm can be used to examine the elevation of the sight line at each of the midpoints between the beginning and end of the sight line. In that method, by substituting the station value of a midpoint in the line equation, the elevation of the line in that specific point was calculated easily and compared to the corresponding roadway elevation at that midpoint. However, the similar method is not applicable in the three-dimensional case because the midpoints and the sight line are not in the same plane. Therefore, it is not possible to substitute the *x* and *y* of a midpoint in the line equation and find the corresponding *z* in order to compare it to the elevation of the midpoint. Instead, an imaginary plane passing through a midpoint and perpendicular to both the axis of the road and the *x*-*y* plane can be used to check the intersection of the sight line and the plane (see Figure 27).

Let's consider G_k as a point located on the center of the travel lane between C_i and C_s, and consider C_k as the point located on the roadway center line and corresponding to G_k (see Figure 27):

$$C_k = \begin{pmatrix} x_{C_k} \\ y_{C_k} \\ z_{C_k} \end{pmatrix}$$

and

$$G_k = \begin{pmatrix} x_{G_k} \\ y_{G_k} \\ z_{G_k} \end{pmatrix}$$

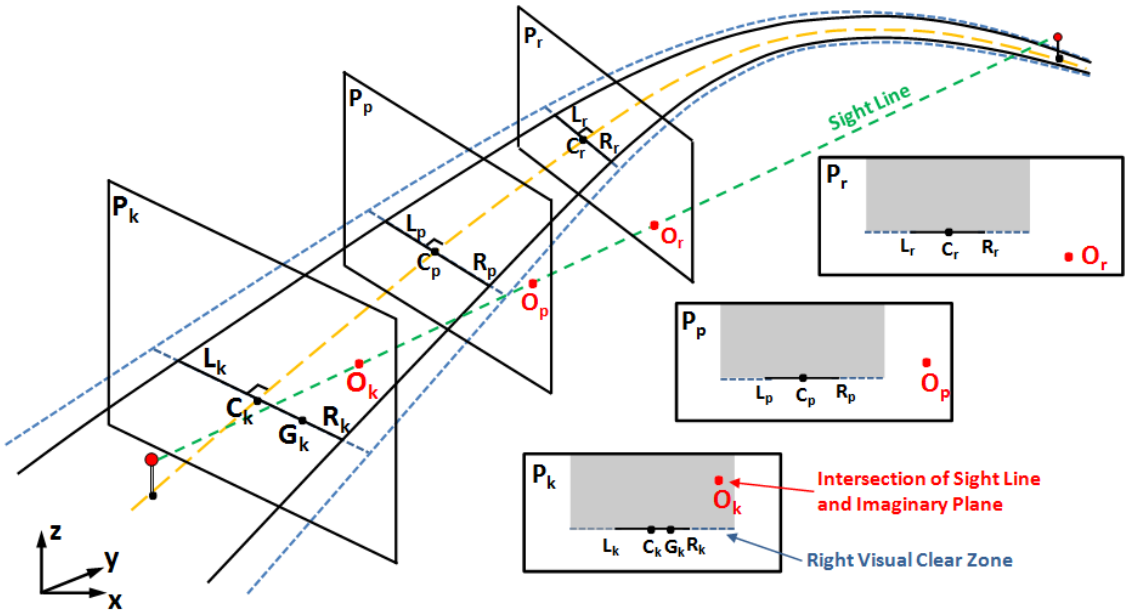

Figure 27. Three-dimensional sight distance evaluation

P_k is an imaginary plane through points C_k and G_k and perpendicular to both the axis of the roadway and the *x*-*y* plane. To find the intersection of the imaginary plane and the sight line, it is necessary to have the equations of both the plane and the sight line. The equation of the sight line was found in the previous step. In order to write the equation of the plane, it is necessary to have two directional vectors that lie in the desired plane (P_k) and one point that is in the plane. One directional vector is $\overrightarrow{C_k G_k}$:

$$\overrightarrow{C_k G_k} = (x_{G_k} - x_{C_k})\,\hat{i} + (y_{G_k} - y_{C_k})\,\hat{j} + (z_{G_k} - z_{C_k})\,\hat{k} \qquad (94)$$

A vector perpendicular to a plane is called a *normal* vector of the plane. Since the desired plane is perpendicular to the *x*-*y* plane, the normal vector of the *x*-*y* plane is also a directional vector of the desired plane: $\overrightarrow{n_{x\text{-}y}}$ (0, 0, 1). The normal vector, *n*, of the desired plane is orthogonal to both directional vectors $\overrightarrow{C_kG_k}$ and $\overrightarrow{n_{x\text{-}y}}$. The cross product can be figured as:

$$\vec{n} = [\overrightarrow{C_kG_k} , \overrightarrow{n_{x\text{-}y}}] = \begin{vmatrix} \hat{\imath} & \hat{\jmath} & \hat{k} \\ x_{G_k} - x_{C_k} & y_{G_k} - y_{C_k} & z_{G_k} - z_{C_k} \\ 0 & 0 & 1 \end{vmatrix}$$

$$= (y_{G_k} - y_{C_k})\,\hat{\imath} + (-x_{G_k} + x_{C_k})\,\hat{\jmath} \qquad (95)$$

After determining a point in the desired plane and the normal vector to the plane, the equation of the plane can be constructed. Let's choose point C_k. Assume that R(*x*, *y*, *z*) is an arbitrary point in the plane. The vector $\overrightarrow{C_kR}$ lies in the plane:

$$\overrightarrow{C_kR} = (x - x_{C_k})\,\hat{\imath} + (y - y_{C_k})\,\hat{\jmath} + (z - z_{C_k})\,\hat{k} \qquad (96)$$

Since the normal vector of a plane is orthogonal to any vector that lies in the plane, and also the dot product of orthogonal vectors is zero:

$$\langle \vec{n} , \overrightarrow{C_kR} \rangle = 0 \qquad (97)$$

This is called the vector equation of the plane. By writing Equation (97) in components, the equation of the plane can be obtained:

$$(y_{G_k} - y_{C_k})(x - x_{C_k}) + (-x_{G_k} + x_{C_k})(y - y_{C_k}) = 0 \qquad (98)$$

Equations (91), (92), (93), and (98) should be solved simultaneously to find the point of the intersection of the line and the plane:

$$(y_{G_k} - y_{C_k})((x_{C_s} - x_{C_i})t + x_{C_i}) - x_{C_k}) + (-x_{G_k} + x_{C_k})((y_{C_s} - y_{C_i})t + y_{C_i}) - y_{C_k}) = 0$$

$$(x_{C_s} - x_{C_i})(y_{G_k} - y_{C_k})t + (x_{C_i} - x_{C_k})(y_{G_k} - y_{C_k}) + (y_{C_s} - y_{C_i})(-x_{G_k} + x_{C_k})t + (y_{C_i} - y_{C_k})(-x_{G_k} + x_{C_k}) = 0$$

$$[(x_{C_s} - x_{C_i})(y_{G_k} - y_{C_k}) + (y_{C_s} - y_{C_i})(-x_{G_k} + x_{C_k})]t + [(x_{C_i} - x_{C_k})(y_{G_k} - y_{C_k}) + (y_{C_i} - y_{C_k})(-x_{G_k} + x_{C_k})] = 0$$

$$t = \frac{(x_{C_k} - x_{C_i})(y_{G_k} - y_{C_k}) + (y_{C_k} - y_{C_i})(x_{G_k} - x_{C_k})}{(x_{C_s} - x_{C_i})(y_{G_k} - y_{C_k}) + (y_{C_s} - y_{C_i})(-x_{G_k} + x_{C_k})} \quad (99)$$

By substituting for *t* from Equation (99) in Equations (91), (92), and (93), the coordinates of O_k (intersection point) can be obtained. Similar methods are applied to determine the intersection points of the sight line and the imaginary planes passing through other midpoints. For example, by solving the equation of sight line and the plane P_p, the intersection point O_p is obtained (see Figure 27).

In order to have adequate sight distance between C_i and C_s, first, the elevation of the intersection point in each imaginary plane must be greater than the elevation of the corresponding point on the pavement surface of the roadway. Second, the horizontal distance of the intersection point and the corresponding point on the center line of the roadway must be smaller than the sum of the lane width and the width of the visual clear zone boundary:

$$z_{O_j} > z_{G_j} \quad ; \quad j = \text{i to s} \quad (100)$$

and

$$((x_{O_j} - x_{C_j})^2 + (y_{O_j} - y_{C_j})^2)^{0.5} < (W_L + W_{VCZ}) \quad ; \quad j = \text{i to s} \quad (101)$$

To better understand the above set criteria, let's think of the goal post analogy. In American football, the goal structure consists of a crossbar and goal posts that are extending above the crossbar. A field goal is scored when the ball is kicked completely over the crossbar and between or directly over the goal posts. Similarly, there is adequate sight distance between C_i and C_s if the intersection points fall inside the gray rectangles in each imaginary plane passing through the midpoints (see Figure 27). In the figure, the intersection point O_k does fall inside the rectangle in the plane P_k since the elevation of O_k is smaller than the elevation of G_k, and the horizontal distance of O_k and C_k is smaller than the sum of the lane width and the width of the visual clear zone boundary. However, farther down the roadway, the intersection point O_p does not fall inside the rectangle in the plane Pp because the elevation of O_p is greater than the elevation of G_p. Therefore, it is concluded that there is not adequate sight distance between C_i and C_s, and no farther points will be checked in the algorithm.

The procedure described above is for the case when the widths of the visual clear zones on the right and left sides of the road are equal. When the widths of the right and the left visual clear zones are not equal, it must be determined which should be used in Equation (101). Following is a procedure that can be used to select which width related to the right or to the left visual clear zone to apply in Equation (101) at each midpoint. Let's consider C_k and C_{k+1} as two consecutive midpoints along the center line of the roadway, and consider O'_k as the projection of O_k, the intersection point of the sight line and the plane P_k (the plane passing through C_k and perpendicular to both the axis of the road and the *x*-*y* plane), on the *x*-*y* plane (see Figure 28). Therefore:

$$x_{O'_k} = x_{O_k} \tag{102}$$

and

$$y_{O'_k} = y_{O_k} \tag{103}$$

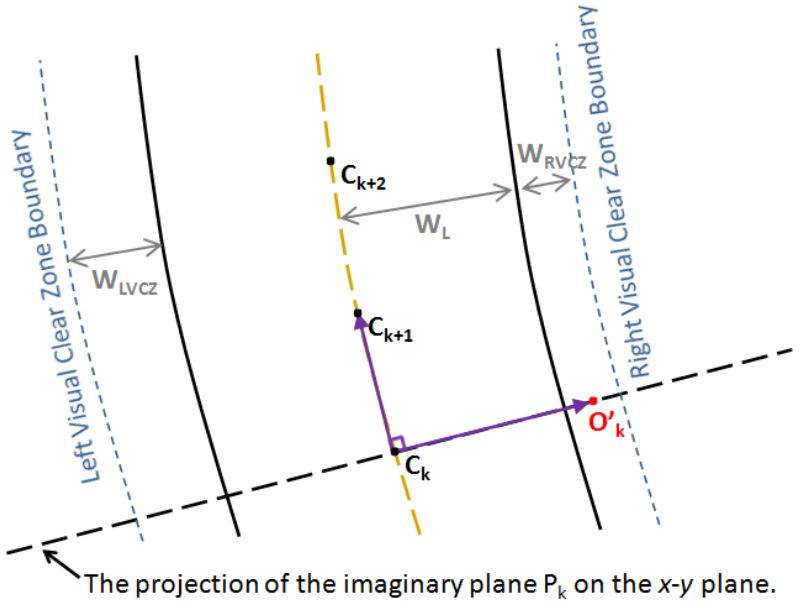

Figure 28. Plan view of the road segment at C_k (when $W_{LVCZ} > W_{RVCZ}$)

Since $\overrightarrow{C_kC_{k+1}}$ and $\overrightarrow{C_kO'_k}$ are in the same *x*-*y* plane, the resulting vector of $[\overrightarrow{C_kC_{k+1}} \, . \, \overrightarrow{C_kO'_k}]$ should point purely in the *z*-direction and lie along the positive or negative *z*-axis depending on whether O'_k is on the left or right side of $\overrightarrow{C_kC_{k+1}}$ (based on the cross product definition; Figure 17):

$$[\overrightarrow{C_kC_{k+1}} \, , \, \overrightarrow{C_kO'_k}] = \begin{vmatrix} \hat{i} & \hat{j} & \hat{k} \\ x_{C_{k+1}} - x_{C_k} & y_{C_{k+1}} - y_{C_k} & 0 \\ x_{O'_k} - x_{C_k} & y_{O'_k} - y_{C_k} & 0 \end{vmatrix}$$

$$= ((x_{C_{k+1}} - x_{C_k})(y_{O'_k} - y_{C_k}) - (y_{C_{k+1}} - y_{C_k})(x_{O'_k} - x_{C_k}))\, \hat{k}$$

$$= \lambda\, \hat{k} \tag{104}$$

where $\hat{k}$ is the unit vector in the direction of the *z*-axis and:

$$\lambda = (x_{C_{k+1}} - x_{C_k})(y_{O'_k} - y_{C_k}) - (y_{C_{k+1}} - y_{C_k})(x_{O'_k} - x_{C_k}) \tag{105}$$

Trying $x_{O'_k} = x_{O_k}$ and $y_{O'_k} = y_{O_k}$ in λ, if $\lambda > 0$, then the vector $[\overrightarrow{C_kC_{k+1}} \,.\, \overrightarrow{C_kO'_k}]$ lies along the positive *z*-axis, meaning that O'_k is on the left side of $\overrightarrow{C_kC_{k+1}}$, and the width of the left visual clear zone must be used in Equation (101). Otherwise, O'_k is on the right side of $\overrightarrow{C_kC_{k+1}}$ and the width of the right visual clear zone must be used in the equation. Similar methods are applied at each midpoint to select the width of the visual clear zone on the right or left side of the road that should be used in Equation (101).

Figure 29 shows the flowchart for evaluating three-dimensional sight distance. The algorithm presented in this section has the ability to evaluate the availability of passing sight distance for any roadway segment with change in horizontal and vertical alignments including tangent sections, reverse horizontal curves, vertical curves, and overlapping horizontal and vertical curves, etc.

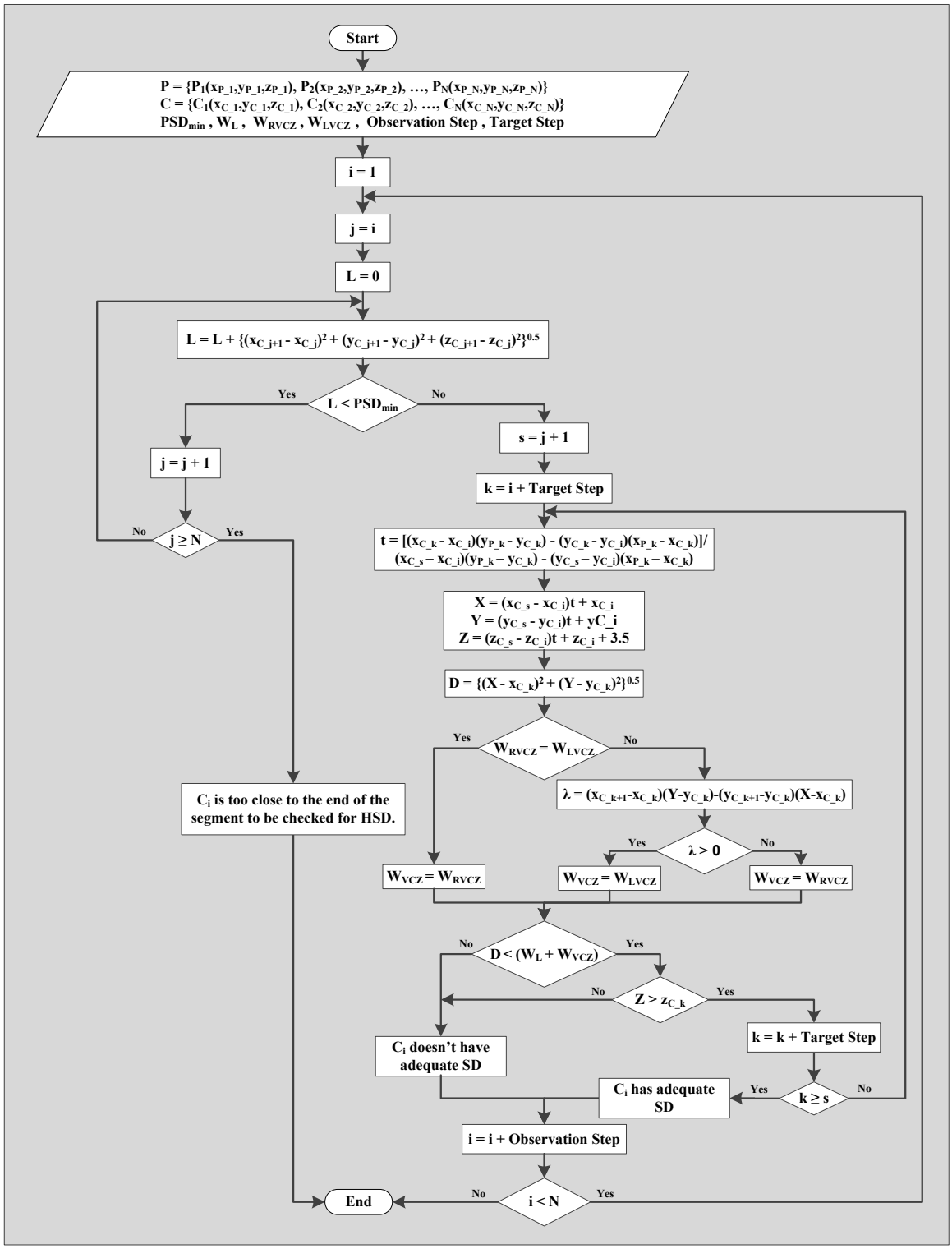

Figure 29. Flowchart for evaluating three-dimensional sight distance

NO-PASSING ZONE MODEL DEVELOPMENT

The algorithms described in the previous sections were incorporated into a computer model to develop an automated method for calculating passing sight distance and locating no-passing zones based on the GPS data. Using the computer model has the potential benefits of saving time, and costs, and eliminating human errors compared to the current methods of field measurements. In the developed model, there are separate and distinct steps as follows:

Step 1: The GPS data (collected by driving on the roadway and using GPS receiver) are converted into the northing and easting values in English units applying the method described in the previous sections. The altitudes related to the GPS data are also converted from metric units to English units. At the end of this step, the result is the coordinates of the collected GPS points, x and y and z, in feet.

Step 2: By applying the cubic B-spline method, the GPS data are smoothed and more data points are generated. At the end of this step, the result is the generated data representing the center of the travel lane (the lane traveled during data collection).

Step 3: Once the GPS data are smoothed, the data that represent the center of a lane are converted to data that represent the center line of the roadway using the algorithm described previously. The result of the process is a series of points that represent the center line of the roadway, sorted in the direction of travel during data collection.

Step 4: The available passing sight distance on a two-lane highway depends on the travel direction. The resulting no-passing zones for the traffic in both directions are independent and may overlap, or there may be a gap between their ends. The

traditional/current field measurement methods for determining the location of no-passing zones require measuring passing sight distance in the field for different travel directions separately, which is time consuming. The three-dimensional sight distance algorithm developed in this research, is based on the evaluation of available three-dimensional sight distance in one direction along the roadway alignment (one directional sight distance algorithm). The developed no-passing zone computer model simply incorporates the algorithm twice (once in each direction) to evaluate the availability of sight distance for a specific roadway segment: once in the direction of travel and once in the opposite direction.

The computer model in this step determines the points on the roadway incrementally and measures the availability of passing sight distance on each point in the direction of travel (data collection) through an iterative process using the developed three-dimensional sight distance algorithm. The first iteration step is to determine the observation points where the availability of sight distances are checked for those locations. Sight distances are checked for the observation points located along the center line of the roadway in the direction of travel. Those points are referred to as O_i, O_{i+1}, O_{i+2}, …, and are not necessarily equally spaced (the distances between the GPS data points depend on the speed of the data collection and also the data collection rate frequency of the GPS receiver). The second iteration step is to examine the iterative target points $T_{i,j}$, $T_{i,j+1}$, $T_{i,j+2}$, …, downstream of the first observation point O_i using the three-dimensional sight distance algorithm described in the previous section. The interval between point O_i and $T_{i,j}$ is tested for sight distance restriction. If a sight

restriction is not found, then $T_{i,j+1}$, the next target point farther down the roadway, is tested for sight restrictions (the location of the current observation point O_i has not been changed yet). Assuming no sight restrictions are found in each successive interval from O_i to the increasing points T_j, the process is repeated until a distance equal to the minimum required passing sight distance as set by the MUTCD (Table 6) is reached (point T_s). In this case, there is not any sight restriction for point O_i, and the algorithm assigns SD_Yes, as a passing attribute, to this point (passing attribute = SD_Yes). T_s is determined by adding the discrete sections of O_iO_{i+1}:

$$\overline{O_iT_s} = \overline{O_iO_{i+1}} + \overline{O_{i+1}O_{i+2}} + \ldots \quad (106)$$

If a sight distance obstruction is found in any successive interval, the iteration (related to this iterative step) stops and the algorithm assigns SD_No, as a passing attribute, to the observation point (passing attribute = SD_No). The next iteration steps are to check the sight distance restrictions for the next observation points, O_{i+1}, O_{i+2}, O_{i+3}, …, individually. For each observation point, a new T_s must be determined. The process is the same as described in the second iteration step. This process is repeated from the beginning to the end of the roadway segment in the direction of travel (data collection). The reason that more than one target point should be examined for each of the observation points in this step (i.e., iterative target points) is to check for probable sight-hidden dips (in vertical curves) or blind spots (in horizontal curves) between the observation point and T_s (the distance equal to the minimum required passing sight distance).

Step 5: After examining the entire segment, the algorithm then identifies the beginning and ending of each no-passing zone segment based on the assigned passing attributes (there would be no-passing zones between the consecutive points having passing attributes of SD_No). At the completion of this step, the result is the locations of the beginning and ending points of theoretical no-passing zones in the direction of travel (data collection). Figure 30 shows the flowchart for determining theoretical no-passing zones.

Step 6: Upon identifying the theoretical no-passing zone segments, the computer model then checks adjacent no-passing zones to see if the distance between segments is less than 400 ft. If this occurs, according to the MUTCD, the no-passing zone should be continuous throughout the entire length, and the solid line should connect those zones to provide a continuous restriction through both zones. Therefore, the model deletes the ending point of the first no-passing zone and the beginning of the next no-passing zone, and one no-passing zone is created (see the flowchart in Figure 31).

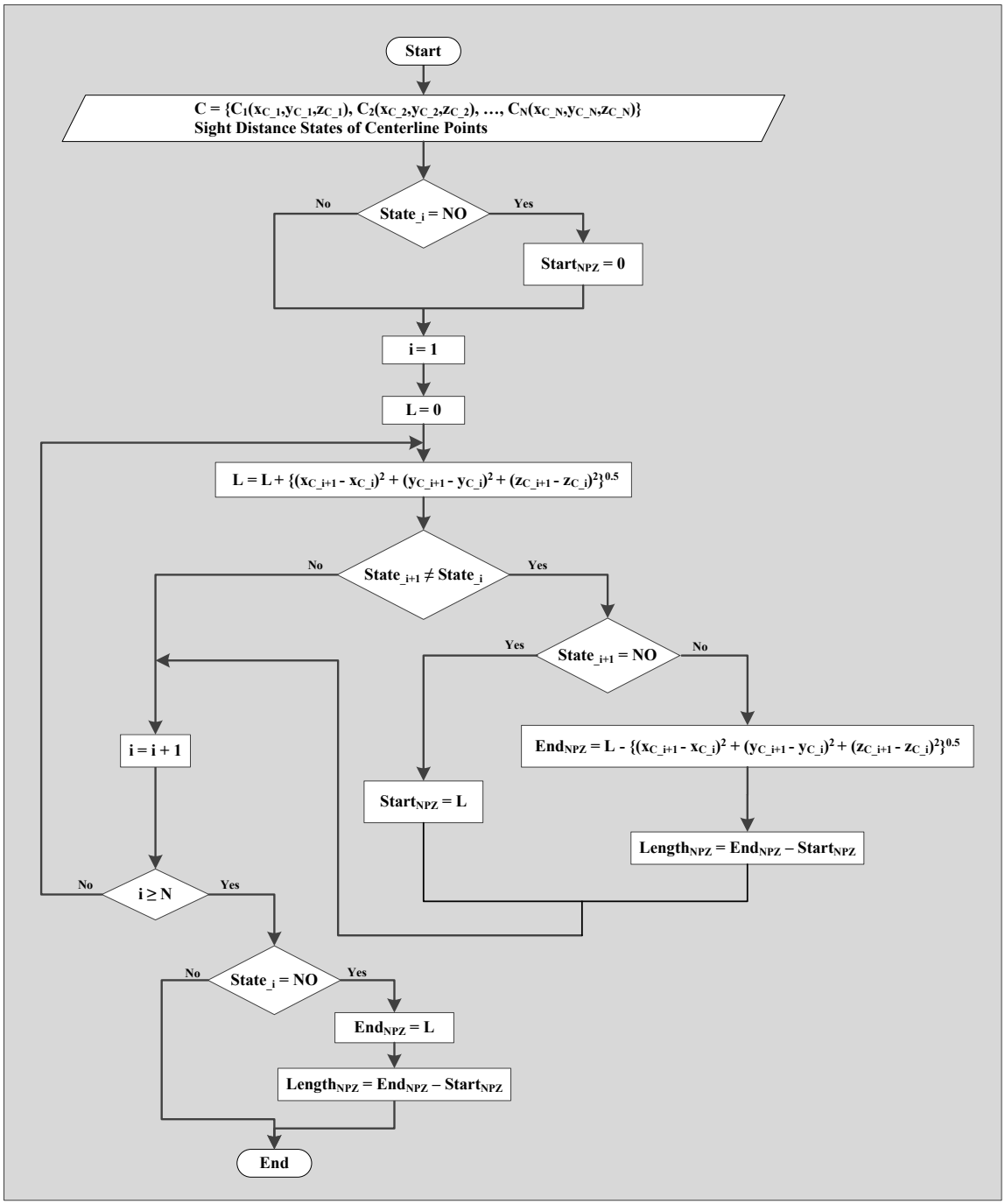

Figure 30. Flowchart for determining theoretical no-passing zone

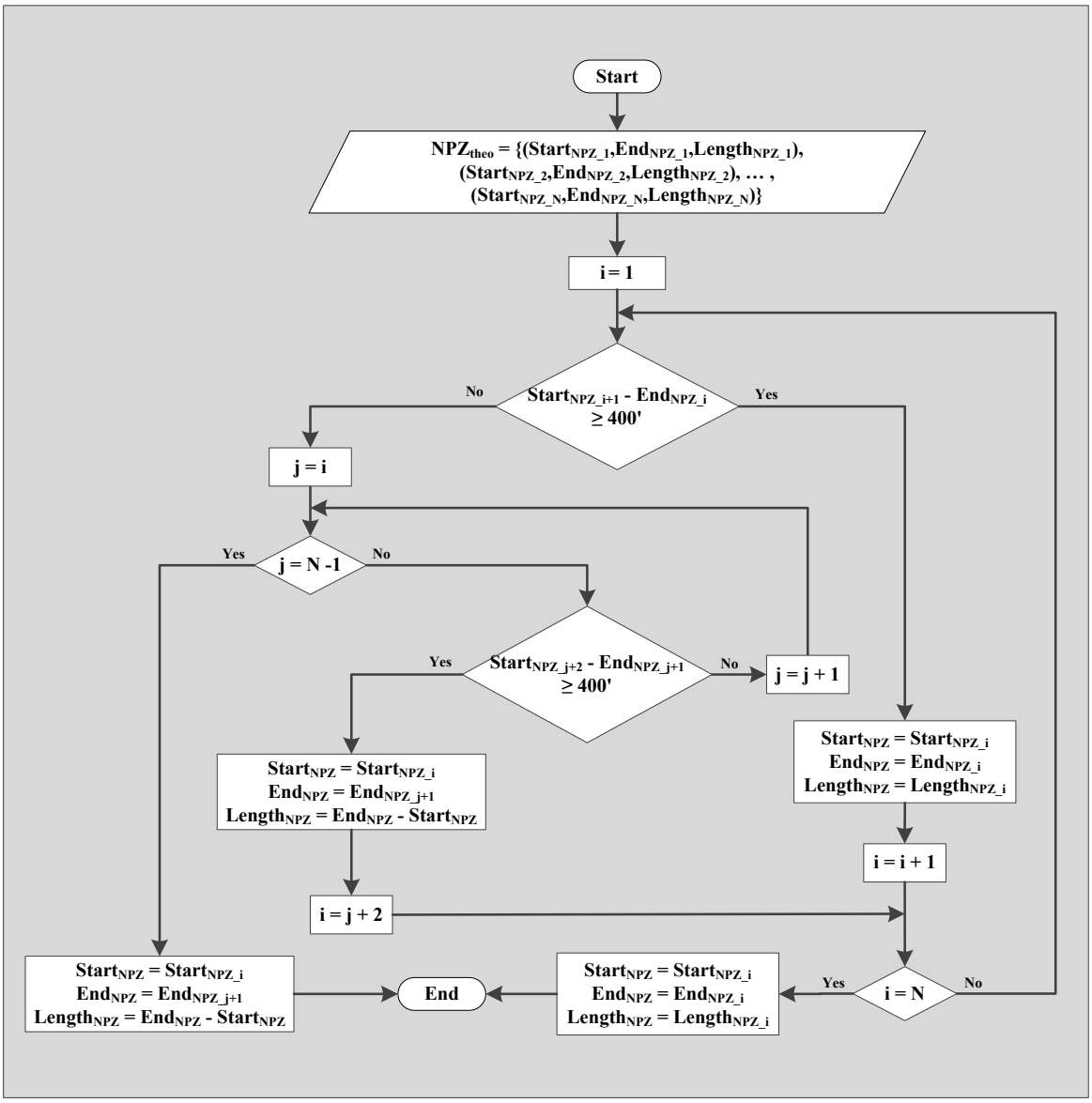

Figure 31. Flowchart for determining no-passing zone

Step 7: Since the GPS data points are collected for one direction of a specific roadway segment, Step 2 and Step 3 produce the geometric models of the center of the travel lane and the roadway center line in the format of sets of data points sorted in the direction of data collection. Step 4, Step 5, and Step 6 evaluate the availability of sight distance and locate no-passing zones in the direction of travel (data collection). The evaluation of

available sight distance in the opposing direction is conducted by reversing the resulting data from Step 2 and 3 and then using the procedure described in Step 4, Step 5, and Step 6 to locate the no-passing zones for the opposing direction.

Figure 32 shows the workflow for the No-Passing Zone computer model. The input to the model is the collected GPS data (longitude, latitude, and altitude), and the output of the model is the locations of no-passing zones for both directions of the roadway (locations along the length of the roadway segment where passing sight distance is not provided).

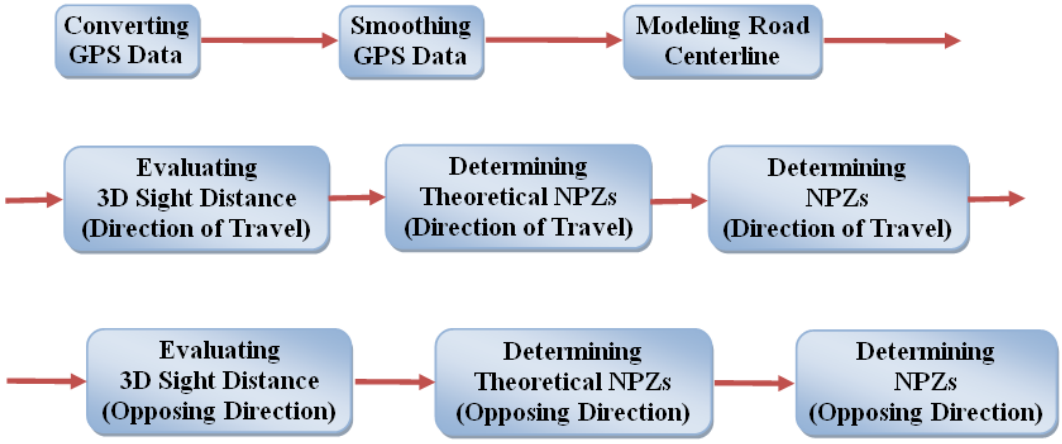

Figure 32. Workflow for No-Passing Zone computer model

CHAPTER IV

SOFTWARE PACKAGE DEVELOPMENT

This chapter presents details on the design and implementation of the NPZ computer program. The NPZ computer program is a user-friendly software package that implements the NPZ computer model described in the previous chapter and integrates the developed algorithms. This includes the algorithms for converting GPS data, smoothing data, modeling roadway center line, evaluating 3D sight distance, determining theoretical no-passing zones, and determining final no-passing zones. The program takes input data (GPS data points), processes the data, and generates output data (location of no-passing zones along a highway).

For coding the software, the main objectives were:

- To have an efficient program with an easy-to-use Graphical User Interface (GUI).
- To have a program convertible to a standalone executable program file.

In the beginning, the computer program was coded in the R programming language in order to test the algorithms. Then, several computer programming languages were examined to find the best one to code the algorithms efficiently and also provide a number of features for GUI applications. Finally, Microsoft (MS) Visual Basic was used to develop the NPZ computer program since it was able to achieve the objectives very well.

By creating an executable program, the author ensured that it can be run independently on any machine (PC or laptop) without the need to install any special or costly software or program. The executable program file can be easily used by both field crews in any location as well as traffic engineers in any local office in order to locate no-passing zones on two-lane highways.

The main suite of the program is a form consisting of five major panels (Figure 33). The panels are:

- Input Parameters Panel.
- Direction of Data Collection Processing Panel.
- Opposing Direction Processing Panel.
- Data Display Panel.
- Output Saving Panel.

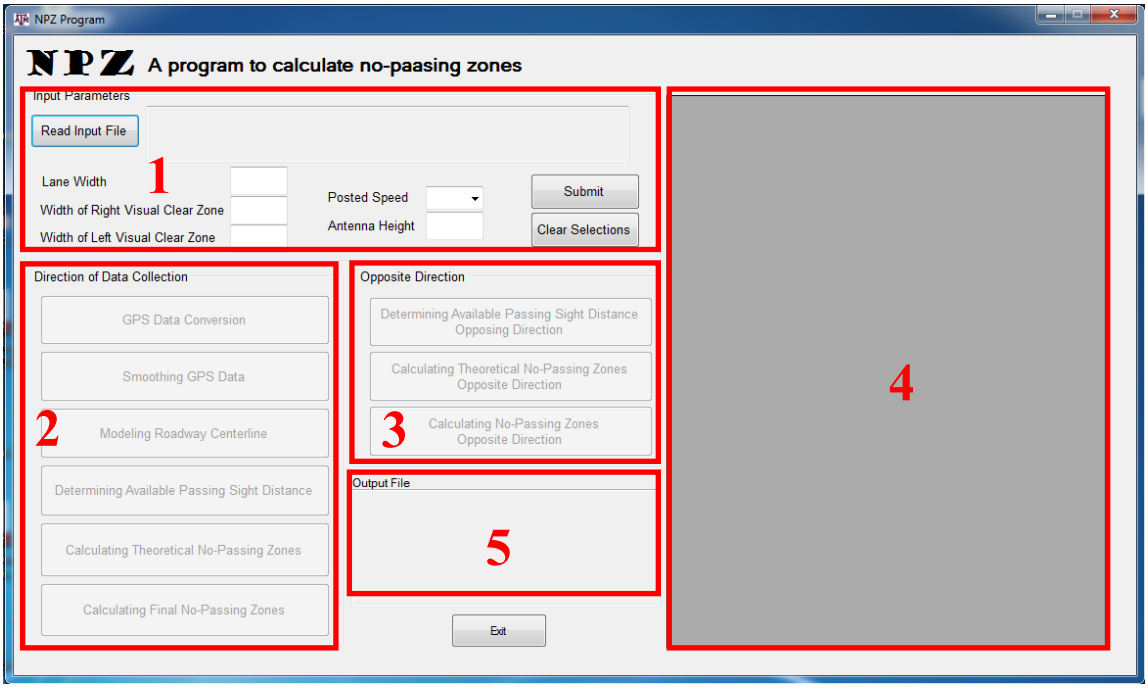

Figure 33. Interface of NPZ program

Each one of the panels has its own self-describing name. One of the first steps in developing the computer program was to identify the important parameters to be used in the program as input parameters to evaluate sight distances. The input parameters such as the parameters related to the geometry of the roadway (e.g. width of the travel lane and width of the visual clear zones on each side of the roadway), posted speed of the highway, and antenna height of the GPS receiver (measured from pavement surface) were identified and included in Panel 1. The major parts of the program are Panel 2 (Direction of Data Collection) and Panel 3 (Opposing Direction). Those panels include several buttons representing the major tasks of the project, as the caption of each button indicates.

The user starts the process by selecting the input file (GPS data points) and then provides the input parameters in Panel 1. The user must prepare the input files in comma separated value (CSV) format beforehand. The file must have three columns (longitude first, latitude second, and altitude third) and the data must start from the first row (without any labels for the columns). Before proceeding further, the program checks the input parameters to avoid any invalid values. Figure 34 shows the program interface after the user left the Lane Width field empty. The red asterisk indicates that this field is mandatory and must be filled.

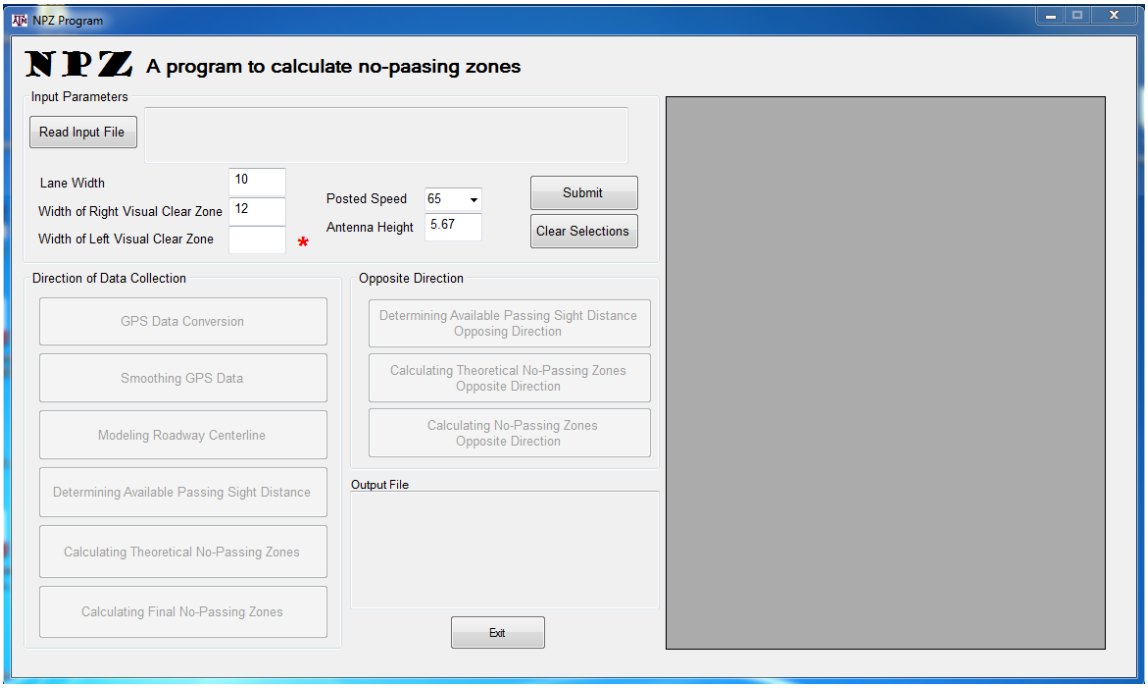

Figure 34. NPZ program, error in input data

After reading the input file and loading the GPS data, the program displays the data in the Data Display Panel in the most right-hand side of the form (Figure 35), which lets the user visually check the data before taking further steps.

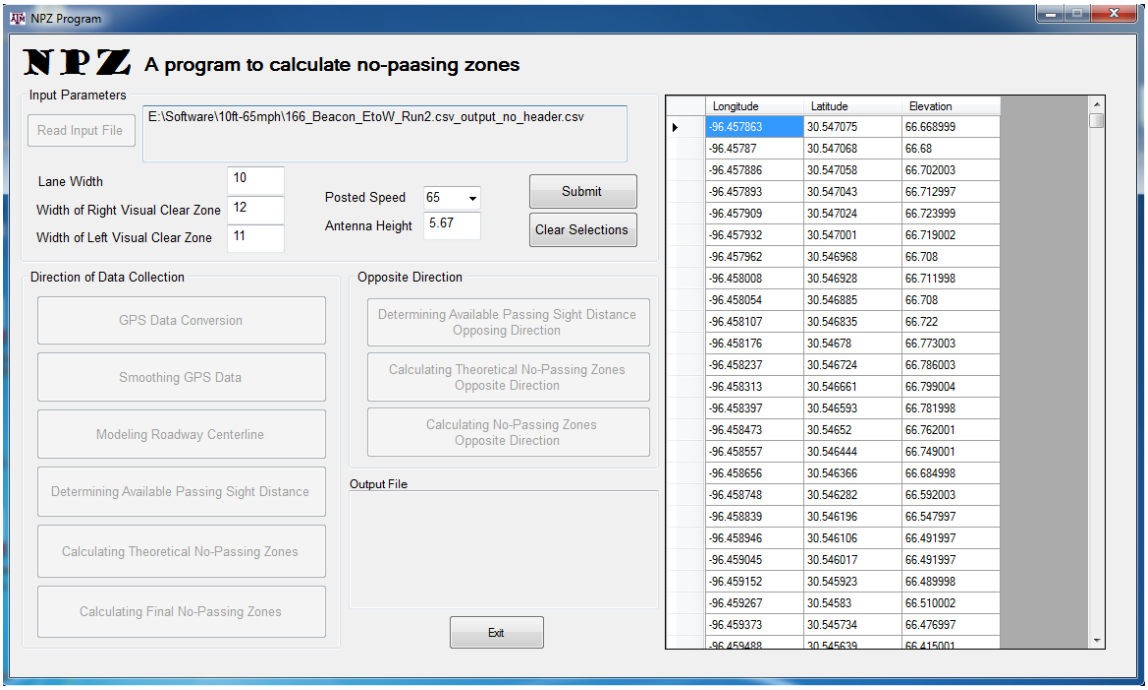

Figure 35. NPZ program, loading the input data

After all the necessary parameters are input, the buttons for the processes are activated one by one in the Direction of Data Collection Panel and Opposing Direction Panel. The first activated button is GPS Data Conversion located in Panel 2 (Direction of Data Collection). No other button will be activated before the conversion process completes. Then, the Smoothing GPS Data button is activated and so on. As each process completes, its results are displayed in the Data Display Panel, and are saved in a CSV file as output. For example, after the user clicks on the GPS Data Conversion

button, longitude, latitude, and altitude are converted to *x*, *y*, and *z*, and the result is displayed in the Data Display Panel. At the same time, Panel 5 shows the information about the output file saved in the computer (see Figure 36).

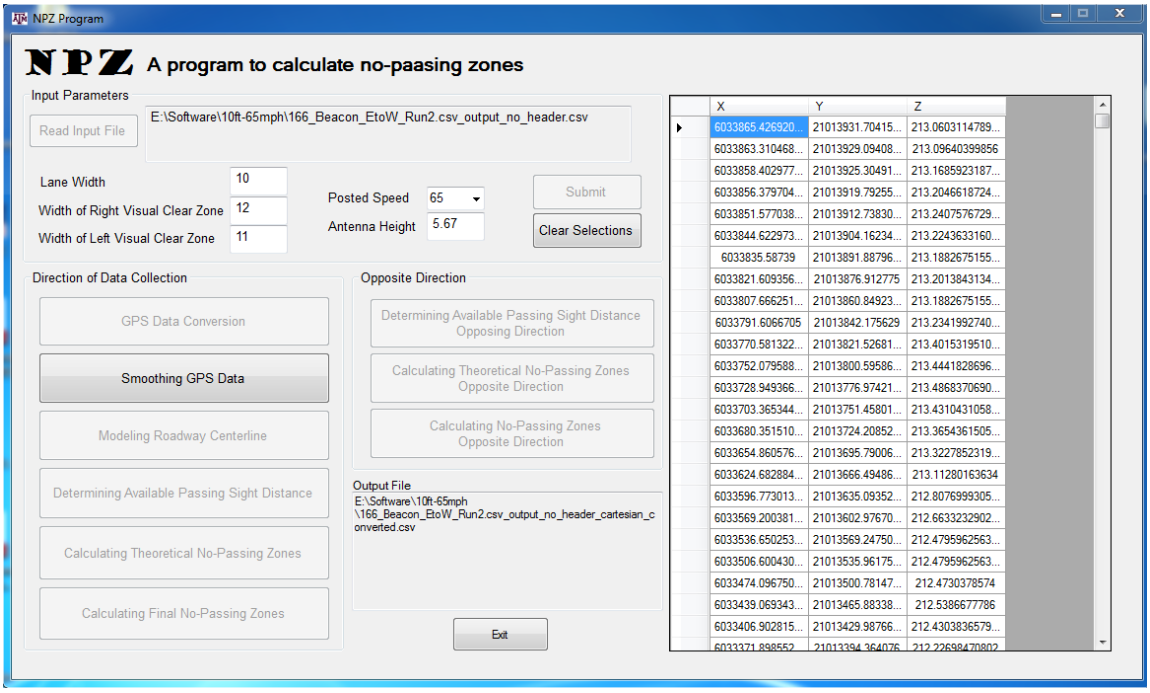

Figure 36. NPZ program, converting GPS data

After each of the next four processes in Panel 2 are completed (i.e., Modeling Roadway Center Line, Evaluating 3D Sight Distance, Theoretical No-Passing Zones, and No-Passing Zones), the results are displayed and also saved in the computer. The last file saved in the computer includes the beginning, ending, and length of each no-passing zone along the direction of the data collection. Then, after the user clicks the first button in Panel 3, the data are reversed along the opposing direction of the roadway. This function enables the program to evaluate sight distance and locate no-passing zones

along the opposing direction, as well. For example, if the original input data had been collected by traveling eastbound, by clicking the button, the last eastbound value became the first value for the westbound study, and so on. In other words, one-direction data collection provides the horizontal sight distance and no-passing zone locations for both directions of the roadway.

CHAPTER V

DATA COLLECTION AND EXPERIMENTAL WORK

This chapter describes the data collection and the experimental work of the research. The data collection was conducted in three main steps. The first step was selecting the data collection sites. Then, the field operation was planned; the appropriate devices and configurations were selected, and the data collection was performed. In the third step, the collected data underwent post-processing, and the redundant data were reduced in order to generate the input files for the NPZ computer program.

SITE SELECTION

The ideal data collection sites were the segments of two-lane highways consisting of both straight and curved segments with significant enough changes in horizontal and vertical alignments to require no-passing zones. The author identified several two-lane highways as ideal sites by asking local engineers and using topographic maps. The test locations provided several different testing lengths and consisted of a variety of horizontal and vertical curves. The highways were driven to select the best segments based on the length of the alignments, number of horizontal and vertical curves, and the other geometric characteristics of the alignments. Ultimately, three sites were selected for the data collection, including segments on Texas Farm-to-Market (FM) Roads 166, 159, and 390. Figure 37 shows the locations of the selected roadway segments.

Figure 37. Selected segments for data collection

Farm-to-Market Road 166

Farm-to-Market Road 166 is in Burleson County, east of Caldwell, Texas (see Figure 38). The roadway is a two-lane highway and is approximately 15.6 mi long. The posted speed limit is 65 mph on this roadway. The dots in Figure 38 represent the beginning and end of the roadway segment evaluated.

Figure 38. Farm-to-Market Road 166 alignment

Farm-to-Market Road 159

Farm-to-Market Road 159 is in Brazos County, northwest of Navasota, Texas. It is a two-lane road, approximately 16.5 mi long and runs from Texas State Highway 6 to Farm-to-Market Road 105. The posted speed limit is 60 mph on this highway. The beginning and end of the roadway segment is marked in Figure 39.

Figure 39. Farm-to-Market Road 159 alignment

Farm-to-Market Road 390

The FM 390 site is located in Washington County, southeast of Somerville Lake, Texas. A part of this road is designated as a scenic route by the State of Texas. The actual test segment is approximately 16.7 mi long and runs from the town of Independence to the intersection of Farm-to-Market Road 1948 N, north of U.S. Highway 290 (see Figure 40). The segment is a two-lane roadway, and the posted speed limit is 65 mph. The dots in Figure 40 represent the beginning and end of the roadway segment evaluated.

Figure 40. Farm-to-Market Road 390 alignment

FIELD OPERATION AND DATA COLLECTION

Data were collected on the studied segments by driving the Texas A&M Transportation Institute (TTI) instrumented vehicle in both directions of the highway. The TTI instrumented vehicle was a 2006 Toyota Highlander that had been upgraded with several different state-of-the-art devices to record various data (see Figure 41). The principal system within the instrumented vehicle was a Dewetron DEWE5000 data acquisition system with several different sensory inputs that could be programmed for different devices. One device was the Trimble® DSM232 GPS that used a single frequency antenna, mounted on the roof of the vehicle, to gather GPS data. Furthermore, the Dewetron data acquisition system allowed the user to record events during the data

collection. The events included but were not limited to the beginning of the run, the end of the run, and every change between passing and no-passing zone pavement markings.

Figure 41. Instrumented vehicle and Dewetron DEWE5000 Data acquisition System

GPS receivers with different technologies are available today to be used in data collection, but it was not in the scope of this research to analyze and evaluate each option. Instead, two accessible GPS devices from different manufacturers that had different high-end technologies (beacon and WAAS) were used for the GPS data collection. The Trimble® DSM232 system was one of the receivers. The DSM232 receiver offers a wide range of GPS positioning methods and associated accuracies. Two methods of GPS positioning that were applied in this research were SBAS-WAAS, and the International Association of Marine Aids to Navigation and Lighthouse Authorities (IALA)-compliant navigation beacon. The DSM232 also has the capability to use a commercial satellite correction service provided by OmniSTAR and provides sub-meter accuracy in real time (see Figure 42). The collection rate capability of the unit is 10 Hz (10 points per second), and accuracy of the device is as follows (*39*):

- X, Y position (differential, RTK): (+/- 0.25m + 1ppm) RMS, (+/- 0.01m + 1ppm).
- Height (differential/RTK): (+/- 0.5m + 1ppm) RMS, (+/- 0.02m + 1ppm).

Figure 42. Trimble® DSM232 differential global positioning system

The other GPS receiver used for the data collection was the GeoChron GPS Logger®, manufactured by SparkFun (see Figure 43). GeoChron is an enclosed GPS logger incorporating an EM408 GPS receiver from GlobalSat, with a high-sensitivity SiRF Star III GPS chipset at its core. The GPS logger has the WAAS feature, and the collection rate capability of this device is 1 Hz (meaning the GPS data can be collected and stored at a 1 sec time interval). For increased accuracy, the WAAS feature of the GPS logger was enabled by setting WAAS equal to 1 in the config file of the device (*40*). The accuracy of the EM408 receiver is 5 m 2DRMS (twice the distance root mean

square) when the WAAS feature is enabled (*41*). The antennas for both the Trimble® DSM232 and GeoChron GPS Logger® were fixed using magnetic mounts on top of the instrumented vehicle.

Figure 43. GeoChron GPS Logger®

The instrumented vehicle was driven while tracking the lane center line (the center of the travel lane) as accurately as possible, and GPS data were collected (at short intervals) as the vehicle traveled on the roadways. Six travel runs of data collection were made through each direction of the roadway segments. For each direction, three runs of data collection were performed setting the DSM232 to the beacon feature, and three runs were conducted setting the DSM232 to the WAAS feature. Simultaneously, the GeoChron GPS Logger® was used, as well. A standard cigarette lighter power adapter provided battery power to the GeoChron. GPS data for each run collected with the DSM232 were sent and stored in the Dewetron DEWE5000 data acquisition system with a unique file name representing the name of the highway, the direction of travel, the number of the run, and the GPS positioning method (beacon or WAAS). Unlike the

DSM232, the GeoChron didn't have the capability of selecting the file names; therefore, it automatically stored the data in its own memory using default file names. A paper diary was kept during the data collection to record any additional trip information that might be used later in the data post-processing and analysis step. In the paper diary, the posted speed limits, travel lane widths, and lateral distances were recorded for each segment of the roadway. The instrumented vehicle was also equipped with a black-and-white video camera to continuously capture the forward view in front of the vehicle. Video data were collected in unison with the horizontal and vertical GPS data. A video feed relayed the video data directly into the data acquisition system. Table 11 summarizes the data collection runs.

Table 11. Data collection runs

Highway Segments		**GPS Receivers**	
		Trimble® DSM232	**GeoChron Logger®***
FM 166	Westbound	3 runs in Beacon	3 runs
	Eastbound	3 runs in WAAS	3 runs
FM 159	Southbound	3 runs in Beacon	3 runs
	Northbound	3 runs in WAAS	3 runs
FM 390	Westbound	3 runs in Beacon	3 runs
	Eastbound	3 runs in WAAS	3 runs

*The DSM232 collected GPS data in the beacon or WAAS mode simultaneously with the GeoChron

DATA POST-PROCESSING AND REDUCTION

After completing the field data collection, the DEWESoft™ software package (version 6.5.1) was used to view the synchronized GPS data that were collected with the DSM232 and the video data. Figure 44 shows an interface of the DEWESoft program.

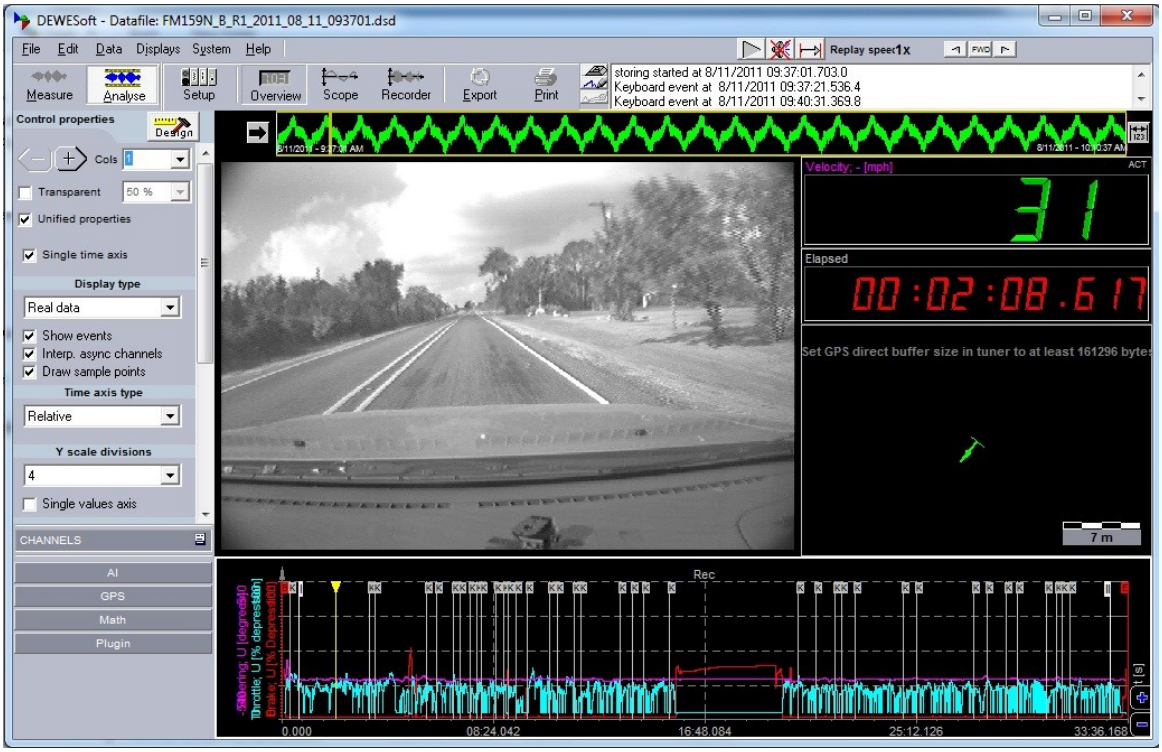

Figure 44. Interface of DEWESoft program

Since DEWESoft is an acquisition package, the acquired data must be exported to other post-processing packages for analysis. This software supports a wide variety of popular formats and makes data files transportable to be imported into any analysis program. The following procedure was performed for each run of the collected data in

order to export the corresponding data into other packages, like Microsoft Excel, during the data post-processing step:

1. The export data properties were set by defining the type of data required to be used (the whole data set or part of it) and determining the time axis (absolute or relative).
2. The channels (variables) longitude, latitude, and altitude (Z) were selected from a displayed channel list among all the various variables.
3. Microsoft Excel was selected from an export option list as the format of data export.
4. After all the settings were defined, the Export Data button was clicked to export the data into Microsoft Excel format.

Figure 45 shows the Export window of the DEWESoft program.

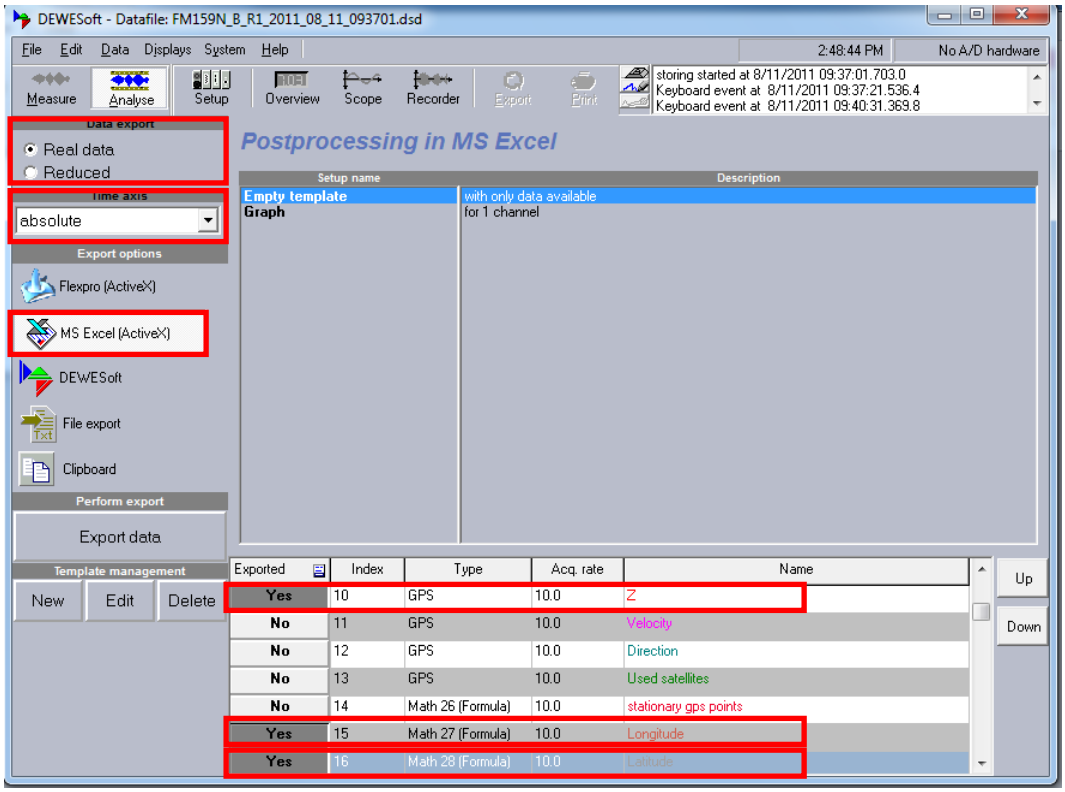

Figure 45. Export window of DEWESoft program

The synchronized data from the DEWESoft program were reduced and exported into spreadsheets that contained all recorded data over the duration of the recording. A separate column containing time was automatically added to the selected variables in the final MS Excel files. Each final file, corresponding to a data collection run, contained multiple worksheets in its raw format--DataInfo, Events, Results--and one or more data worksheets (see Figure 46). The data worksheet(s) included data points for four variables: time, Z, longitude, and latitude (the time variable was not in the channel list as a possible variable, so it was added to the Excel files automatically).

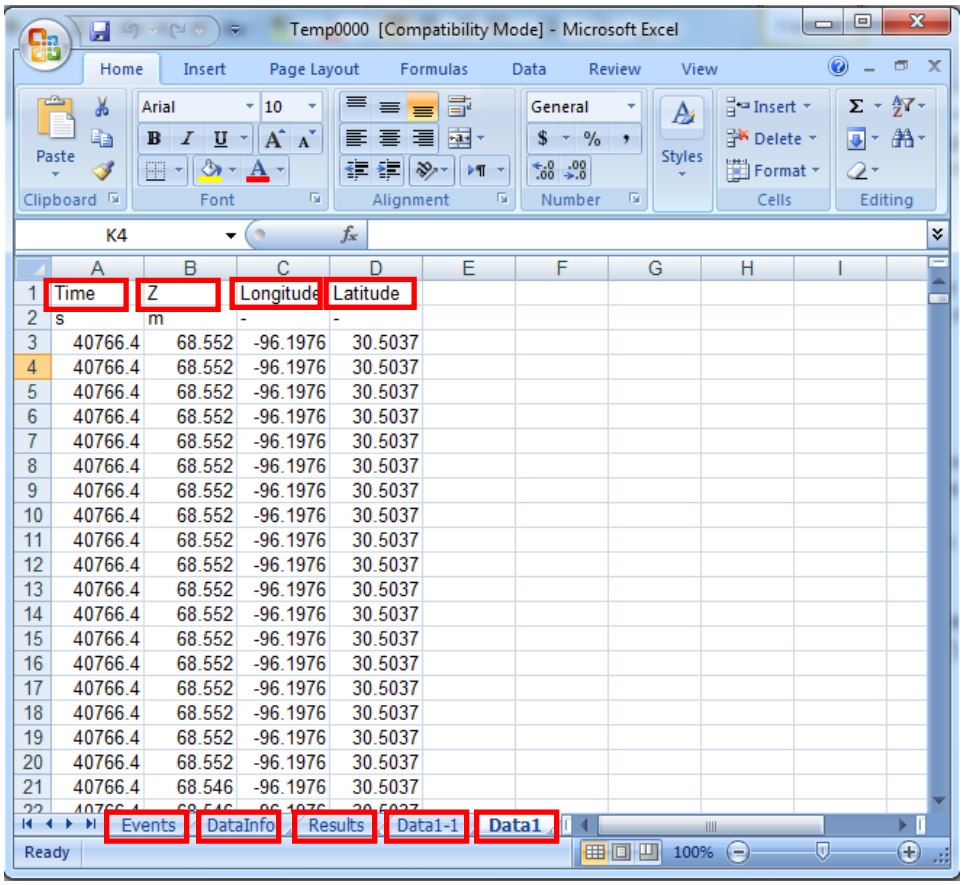

Figure 46. Raw data exported from DEWESoft

The DEWESoft program splits data into multiple data worksheets within an Excel workbook when there are large amounts of data because the DEWESoft MS Excel export function was designed for Microsoft Office 2003 (the maximum worksheet size in Microsoft Excel 2003 is 65,536 rows by 256 columns). For example, the sample exported file in Figure 46 contains two data worksheets since the data include more than 65,536 GPS data points.

To prepare the input file for the NPZ computer program, the Events, DataInfo, and Results worksheets were removed from each MS Excel file, and the Data1 and

Data1-1 worksheets were merged. Furthermore, the columns containing the time variable were removed from each file and the rest of the columns were organized with longitude first, latitude second, and Z third. The files were saved in CSV format with the data starting from the first row (without any labels for the columns).

After retrieving the GPS raw data, three runs were rejected because their data were corrupted: FM 166 eastbound (run 3 of data collection in the beacon mode), FM 166 westbound (run 1 of data collection in the WAAS mode), and FM 159 southbound (run 3 of data collection in the beacon mode).

The data stored in the GeoChron GPS Logger® were also downloaded on the computer. The raw data were saved automatically in a text document file in the format of NMEA-0183. Each collected GPS point in the stored files consisted of three NMEA sentences (RMC, GGA, and GSA). The first word of each sentence, called a *data type*, defines the interpretation of the rest of the sentence (see Figure 47). Each data type has its own unique interpretation in the NMEA standard. The format and description of each NMEA sentence is described in the Appendix.

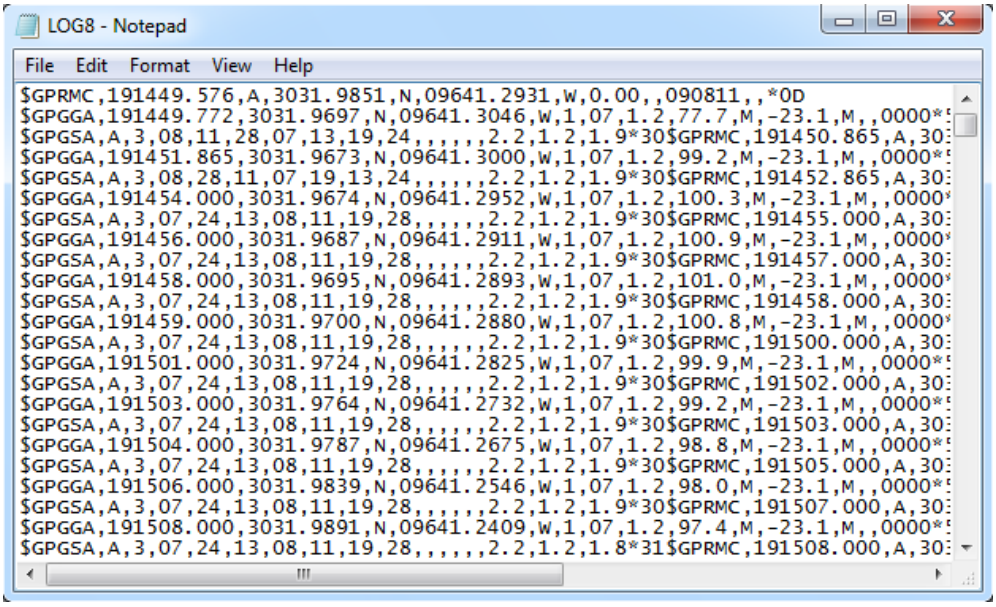

Figure 47. Raw data stored in the GeoChron GPS Logger®

Among RMC, GGA, and GSA, the GSA sentence provides PDOP values of the GPS data points, and the GGA sentence contains longitude, latitude, and altitude. In order to prepare the input file for the NPZ program, the RMC and GSA sentences were first removed from each text document file since the input file must include longitude, latitude, and altitude. Then, from each GGA sentence, redundant variables were removed, and the information related to each data point was sorted in the order of longitude, latitude, and altitude. The files were saved in CSV format with the data starting from the first row (without any labels for the columns). Finally, raw data were converted to the format of longitudes and latitudes. NMEA sentences provide the longitudes and latitudes in degrees-minutes. Therefore, the longitudes and latitudes were converted from degrees-minutes to the decimal degrees required for the NPZ computer program.

After retrieving the GPS raw data collected using GeoChron, two runs were rejected because their data were corrupted: FM 166 eastbound (run 3) and FM 166 westbound (run 4). The results of the NPZ program will be verified in the next chapter.

CHAPTER VI

RESULTS AND MODEL VALIDATION

This part of the study focused on a field evaluation of the result of the developed model, which included a comparison of the calculated no-passing zone results with the actual no-passing zone markings in the field at the study sites. Furthermore, the differences between the calculated no-passing zones and also the differences with the existing field no-passing zones are determined by using mathematical measurements.

The locations of the existing no-passing zones were recorded by the TTI fleet vehicles equipped with DMIs traveling to the field. The Texas A&M Transportation Institute has Ford Taurus sedans equipped with Nitestar NS-50 DMIs manufactured by Nu-Metrics, Inc. Each DMI receives its power and data input from the vehicle's transmission. It measures the number of shaft rotations in the vehicle by monitoring the number of electronic pulses received from the DMI sensors attached to the vehicle's transmission. Each drive shaft rotation is converted into distance traveled as a function of the differential gear ratio and tire diameter. According to the DMI specifications sheet, the accuracy of DMI is up to +/-1 ft per mi.

Figure 48. Nu-Metrics Nitestar Distance Measuring Instrument (DMI)

Before the experiments, the DMIs were calibrated following the manufacturer's standard calibrating procedure (*42*). The calibrations were performed at unused runways of a retired airbase that now serves as the Texas A&M Riverside Campus in Bryan (runways 17C and 35C in Figure 49) by traveling a known distance and correlating that distance with the number of pulses recorded.

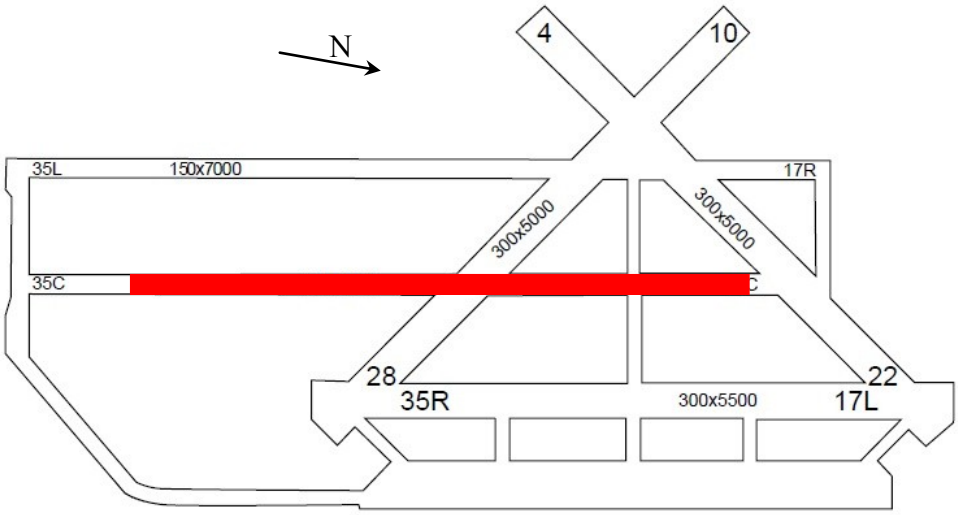

Figure 49. Runway configuration at Texas A&M Riverside Campus and DMI calibration

Field trips were made to record the locations of the existing no-passing zones. The DMI was set to zero at the beginning of each direction of the segments. Then, the sedan was driven along the segments to collect the data. The Nitestar NS-50 DMI shows the data including the measured distance and the speed, but it does not have the capability to save the data. Therefore, the beginning and ending of solid lines, determined by reading the values from the DMI while the vehicle was passing through them, were recorded in the paper diary.

The data were collected for each direction of the highway segments two times, each time using a different sedan equipped with a DMI to achieve the highest level of accuracy and eliminate human errors in reading and recording the data. The beginning and ending of each no-passing zone were calculated by taking the average of the two values collected in each field trip. The horizontal curves, vertical crest curves, railroad grade crossings (RR Xing), underpasses, and intersections or road junctions (JCT) were recorded for each direction of the study segments by watching the videos recorded during the data collection. The locations of the existing no-passing zones were also verified through video analyses in the DEWESoft program.

The summary statistics of the existing no-passing zones for Farm-to-Market Road 166, westbound and eastbound, are illustrated in Tables 12 and 13, respectively. The information presented in the tables is based on visual observation and may not be accurate.

Table 12. Summary statistics for horizontal and crest vertical curves on FM 166 westbound

NPZs, RR Xings, JCTs, and Underpasses	Horizontal Curves	Crest Vertical Curves
NPZ 0	due to the intersection at the beginning of the segment	
NPZ 1	1 (right curve)	0
NPZ 2	5 (2 right curves, 3 left curves)	0
NPZ 3	1 (left curve)	1
NPZ 4	3 (2 right curves, 1 left curve)	0
T-Junction	1 (right curve)	-
NPZ 4	5 (2 right curves, 3 left curves)	0
NPZ 5	0	1
NPZ 6	7 (3 right curves, 4 left curves)	0
NPZ 7	0	1
NPZ 8	3 (1 right curve, 2 left curves)	1
NPZ 9	6 (3 right curves, 3 left curves)	1
NPZ 10	2 (1 right curve, 1 left curve)	0
NPZ 11	3 (2 right curves, 1 left curve)	1
NPZ 12	9 (4 right curves, 5 left curves)	4
NPZ 13	2 (1 right curve, 1 left curve)	0
One-Lane Underpass	-	-
NPZ 13	1 (left curve)	0

Table 13 presents the summary statistics of the existing no-passing zones for the eastbound direction of this segment.

Table 13. Summary statistics for horizontal and crest vertical curves on FM 166 eastbound

NPZs, RR Xings, JCTs, and Underpasses	Horizontal Curves	Crest Vertical Curves
NPZ 1	2 (right curves)	0
One-Lane Underpass	-	-
NPZ 1	1 (left curve)	0
NPZ 2	1 (right curve)	0
-	1 (left curve)	0
NPZ 3	7 (4 right curves, 3 left curves)	5
NPZ 4	3 (1 right curve, 2 left curves)	0
NPZ 5	9 (4 right curves, 5 left curves)	4
NPZ 6	1 (right curve)	0
NPZ 7	6 (3 right curves, 3 left curves)	1
NPZ 8	1 (right curve)	0
NPZ 9	6 (3 right curves, 3 left curves)	0
T-Junction	1(left curve)	-
NPZ 9	2 (1 right curve, 1 left curve)	0
NPZ 10	1 (right curve)	0
NPZ 11	6 (4 right curves, 2 left curves)	0
NPZ 12	1 (left curve)	0
NPZ 13	due to the intersection at the end of the segment	

The summary statistics of the existing no-passing zones for Farm-to-Market Road 159, southbound and northbound, are illustrated in Tables 14 and 15, respectively.

Table 14. Summary statistics for horizontal and crest vertical curves on FM 159 southbound

NPZs, RR Xings, JCTs, and Underpasses	Horizontal Curves	Crest Vertical Curves
NPZ 1	6 (3 right curves, 3 left curves)	3
NPZ 2	3 (2 right curves, 1 left curve)	0
Junction	-	-
RR Xing	-	-
NPZ 2	1 (right curve)	0
NPZ 3	1 (left curve)	0
NPZ 4	0	1
NPZ 5	0	1
NPZ 6	0	1
NPZ 7	0	1
NPZ 8	1 (right curve)	2
NPZ 9	1 (right curve)	1
NPZ 10	2 (1 right curve, 1 left curve)	0
NPZ 11	0	1
RR Xing	-	-
NPZ 12	1 (left curve)	0
NPZ 13	2 (1 right curve, 1 left curve)	0
NPZ 14	1 (left curve)	0
-	1 (left curve)	0
NPZ 15	1 (right curve)	0
NPZ 16	1 (right curve)	0
NPZ 17	1 (right curve)	0
NPZ 18	0	1
NPZ 19	1 (right curve)	0
NPZ 20	due to the intersection at the end of the segment	

Table 15. Summary statistics for horizontal and crest vertical curves on FM 159 northbound

NPZs, RR Xings, JCTs, and Underpasses	Horizontal Curves	Crest Vertical Curves
NPZ 0	due to the intersection at the beginning of the segment	
NPZ 1	2 (left curves)	0
NPZ 2	1 (left curve)	0
NPZ 3	1 (left curve)	0
-	2 (1 right curve, 1 left curve)	0
NPZ 4	1 (left curve)	0
NPZ 5	1 (right curve)	0
NPZ 6	1 (right curve)	0
NPZ 7	3 (1 right curve, 2 left curves)	0
NPZ 8	1 (right curve)	0
RR Xing	-	-
NPZ 9	0	1
NPZ 10	0	1
NPZ 11	2 (1 right curve, 1 left curve)	0
NPZ 12	1 (left curve)	1
NPZ 13	2 (left curves)	2
NPZ 14	0	1
NPZ 15	1 (right curve)	1
NPZ 16	0	1
NPZ 17	0	1
NPZ 18	1 (right curve)	0
NPZ 19	1 (left curve)	0
RR Xing	-	-
Junction	-	-
NPZ 19	3 (1 right curve, 2 left curves)	1
NPZ 20	1 (right curve)	0
NPZ 21	4 (2 right curves, 2 left curves)	0
NPZ 22	due to the intersection at the end of the segment	

The summary statistics of the existing no-passing zones for Farm-to-Market Road 390, westbound and eastbound, are illustrated in Tables 16 and 17, respectively.

Table 16. Summary statistics for horizontal and crest vertical curves on FM 390 westbound

NPZs, RR Xings, JCTs, and Underpasses	Horizontal Curves	Crest Vertical Curves
NPZ 1	3 (1 right curve, 2 left curves)	1
NPZ 2	1 (right curve)	1
NPZ 3	1 (left curve)	3
NPZ 4	7 (4 right curves, 3 left curves)	6
NPZ 5	0	2
NPZ 6	3 (1 right curve, 2 left curves)	2
NPZ 7	1 (right curve)	1
NPZ 8	1 (left curve)	1
NPZ 9	0	1
Junction	-	1
NPZ 10	0	1
NPZ 11	3 (1 right curve, 2 left)	1
One-Lane Underpass	-	-
NPZ 11	13 (5 right curves, 8 left curves)	7
NPZ 12	0	2
Junction	-	-
NPZ 13	2 (1 right curve, 1 left curves)	2
NPZ 14	0	1
NPZ 15	0	1
NPZ 16	5 (2 right curves, 3 left curves)	2

Table 17. Summary statistics for horizontal and crest vertical curves on FM 390 eastbound

NPZs, RR Xings, JCTs, and Underpasses	Horizontal Curves	Crest Vertical Curves
NPZ 1	5 (3 right curves, 2 left curves)	5
NPZ 2	0	1
NPZ 3	0	1
NPZ 4	2 (1 right, 1 left)	1
NPZ 5	0	0
Junction	-	-
NPZ 5	0	4
NPZ 6	10 (6 right curves, 4 left curves)	10
One-Lane Underpass	-	-
NPZ 6	2 (1 right curve, 1 left curve)	1
NPZ 7	0	1
Junction	-	-
NPZ 7	0	0
NPZ 8	0	1
NPZ 9	1 (right curve)	1
NPZ 10	1 (left curve)	1
NPZ 11	3 (2 right curves, 1 left curve)	2
NPZ 12	2 (1 right curve, 1 left curve)	2
NPZ 13	0	0
Junction	-	-
NPZ 13	3 (2 right curves, 1 left curve)	4
-	1 (right curve)	0
NPZ 14	3 (1 right curve, 2 left curves)	3
NPZ 15	2 (1 right curve, 1 left curve)	4
NPZ 16	0	1
-	1 (left curve)	0
NPZ 17	3 (2 right curves, 1 left curve)	3

COMPARISON STUDY

As it was discussed earlier in chapter II, the geometry of satellites in the sky affects the accuracy of GPS data points. To check the quality of satellite geometry for collected data, the PDOP values were extracted from the GSA NMEA sentence that had been downloaded from the GeoChron GPS Logger. Table 18 lists the maximum and the average PDOP values for all the data collection runs. As the table shows, the average values of PDOP are less than 2.4, indicating the high probability of positional accuracy of the GPS data points.

After the NPZ program was run for each data set, the program calculated the lengths and the locations of no-passing zones, and the results were stored in separate files. To visually compare the no-passing zones that are calculated by the program with the existing no-passing zones, whose information was collected during site visits, the no-passing zones were displayed on a series of plots.

Table 18. PDOP Values for different runs of data collection

Roadway Direction	Data Collection Runs		PDOP	
			Maximum	Average
FM 166 WB	Beacon, Run 1	GeoChron, Run 1	4.6	2.0
	Beacon, Run 2	GeoChron, Run 2	2.6	1.5
	Beacon, Run 3	GeoChron, Run 3	2.7	1.6
	WAAS, Run 2	GeoChron, Run 5	2.2	1.5
	WAAS, Run 3	GeoChron, Run 6	1.7	1.4
FM 166 EB	Beacon, Run 1	GeoChron, Run 1	2.2	1.8
	Beacon, Run 2	GeoChron, Run 2	1.9	1.5
	WAAS, Run 1	GeoChron, Run 4	3.0	1.9
	WAAS, Run 2	GeoChron, Run 5	1.9	1.4
	WAAS, Run 3	GeoChron, Run 6	1.7	1.5
FM 159 SB	Beacon, Run 1	GeoChron, Run 1	2.2	1.5
	Beacon, Run 2	GeoChron, Run 2	2.9	1.9
	-	GeoChron, Run 3	1.9	1.5
	WAAS, Run 1	GeoChron, Run 4	3.2	2.4
	WAAS, Run 2	GeoChron, Run 5	2.1	1.7
	WAAS, Run 3	GeoChron, Run 6	2.2	1.8
FM 159 NB	Beacon, Run 1	GeoChron, Run 1	4.0	1.7
	Beacon, Run 2	GeoChron, Run 2	2.6	1.6
	Beacon, Run 3	GeoChron, Run 3	2.3	1.5
	WAAS, Run 1	GeoChron, Run 4	3.4	2.2
	WAAS, Run 2	GeoChron, Run 5	2.2	1.8
	WAAS, Run 3	GeoChron, Run 6	1.9	1.7
FM 390 WB	Beacon, Run 1	GeoChron, Run 1	9.5	1.6
	Beacon, Run 2	GeoChron, Run 2	2.2	1.8
	Beacon, Run 3	GeoChron, Run 3	1.9	1.5
	WAAS, Run 1	GeoChron, Run 4	3.1	1.6
	WAAS, Run 2	GeoChron, Run 5	5.1	1.8
	WAAS, Run 3	GeoChron, Run 6	2.5	1.5
FM 390 EB	Beacon, Run 1	GeoChron, Run 1	2.7	2.0
	Beacon, Run 2	GeoChron, Run 2	4.0	1.6
	Beacon, Run 3	GeoChron, Run 3	1.7	1.5
	WAAS, Run 1	GeoChron, Run 4	2.4	1.8
	WAAS, Run 2	GeoChron, Run 5	3.3	1.7
	WAAS, Run 3	GeoChron, Run 6	1.9	1.4

Farm-to-Market Road 166 - Westbound

Figure 50 shows the calculated no-passing zones in the westbound direction of Farm-to-Market Road 166 for different runs of data collection using DSM232's beacon mode. The figure also shows the existing no-passing zones (field) for the westbound direction. The lines represent no-passing zones. For the first three runs (Run 1, Run 2, and Run 3), the data were collected by traveling westbound. In the figure, "Run 1 (Opp. Dir.)" and "Run 2 (Opp. Dir.)" mean that the original data have been collected by traveling opposite of the study direction (i.e. the data collected by traveling eastbound) and then, the data points were reversed, so that the last eastbound value became the first westbound value. The figure does not illustrate any result for Run 3 (Opp. Dir.) since the GPS raw data collected in run 3 of FM 166 eastbound data collection (beacon mode) were rejected after the GPS raw data had been retrieved (as it was described in Chapter V).

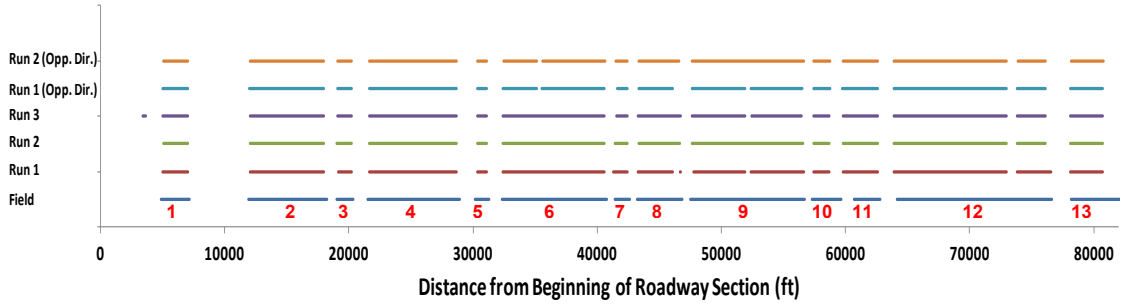

Figure 50. Farm-to-Market 166 westbound (DSM232--beacon mode), existing and calculated no-passing zones

Figure 51 and Figure 52 show the calculated no-passing zones in the westbound direction of Farm-to-Market Road 166 for different runs of data collection using DSM232's WAAS mode and GeoChron, respectively. The figures also illustrate the existing no-passing zones (field).

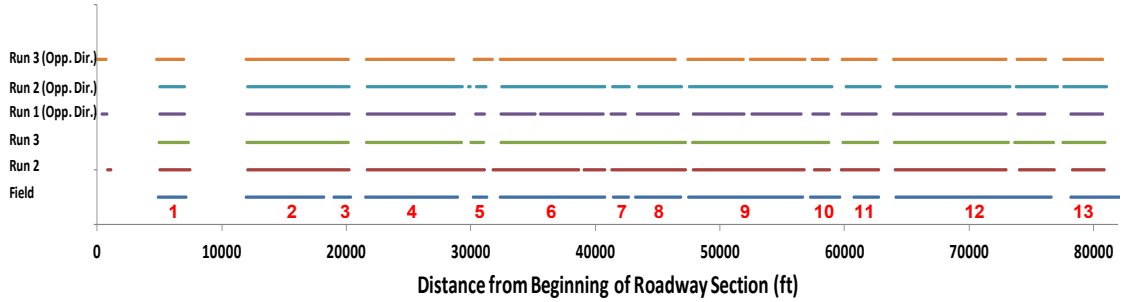

Figure 51. Farm-to-Market 166 westbound (DSM232--WAAS mode), existing and calculated no-passing zones

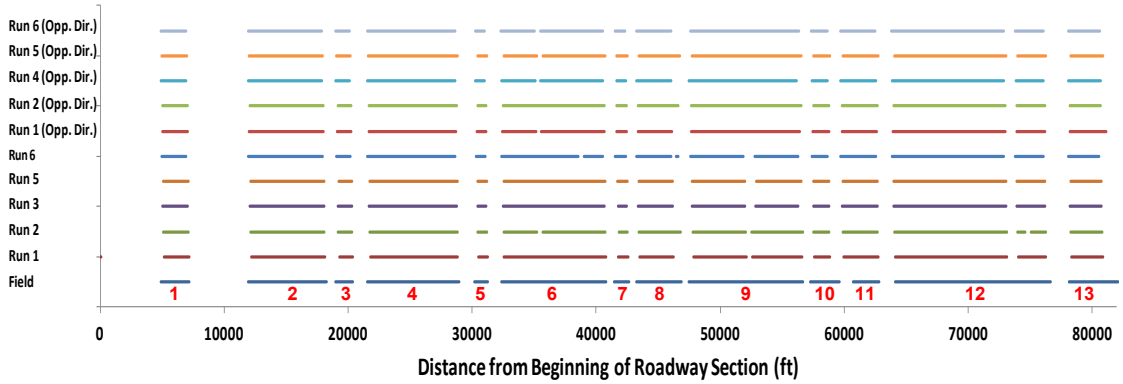

Figure 52. Farm-to-Market 166 westbound (GeoChron), existing and calculated no-passing zones

Discussion

1) A majority of the existing field no-passing zones match with the output of the program. However, the figures show that for some portions of the roadway, the results of the program show multiple no-passing zones while there is one continuous no-passing zone in the field. To validate the output of the program, the distances between the short no-passing zones were calculated and confirmed to be no shorter than 400 ft. It means that the adjacent no-passing zones that are located close to each other were connected in the field, even if they were more than 400 ft apart.
2) Comparing those Figures 51 and 52 with Figure 50, there is less variability in the results of different data collection runs using DSM232's beacon mode. Figure 52 shows the clear compatibility of the no-passing zones between the field and the output of the developed program.

Farm-to-Market Road 166 - Eastbound

Figure 53 and Figure 54 compare the calculated and existing no-passing zones in the eastbound direction of Farm-to-Market Road 166 using DSM232's beacon and WAAS modes, respectively.

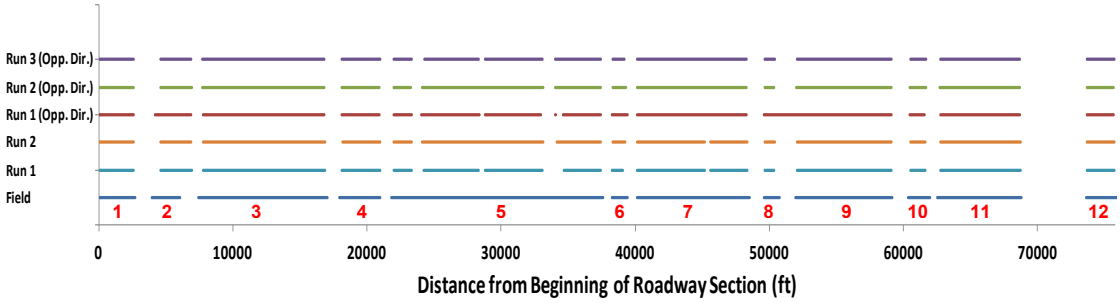

Figure 53. Farm-to-Market 166 eastbound (DSM232--beacon mode), existing and calculated no-passing zones

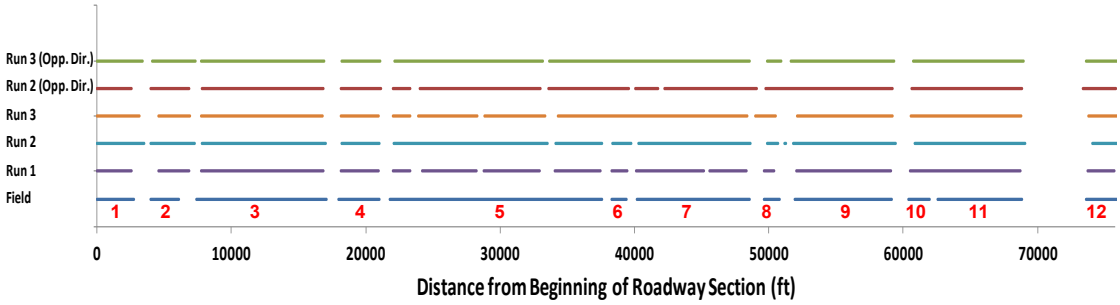

Figure 54. Farm-to-Market 166 eastbound (DSM232--WAAS mode), existing and calculated no-passing zones

Figure 55 shows the calculated no-passing zones along with the existing no-passing zones for the data collected on Farm-to-Market Road 166 in the eastbound direction using GeoChron.

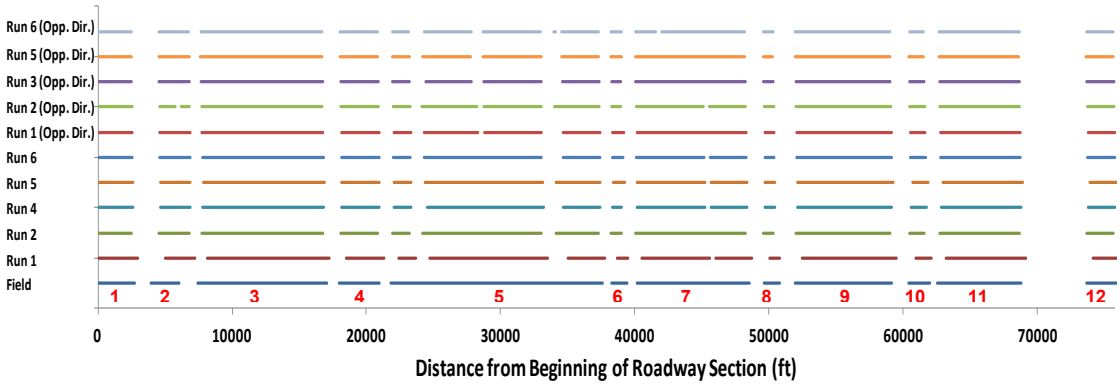

Figure 55. Farm-to-Market 166 eastbound (GeoChron), existing and calculated no-passing zones

Discussion

As illustrated in the figures, the outputs of the program are matching with the existing field no-passing zones in almost all cases, with minor negligible differences.

Farm-to-Market Road 159 - Southbound

The calculated no-passing zones along with the existing no-passing zones for the data collected on Farm-to-Market Road 159 in the southbound direction using DSM232's beacon mode, DSM232's WAAS mode, and GeoChron are illustrated in Figures 56, 57, and 58, respectively.

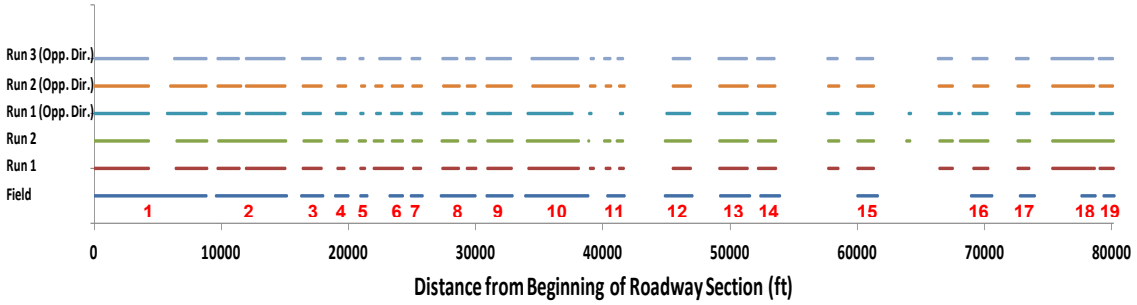

Figure 56. Farm-to-Market 159 southbound (DSM232--Beacon mode), existing and calculated no-passing zones

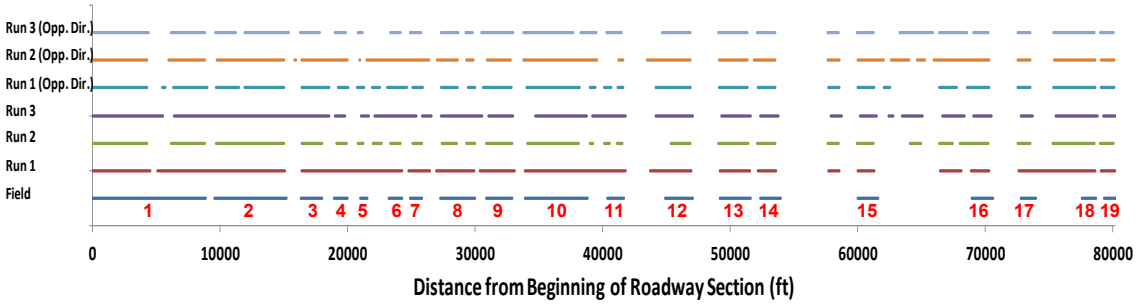

Figure 57. Farm-to-Market 159 southbound (DSM232--WAAS mode), existing and calculated no-passing zones

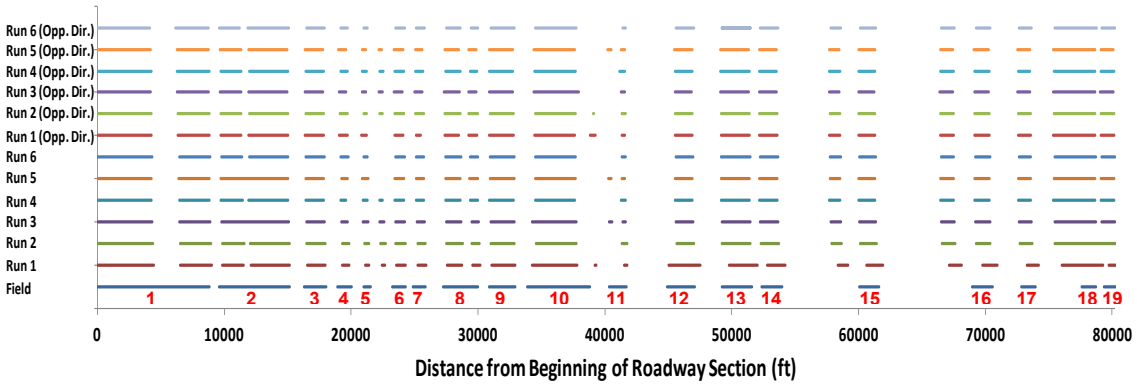

Figure 58. Farm-to-Market 159 southbound (GeoChron), existing and calculated no-passing zones

Discussion

1) In the Figures 56 to 58, the second existing field no-passing zone is a continuous zone. However, the program calculated more than one no-passing zone corresponding to this zone for each run of the data collection. The author further investigated this specific case and found that there are a junction and a railroad crossing in that segment of the roadway (see Table 14). During the field observation, the existing solid lines before and after the junction and the railroad crossing were considered to be connected, and the existing no-passing zone was recorded continuously. Therefore, the NPZ program made the correct calculation based solely on that input data.
2) Furthermore, the NPZ program calculated a no-passing zone between the fourteenth and fifteenth existing field no-passing zones. The field observation (Table 14) showed that there is at least one horizontal curve in that location, although no solid line is marked on the pavement. This means the NPZ program correctly calculated the no-passing zone for this segment of the roadway.

Farm-to-Market Road 159 - Northbound

Figures 59 to 61 present the results of the NPZ program for the data collected on Farm-to-Market Road 159 in the northbound direction using DSM232's beacon mode, DSM232's WAAS mode, and GeoChron, respectively.

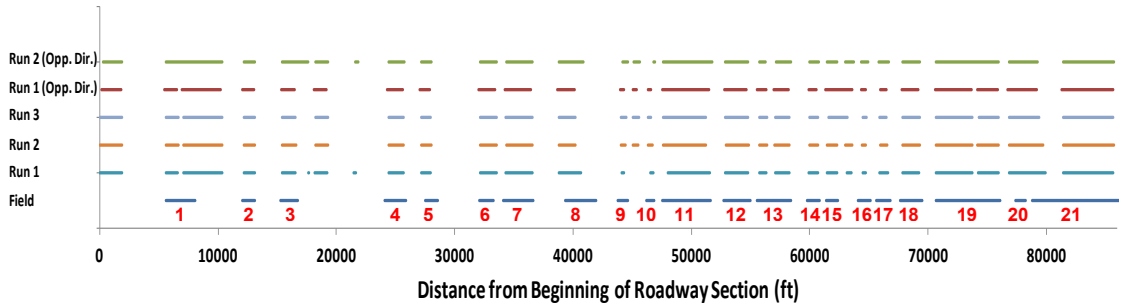

Figure 59. Farm-to-Market 159 northbound (DSM232--Beacon mode), existing and calculated no-passing zones

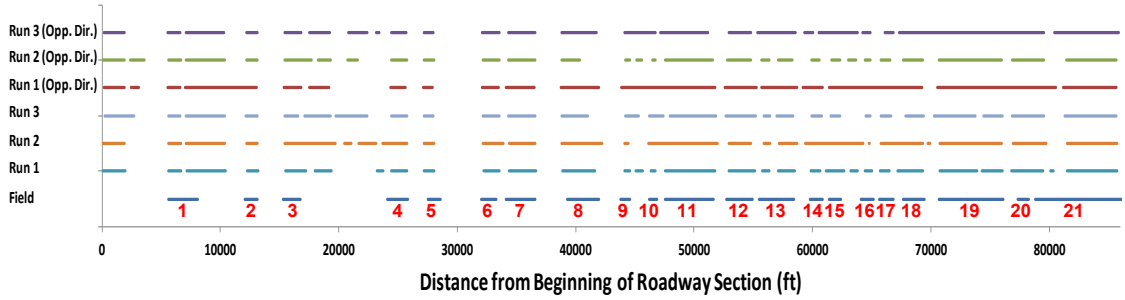

Figure 60. Farm-to-Market 159 northbound (DSM232--WAAS mode), existing and calculated no-passing zones

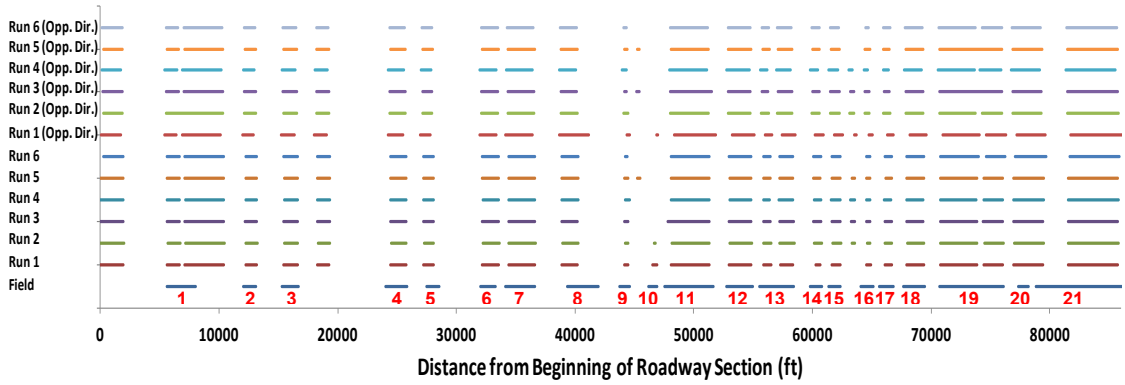

Figure 61. Farm-to-Market 159 northbound (GeoChron), existing and calculated no-passing zones

Discussion

1) The results of the NPZ program for all the data collection runs (Figures 59 to 61) indicate that there is a no-passing zone (due to the roadway alignment) at the beginning of the roadways, however no existing field no-passing zone is present in the graphs corresponding to those calculated ones. Further investigations revealed that Farm-to-Market road 159 (northbound) starts at its intersection with the State Highway 105 with a crest vertical curve. The solid line at the beginning of the roadway was not recorded during the field visit since it was assumed that the pavement markings are due to the existence of the intersection rather than any changes in the roadway alignment. Therefore, the NPZ correctly calculated a no-passing zone for the beginning of this roadway.
2) Also, the figures show that the NPZ program calculated at least one no-passing zone between the third and fourth existing no-passing zones for FM 159 northbound direction. Based on Table 15, there are two horizontal curves in that location; although, no solid lines are marked on the pavement. This means the NPZ program correctly calculated the no-passing zone for this segment of the roadway.
3) Table 15 also shows that there is a railroad crossing after the eighth exiting no-passing zone, and it was observed in the field that the solid line has been extended to the railroad crossing. That is the reason for the corresponding calculated no-passing zones which are shorter compared to the existing one in the field.

Farm-to-Market Road 390 - Westbound

The no-passing zones (existing and calculated) along Farm-to-Market Road 390 westbound are displayed in Figure 62.

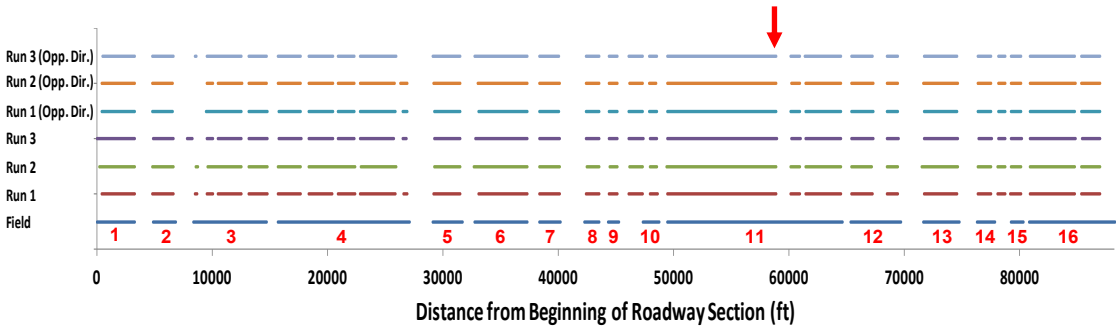

Figure 62. Farm-to-Market 390 westbound (DSM232--beacon mode), existing and calculated no-passing zones

The results for the different runs of data collection in the westbound direction of Farm-to-Market Road 166 using DSM232's WAAS mode and GeoChron are also illustrated in Figure 63 and Figure 64, respectively.

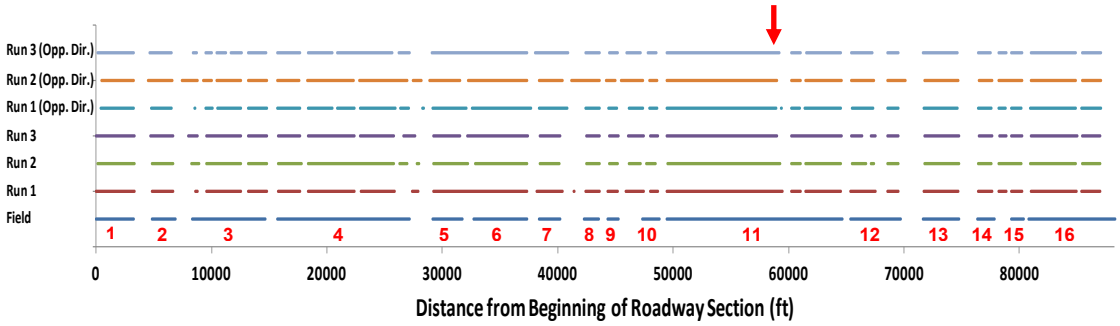

Figure 63. Farm-to-Market 390 westbound (DSM232--WAAS mode), existing and calculated no-passing zones

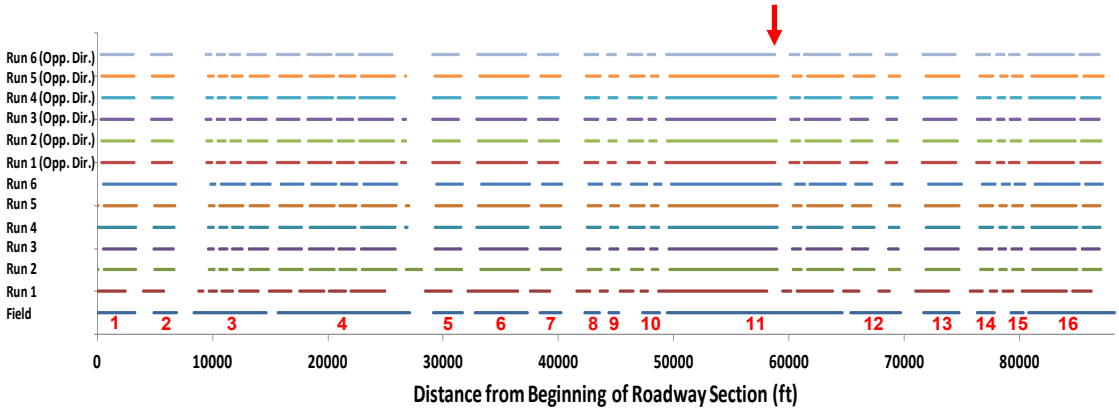

Figure 64. Farm-to-Market 390 westbound (GeoChron), existing and calculated no-passing zones

Discussion

1) There are 16 no-passing zones marked in the field along this direction of the highway. The eleventh existing field no-passing zone is a continuous zone, unlike the corresponding calculated no-passing zone. There is a gap between the two consecutive no-passing zones (showed with a red arrow in the figures), but the gap does not exist in the field. The author studied this case in the field and also intensively reviewed video recorded during the data collection (the results were summarized in Tables 12 to 17), and discovered that there is an underpass along that segment of the roadway between the two individual calculated no-passing zones. That is the reason the no-passing zone is continuously marked in the field along that portion of the roadway.
2) The detailed investigation on the third existing field no-passing zone revealed that the segment includes one horizontal curve and three vertical crest curves. Therefore, it confirms to the results of the program for this section of the

roadway. The program calculated four individual no-passing zones in most of the data collection runs which is the correct approach based on the given data.

3) There are at least two individual no-passing zones corresponding to the twelfth existing no-passing zone in the figures. By analyzing the field observations, it was verified that there are two crest vertical curves located at this section of the roadway. Therefore, the output of the program is correct.
4) The figures show that the NPZ program calculated one no-passing zone between the existing ninth and the tenth no-passing zones for the different data collection runs. However, there is no existing field no-passing zone corresponding to that no-passing zone. The reason is the existing no-passing zones were recorded in the field based on the pavement markings (solid lines). The further study of the field observations confirms that there is a junction with a vertical crest curve in that location of the roadway. Hence, the output no-passing zone of the program was correctly calculated.

Farm-to-Market Road 390 - Eastbound

Figures 65 to 67 present the results of the NPZ program for the data collected on Farm-to-Market Road 390 in the eastbound direction using DSM232's beacon mode, DSM232's WAAS mode, and GeoChron, respectively.

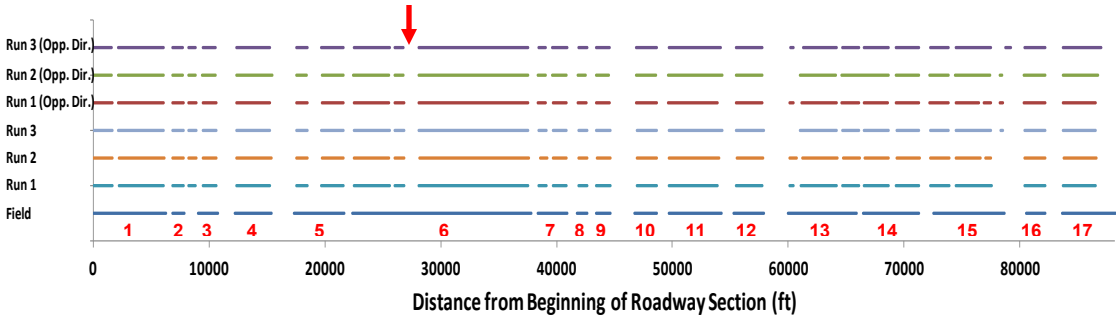

Figure 65. Farm-to-Market 390 eastbound (DSM232--Beacon mode), existing and calculated no-passing zones

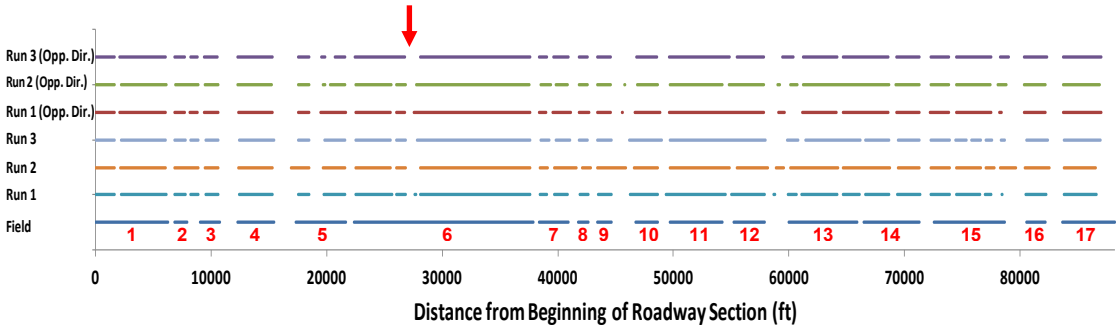

Figure 66. Farm-to-Market 390 eastbound (DSM232--WAAS mode), existing and calculated no-passing zones

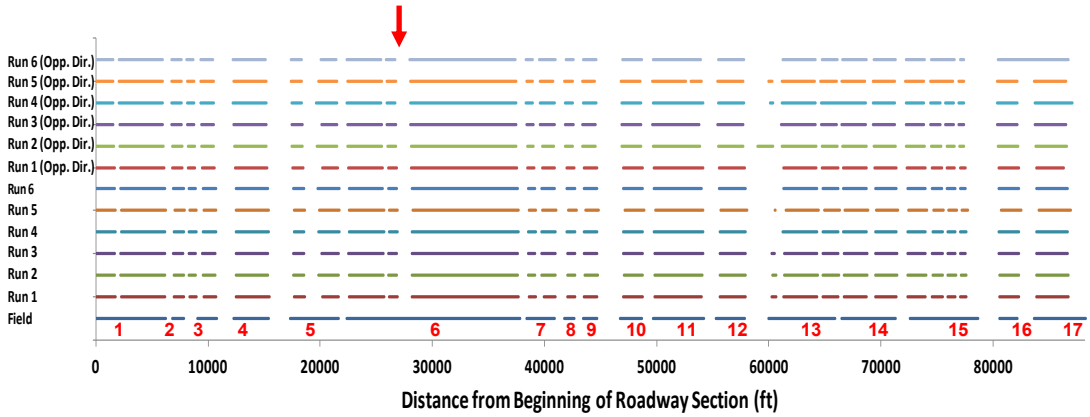

Figure 67. Farm-to-Market 390 eastbound (GeoChron), existing and calculated no-passing zones

Discussion

1) In the Figures 65 to 67, the fifth, seventh, and thirteenth existing no-passing zones are continuous zones. However, the program calculated more than one no-passing zone corresponding to these zones for each run of the data collection. In order to clarify those differences, the author examined the field observations (see Table 17) and discovered that there are junctions in those segments of the roadway. The existing solid lines before and after the junctions were considered to be connected during the field observation, and they were recorded continuously.
2) Furthermore, the sixth existing field no-passing zone is a continuous zone, unlike the corresponding calculated no-passing zones. There is a gap between the two consecutive no-passing zones (showed with a red arrow in the figures), but the gap does not exist in the field. Field observation revealed that there is an underpass along that segment of the roadway between the two individual calculated no-passing zones. That is the reason the no-passing zone is continuously marked in the field along that portion of the roadway.

DIFFERENCE MEASUREMENT ANALYSIS

Two methods were used to evaluate the differences between the calculated no-passing zones and the differences with the existing field no-passing zones: statistical analysis of differences and linear difference analysis.

Statistical Analysis of Differences

In order to compare the accuracy of the GPS receivers and also to verify the ability of the developed model in working with different receivers as data input resources, two methodologies were used: Mean Absolute Percentage Difference (MAPD) and Root Mean Square Difference (RMSD) measurements. For this study, lower values are desirable.

To determine MAPD (Equation 107), the difference between the length of the existing no-passing zone and the length of the corresponding calculated no-passing zone is divided by the length of the existing no-passing zone, again. The absolute value in this calculation is summed for every calculated no-passing zone in time and divided again by the number of calculated no-passing zones, *n*. Multiplying by 100 gives the results as percentage difference.

$$\text{MAPD} = \frac{100\%}{n}\sum_{i=1}^{n}\left|\frac{L\_ENPZ_i - L\_CNPZ_i}{L\_ENPZ_i}\right| \tag{107}$$

L_ENPZ_i denotes the length of the *i*-th existing no-passing zone as measured in the field using DMI, and L_CNPZ_i denotes the length of the *i*-th no-passing zone calculated by the NPZ program.

RMSD is a quadratic scoring rule which measures the average magnitude of the difference. To determine RMSD (Equation 108), the difference between lengths of calculated and corresponding existing no-passing zones are each squared and then averaged. Finally, the square root of the average is taken. The RMSD is sensitive to large differences. Since the differences are squared before they are averaged, the RMSD

results in a relatively large difference. In other words, the squaring process gives disproportionate weight to large differences.

$$RMSD = \sqrt{\frac{\sum_{i=1}^{n} (L\_ENPZ_i - L\_CNPZ_i)^2}{n}} \quad (108)$$

The values of MAPD and RMSD were determined using the output of the program (i.e. the lengths of the calculated no-passing zones for each run of data collection) and the lengths of the existing field no-passing zones. It was discussed earlier in this chapter that the beginning and ending of solid lines in the field were determined using the DMI, and the existing locations of the no-passing zones were recorded. When examining the results of the NPZ program, the calculated no-passing zones for some segments of the roadways include several no-passing zones that when grouped together resemble more closely the existing field markings for the no-passing zones. In other words, the length of the grouped calculated no-passing zones might be roughly equal to the measured length of one existing no-passing zone. To analyze the data to determine the MAPD and RSMD, the judgment was made by the author to group the no-passing zones where they seemed similar to the existing field no-passing zones in order to address this issue. Tables 19 and 20 list all the MAPD and RSMD values for different runs of the data collection and different GPS devices. Furthermore, the average of the results of different data collection runs was calculated for each GPS device applied in the roadways and listed in the tables.

Table 19. Mean Average Percentage Difference (MAPD) in no-passing zone length calculated for different runs of data collection

		Run 1	Run 2	Run 3	Run 4	Run 5	Run 6	Run 1 (Opp. Dir.)	Run 2 (Opp. Dir.)	Run 3 (Opp. Dir.)	Run 4 (Opp. Dir.)	Run 5 (Opp. Dir.)	Run 6 (Opp. Dir.)	Ave.
FM 166 WB	**Beacon**	16.3%	16.5%	17.2%	-	-	-	19.3%	17.2%	-	-	-	-	17.3%
	WAAS	-	16.3%	9%	-	-	-	15.4%	11.2%	15.1%	-	-	-	13.4%
	GeoChron	19.5%	19%	20.5%	-	19.7%	18.6%	18.5%	18.5%	-	20%	17.5%	19%	19.1%
FM 166 EB	**Beacon**	11.8%	10.4%	-	-	-	-	11.4%	10.1%	10.7%	-	-	-	10.9%
	WAAS	7.5%	16.2%	8.5%	-	-	-	-	7.4%	12%	-	-	-	10.3%
	GeoChron	11.7%	11.8%	-	12%	10.7%	11.3%	11.6%	12.8%	12.7%	-	11.9%	12%	11.8%
FM 159 SB	**Beacon**	31.2%	33.8%	-	-	-	-	32.1%	30.2%	28.5%	-	-	-	31.2%
	WAAS	17.8%	23.4%	42.4%	-	-	-	23.5%	45.5%	23.5%	-	-	-	29.3%
	GeoChron	30.7%	26%	27.7%	32.1%	27.4%	32.5%	33%	32.3%	32.4%	31.5%	28.8%	32.2%	30.6%
FM 159 NB	**Beacon**	28.9%	27.3%	31.4%	-	-	-	34%	27.1%	-	-	-	-	29.7%
	WAAS	23.9%	31.4%	24.9%	-	-	-	12.9%	28.7%	32.7%	-	-	-	25.7%
	GeoChron	30.9%	32%	29.2%	28.6%	29.8%	29.4%	29.6%	28.6%	29.7%	29.2%	29.6%	29.8%	29.7%
FM 390 WB	**Beacon**	13.5%	13%	13.2%	-	-	-	14.3%	14.4%	13.3%	-	-	-	13.6%
	WAAS	12.3%	15.9%	11.6%	-	-	-	15.2%	22.4%	14.3%	-	-	-	15.3%
	GeoChron	16.6%	15.5%	15.4%	13.6%	13.5%	14.9%	15%	14.9%	14.9%	14.7%	14.1%	15%	14.8%
FM 390 EB	**Beacon**	11.1%	11.2%	10.6%	-	-	-	10.7%	10.9%	10.1%	-	-	-	10.8%
	WAAS	11.5%	23.7%	11.7%	-	-	-	9.9%	15.8%	11.2%	-	-	-	13.9%
	GeoChron	11.3%	11%	11.4%	12%	11.1%	11.9%	13.2%	12.9%	12%	11%	10.9%	11.5%	11.7%

Table 20. Root Mean Square Difference (RMSD) in no-passing zone length calculated for different runs of data collection

		Run 1	Run 2	Run 3	Run 4	Run 5	Run 6	Run 1 (Opp. Dir.)	Run 2 (Opp. Dir.)	Run 3 (Opp. Dir.)	Run 4 (Opp. Dir.)	Run 5 (Opp. Dir.)	Run 6 (Opp. Dir.)	Ave.
FM 166 WB	Beacon	579.3	580.2	585.5	-	-	-	628.5	580.7	-	-	-	-	590.8
	WAAS	-	701.9	537.7	-	-	-	603.1	414.1	545.2	-	-	-	560.4
	GeoChron	642.6	609.2	667.5	-	660.9	621	583.3	612.2	-	649	580.8	639.5	626.6
FM 166 EB	Beacon	319.4	307.3	-	-	-	-	359.3	302.4	304.6	-	-	-	318.6
	WAAS	274.4	587.3	313.1	-	-	-	-	401	500.3	-	-	-	415.2
	GeoChron	321.7	325.2	-	330.5	311.2	318.6	325.8	341.6	332.7	-	324.6	335.5	326.7
FM 159 SB	Beacon	643.5	940	-	-	-	-	646.8	628.2	593.3	-	-	-	690.4
	WAAS	422.8	562	898.6	-	-	-	571.5	1119.7	566.1	-	-	-	690.1
	GeoChron	691.7	750.7	673.6	760.4	711.3	745.9	753	744	710.8	732.1	704.3	741.5	726.6
FM 159 NB	Beacon	663	680.2	704.7	-	-	-	735.4	635.1	-	-	-	-	683.7
	WAAS	593.5	970	607.9	-	-	-	319.8	671.8	833.5	-	-	-	666.1
	GeoChron	718.5	721.2	716.6	721.6	732.5	726.9	646.8	727.4	721.8	733.9	730.5	731.3	719.1
FM 390 WB	Beacon	476.2	541.1	529.9	-	-	-	538.6	543.7	544.8	-	-	-	529
	WAAS	577.5	495.7	490.8	-	-	-	498.9	654.8	514.2	-	-	-	538.6
	GeoChron	675.8	653.5	657.4	555.8	553.7	681.6	539	549.7	543.1	614.9	532.1	644	600
FM 390 EB	Beacon	535.9	535.3	528.6	-	-	-	497.7	526.4	449.3	-	-	-	512.2
	WAAS	511.2	692.8	488.5	-	-	-	511.5	507	477	-	-	-	531.3
	GeoChron	538.8	540.9	539.1	586	535.6	600.4	672	605.6	597.1	469.4	538.8	560.6	565.3

Figures 68 and 69 graphically display the average MAPD and RMSD. The values were calculated for each roadway and each GPS receiver.

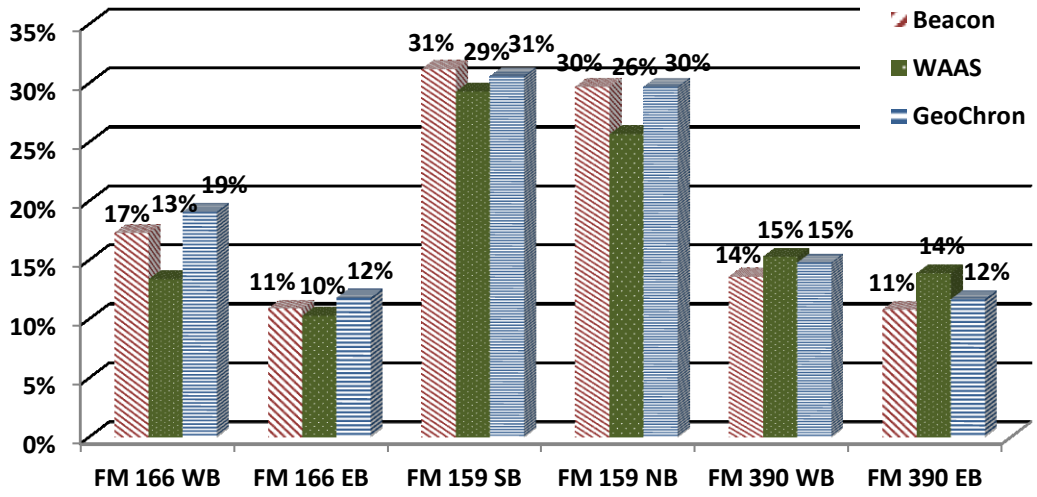

Figure 68. Average MAPD in no-passing zone lengths for different roadways

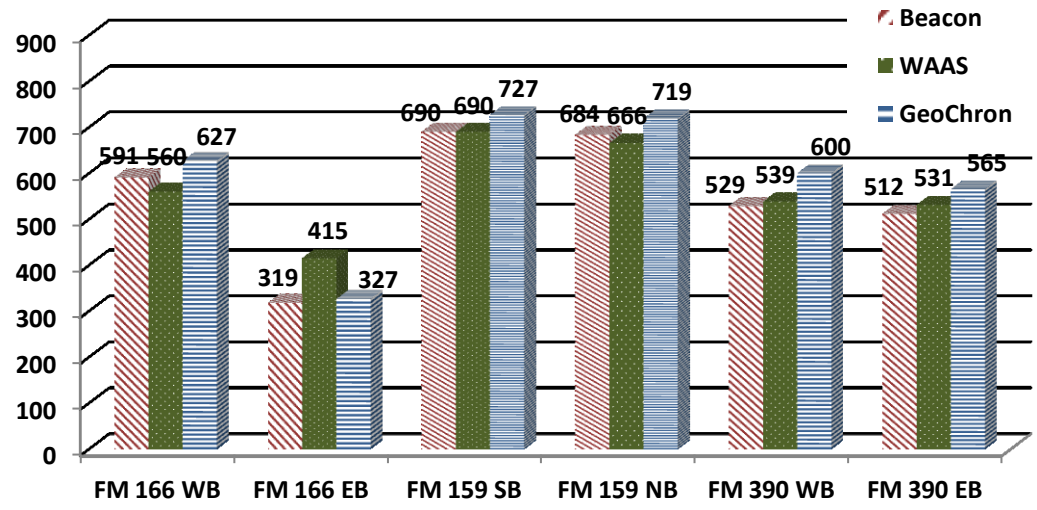

Figure 69. Average RMSD in no-passing zone lengths for different roadways

Figures 68 show that the results of the developed model and the existing field no-passing zones, on average, have low MAPD values in most of the cases. The MAPD for FM 166 and FM 390 is less than 18%. The FM 159 has a maximum of 31% MAPD, which the author suspects it is due to difficulty in accessing GPS satellites. The developed analytical model is highly accurate, provided that its input data and parameters are precise. However, to validate our model, the author had to collect data from various steps/resources that are prone to errors: collected GPS data, existing field no-passing zone markings, human error in collecting the existing field no-passing zones, etc. Considering all of the contributing error producing factors of the process, the author still believes that the results are significant.

Figures 68 and 69 shows that the MAPD and RMSD values calculated for each roadway are in the same range for all the GPS devices used, and they are not far from each other.

The main point that can be seen from Figures 68 and 69 is that the developed model is not biased toward any of these devices. As the figures show, the GeoChron has MAPD values that are close to DSM232 in either Beacon or WASS modes. This may be an interesting observation considering the high price difference of DSM232 and GeoChron, which is advertised to be an important factor in determining the coordinates of location (GeoChron is considerably lower price than DSM232). As it was discussed in the background section of this research, it been noted by Young and Miller (*23*) that the relative accuracy of GPS data points is much greater than what is expected, and the spatial error from successive GPS data is highly correlated (see Figure 10). This, in fact,

confirms the robustness of the developed model because it shows that the model performs fairly consistently with different GPS devices, however, further studies are required to investigate whether the results of the GeoChron is close enough to the results of the DSM232' beacon and WAAS option or not.

The figures also show that the results related to the roadways FM 166 and FM 390 are better than FM 159 in terms of MAPD and RMSD, and one possible reason for this observation is that there might be more difficulties in receiving the signals from the satellite throughout route FM 159. In fact, the data collected by a GPS receiver depends highly on the number of visible GPS satellites. Furthermore, for the case of differential GPS systems, the coverage and the quality of Beacon and WAAS signals in the study location is an important factor.

The MAPD and RMSD are the values measured based on the differences between the existing field no-passing zones and the no-passing zones that are calculated by the developed model. In those calculations, the existing field no-passing zones are treated as the ground truth. This assumption is necessary for having a benchmark for the comparisons. However, throughout this project it was discovered that there are cases that the existing no-passing zones in the field are not marked correctly, as described earlier in the Comparison Study section. This fact was verified by studying the characteristics of the highways (that was later listed in Tables 12 to 17) through field observations and furthermore by intensively reviewing the videos of the data collection. This may be problematic in the verification step, because the output of the program is validated against the existing field no-passing zones. This issue cannot be avoided or

fixed. Additionally, this is not a very common issue, and the author decided to ignore the discrepancies, however, this will be a factor in validating it against the existing no-passing zones that affect the values of MAPD and RSMD.

Linear Difference Analysis

As a second effort to compare and evaluate the differences between the calculated no-passing zones, a method of linear difference analysis was used. To compare the beginnings of no-passing zones with each other and also the ending points with each other, the maximum differences between the beginnings (or ends) are calculated by using the following equations:

$$\text{Maximum Difference for the Beginning Point} = \text{Max}(B\_CNPZ_1, B\_CNPZ_2, B\_CNPZ_3, \ldots, B\_CNPZ_n) - \text{Min}(B\_CNPZ_1, B\_CNPZ_2, B\_CNPZ_3, \ldots, B\_CNPZ_n) \quad (109)$$

$$\text{Maximum Difference for the Ending Point} = \text{Max}(E\_CNPZ_1, E\_CNPZ_2, E\_CNPZ_3, \ldots, E\_CNPZ_n) - \text{Min}(E\_CNPZ_1, E\_CNPZ_2, E\_CNPZ_3, \ldots, E\_CNPZ_n) \quad (110)$$

where B_CNPZ_n and E_CNPZ_n are the beginning and the ending points of the n^{th} calculated no-passing zones, respectively.

In other words, the maximum difference shows the range between the first and the last beginning (ending) points for each calculated no-passing zone. The maximum differences for the calculated no-passing zones (in Beacon mode) for both directions on all three highways were calculated and listed in Tables 21 to 26. Beacon mode was

selected since it appeared to have more accurate data. In the tables, all the values were rounded to the nearest feet.

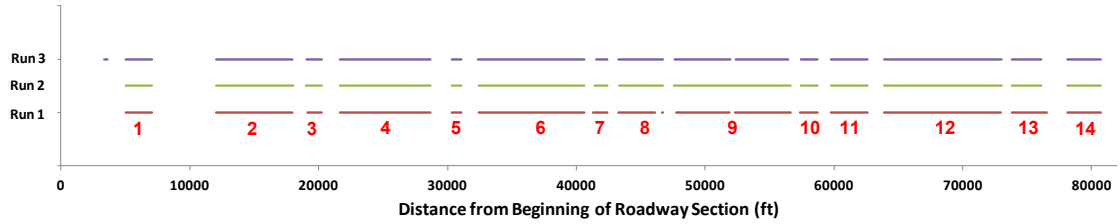

Figure 70. FM 166 westbound (Beacon mode), calculated no-passing zones

Table 21. Calculated no-passing zones for FM 166 westbound (Beacon mode)

Calculated No-Passing Zone	Run 1		Run 2		Run 3		Max Difference	
	Begin (ft)	End (ft)	Begin (ft)	End (ft)	Begin (ft)	End (ft)	Begin (ft)	End (ft)
1	5016	7043	5030	7055	5016	7051	14	12
2	12026	17987	12032	18008	12021	17986	11	22
3	19124	20228	19029	20244	19042	20232	95	16
4	21626	28693	21633	28700	21629	28695	7	7
5	30325	31093	30343	31097	30332	31097	18	4
6	32418	40601	32412	40611	32400	40602	18	10
7	41308	42433	41415	42427	41517	42429	209	6
8	43294	46713	43312	46697	43301	46725	18	28
9	47746	56668	47609	56612	47632	56475	137	193
10	57403	58703	57426	58711	57417	58719	23	16
11	59765	62597	59780	62607	59764	62601	16	10
12	63896	72956	63906	72995	63896	72996	10	40
13	73820	76558	73802	76118	73823	76123	21	440
14	78126	80722	78125	80734	78123	80738	3	16
						Average	43	59
						No. of Outliers (No-Passing Zones > Average)	3	2
						Average w/o Outliers	14	16

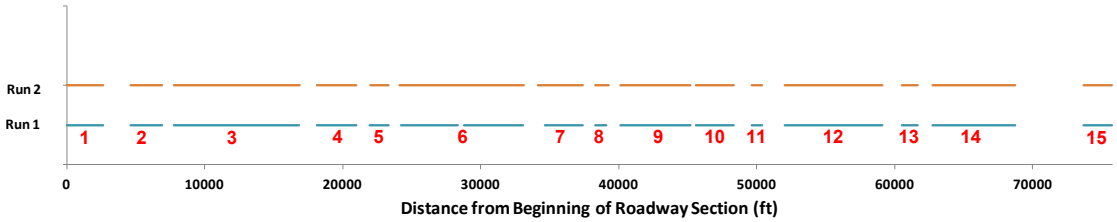

Figure 71. FM 166 eastbound (Beacon mode), calculated no-passing zones

Table 22. Calculated no-passing zones for FM 166 eastbound (Beacon mode)

Calculated No-Passing Zone	Run 1		Run 2		Max Difference	
	Begin (ft)	End (ft)	Begin (ft)	End (ft)	Begin (ft)	End (ft)
1	0	2620	0	2625	0	5
2	4611	6933	4632	6904	21	29
3	7775	16857	7784	16871	9	14
4	18143	20980	18157	20990	14	10
5	21985	23341	22016	23329	31	12
6	24215	33088	24135	33135	80	47
7	34658	37422	34137	37424	521	2
8	38293	39117	38313	39280	20	163
9	40131	45202	40137	45200	6	2
10	45607	48345	45615	48343	8	2
11	49639	50391	49644	50409	5	18
12	52045	59127	52064	59127	19	0
13	60525	61666	60523	61670	2	4
14	62770	68745	62767	68746	3	1
15	73718	75738	73713	75742	5	4
				Average	50	21
				No. of Outliers (No-Passing Zones > Average)	2	3
				Average w/o Outliers	11	6

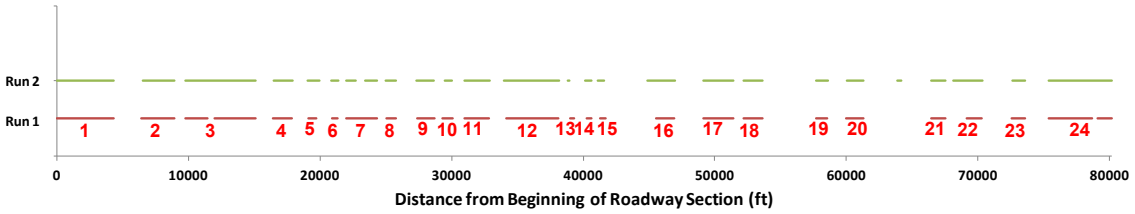

Figure 72. FM 159 southbound (Beacon mode), calculated no-passing zones

Table 23. Calculated no-passing zones for FM 159 southbound (Beacon mode)

Calculated No-Passing Zone	Run 1		Run 2		Max Difference	
	Begin (ft)	End (ft)	Begin (ft)	End (ft)	Begin (ft)	End (ft)
1	0	4308	0	4322	0	14
2	6396	8884	6502	8901	106	17
3	9730	15062	9760	15083	30	21
4	16427	17865	16443	17891	16	26
5	19127	19701	19047	19943	80	242
6	20902	21294	20829	21381	73	87
7	21994	24299	22007	24313	13	14
8	25063	25728	25007	25772	56	44
9	27378	28687	27343	28612	35	75
10	29301	30074	29446	30020	145	54
11	30944	32847	30948	32894	4	47
12	34129	38104	33994	38137	135	33
13	38999	39306	38840	38930	159	376
14	40239	40598	40134	40630	105	32
15	41289	41673	41115	41609	174	64
16	45514	46934	44855	46950	659	16
17	49156	51412	49147	51422	9	10
18	52184	53600	52197	53620	13	20
19	57731	58561	57733	58580	2	19
20	59998	61315	60020	61330	22	15
21	66460	67533	66468	67543	8	10
22	69145	70316	68111	70328	1034	12
23	72585	73570	72605	73609	20	39
24	75374	80166	75370	80179	4	13
				Average	121	54
				No. of Outliers (No-Passing Zones > Average)	6	5
				Average w/o Outliers	33	24

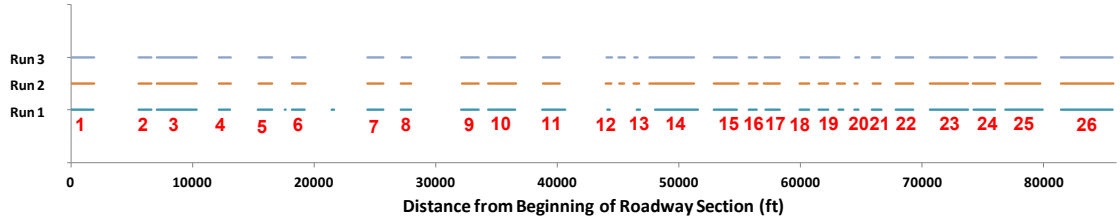

Figure 73. FM 159 northbound (Beacon mode), calculated no-passing zones

Table 24. Calculated no-passing zones for FM 159 northbound (Beacon mode)

Calculated No-Passing Zone	Run 1		Run 2		Run 3		Max Difference	
	Begin (ft)	End (ft)	Begin (ft)	End (ft)	Begin (ft)	End (ft)	Begin (ft)	End (ft)
1	0	1883	0	1898	0	1916	0	33
2	5571	6617	5601	6650	5564	6646	37	33
3	7056	10379	7073	10381	7061	10355	17	26
4	12153	13124	12152	13144	12153	13139	1	20
5	15406	16571	15417	16590	15415	16572	11	19
6	18193	19265	18214	19295	18213	19281	21	30
7	24400	25714	24409	25722	24410	25711	10	11
8	27157	28006	27153	28014	27174	28007	21	8
9	32119	33526	32140	33550	32119	33536	21	24
10	34298	36574	34330	36593	34315	36578	32	19
11	38795	40687	38819	40200	38802	40181	24	506
12	44091	44336	44025	44467	44057	44503	66	167
13	46539	46784	46305	46748	46336	46595	234	189
14	48032	51563	47587	51251	47591	51234	445	329
15	52875	54786	52902	54869	52859	54787	43	83
16	55772	56371	55719	56442	55748	56436	53	71
17	57107	58285	57003	58309	57085	58294	104	24
18	59924	60720	59964	60699	59994	60695	70	25
19	61473	63520	61473	63623	61564	63204	91	419
20	64467	64751	64409	64717	64480	64804	71	87
21	65887	66659	65929	66597	65875	66496	54	163
22	67838	69285	67861	69304	67845	69294	23	19
23	70644	73754	70660	73763	70650	73741	16	22
24	74232	75985	74164	75995	74296	75981	132	14
25	76830	79947	76861	79716	76832	79393	31	554
26	81395	85675	81420	85726	81412	85654	25	72
						Average	64	114
						No. of Outliers (No-Passing Zones > Average)	8	7
						Average w/o Outliers	24	34

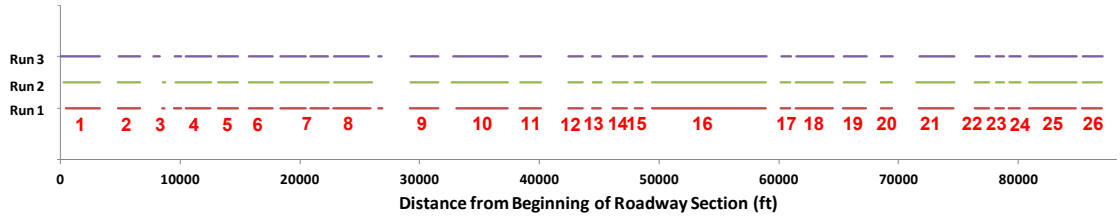

Figure 74. FM 390 westbound (Beacon mode), calculated no-passing zones

Table 25. Calculated no-passing zones for FM 390 westbound (Beacon mode)

Calculated No-Passing Zone	Run 1		Run 2		Run 3		Max Difference	
	Begin (ft)	End (ft)	Begin (ft)	End (ft)	Begin (ft)	End (ft)	Begin (ft)	End (ft)
1	437	3264	231	3296	0	3288	437	32
2	4817	6649	4806	6643	4835	6643	29	6
3	8463	8694	8540	8739	7773	8305	767	434
4	9490	12527	9569	12558	9536	12559	79	32
5	13128	14776	13138	14789	13150	14793	22	17
6	15700	17680	15714	17699	15730	17707	30	27
7	18370	22382	18336	22366	18363	22337	34	45
8	22795	25872	22879	25989	22826	25763	84	226
9	29189	31525	29236	31528	29228	31541	47	16
10	33055	37330	32649	37341	32822	37349	406	19
11	38365	40113	38375	40111	38373	40132	10	21
12	42428	43584	42439	43595	42419	43588	20	11
13	44416	45141	44440	45171	44385	45136	55	35
14	46132	47320	46141	47359	46134	47387	9	67
15	47931	48614	47947	48590	47930	48596	17	24
16	49436	58894	49412	58910	49475	58953	63	59
17	60164	60959	60180	60975	60219	61011	55	52
18	61419	64514	61436	64539	61457	64560	38	46
19	65395	67280	65414	67229	65448	67372	53	143
20	68505	69456	68535	69469	68540	69523	35	67
21	71709	74610	71501	74648	71751	74688	250	78
22	76378	77539	76402	77576	76442	77601	64	62
23	78120	78782	78131	78794	78183	78801	63	19
24	79223	80144	79266	80186	79275	80202	52	58
25	80918	84832	80908	84846	80937	84889	29	57
26	85344	86985	85372	86984	85408	87026	64	42
						Average	108	65
						No. of Outliers (No-Passing Zones > Average)	4	6
						Average w/o Outliers	43	34

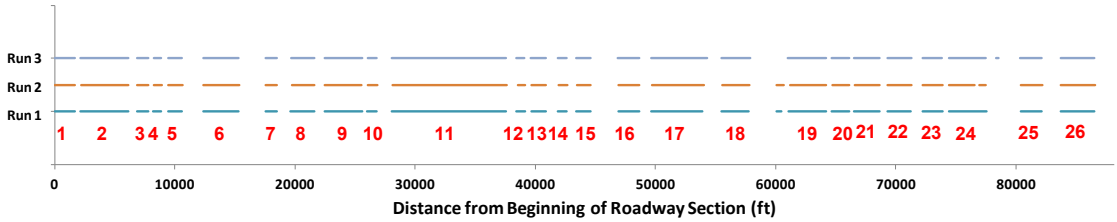

Figure 75. FM 390 eastbound (Beacon mode), calculated no-passing zones

Table 26. Calculated no-passing zones for FM 390 eastbound (Beacon mode)

Calculated No-Passing Zone	Run 1		Run 2		Run 3		Max Difference	
	Begin (ft)	End (ft)	Begin (ft)	End (ft)	Begin (ft)	End (ft)	Begin (ft)	End (ft)
1	0	1658	0	1680	0	1650	0	30
2	2176	6106	2186	6116	2167	6101	19	15
3	6845	7772	6858	7785	6842	7763	16	22
4	8217	8850	8245	8899	8242	8868	28	49
5	9427	10619	9481	10626	9446	10607	54	19
6	12374	15285	12359	15385	12371	15274	15	111
7	17541	18496	17553	18507	17541	18485	12	22
8	19639	21613	19726	21624	19700	21610	87	14
9	22489	25585	22511	25562	22469	25600	42	38
10	26035	26830	26048	26835	26038	26832	13	5
11	28092	37575	28130	37608	28095	37574	38	34
12	38455	39133	38552	39170	38422	39097	130	73
13	39666	40873	39695	40886	39655	40872	40	14
14	41885	42638	41922	42653	41877	42624	45	29
15	43434	44628	43452	44642	43435	44624	18	18
16	46905	48657	46909	48669	46897	48643	12	26
17	49689	53931	49697	54016	49683	54288	14	357
18	55501	57758	55547	57852	55500	57906	47	148
19	61112	64204	61223	64243	61033	64203	190	40
20	64687	66113	64712	66158	64681	66124	31	45
21	66555	68640	66587	68665	66545	68657	42	25
22	69322	71279	69352	71329	69327	71307	30	50
23	72246	73884	72280	73915	72244	73870	36	45
24	74464	77540	74466	77520	74462	77513	4	27
25	80402	82188	80434	82225	80395	82184	39	41
26	83730	86568	83752	86605	83733	86562	22	43
						Average	39	52
						No. of Outliers (No-Passing Zones > Average)	9	4
						Average w/o Outliers	20	30

The average of the maximum differences was calculated for the beginnings and the ends of the calculated no-passing zones in each table. For example, the averages of the maximum differences are 43 and 59 feet for the beginnings and the ends of all the calculated no-passing zones, respectively, in the westbound of FM 166 (see Table 21). The averages were compared with the maximum differences in the beginnings and the ends of the calculated no-passing zones in each table, and the numbers of the no-passing zones with the maximum difference values greater than the average (i.e., outliers) were determined and listed in the tables. Although the outliers represent the uncertainty in the results, the small number of outliers in this research study indicates the reasonably of the results and the robustness of the developed model. Further studies are required to investigate the reason for the variability among the results. For example, there are 3 and 2 outliers related to the beginnings and the ends of the no-passing zones, respectively, calculated for the westbound direction of FM 166 (Table 21). If we eliminate the outliers for this roadway, the averages of the maximum difference values will be 14 and 16 feet for the beginning and the end of the no-passing zones, respectively. Those are the averages without considering the outliers, calculated for both directions of all three highways under the study (Tables 21 to 26). Furthermore, the averages of those six averages are calculated for the beginning and the end of the no-passing zones as follows:

For the beginning points: $(14 + 11 + 33 + 24 + 43 + 20)/6 = 24.2$ ft

For the ending points: $(16 + 6 + 24 + 34 + 34 + 30)/6 = 24$ ft

The results of the above calculations show a consistent average of the maximum differences for the beginning and the ending points of all the calculated no-passing

zones. This means that adding a length of 24 feet to both the beginning and the end of each calculated no-passing zone does compensate for the probable inaccuracies in the GPS data points and the resulting uncertainties.

CHAPTER VII

SUMMARY AND CONCLUSION

A majority of the existing roadways were designed and constructed a long time ago, and locating no-passing zone for them after years of maintenance and restructuring has always been a challenging task for highway agencies. Either there may be no design information related to all of those roadways at the present time, or checking the design plans is not helpful, as the roadway surface may not always comply with the designs. Furthermore, surveying the existing roadway surface is time consuming and not feasible. On the other hand, highway agencies have to locate or reestablish no-passing zones whenever the speed limit changes, and sometimes when the pavement is resurfaced. Various methods of field measurements exist for calculating passing sight distance and determining the location of no-passing zones. However, there are one or more weaknesses in these methods due to the amount of time required, accuracy obtained, and/or related safety issues presented. Therefore, there was a need for an automated method to locate no-passing zones for implementation by transportation agencies. The goal of this research study was to develop a new analytical algorithm to determine the availability of passing sight distance with less data input than other existing models, yet yielding the desired level of accuracy. The algorithm can be ultimately applied in a system which automates the process for locating no-passing zones on two-lane highways.

Several new analytical algorithms were developed and presented in this research study. Vector product calculations were used to develop an algorithm for modeling the geometry of the roadway center line based on the spatial coordinates of available data points representing the center of a travel lane. Next, an algorithm was developed to capture mathematically the visual clear zone boundaries on both sides of the roadway. Based on the geometry of the roadway center line and the visual clear zone boundaries, a horizontal sight distance algorithm was developed. The algorithm uses vector operations to examine the intersection of the sight line that originated from points located on the roadway center line, and the visual clear zones boundaries on both side of the roadway. The algorithm is appropriate for the areas where the terrain is flat (level terrain). Furthermore, another algorithm was developed for analyzing the availability of sight distance along the vertical profiles of two-lane highways. The algorithm is applicable to the straight alignments of two-lane highways. Finally, the main analytical algorithm was developed for evaluating the available three-dimensional passing sight distance for two-lane highways. The algorithm determines the available sight distance by examining the intersection of sight line and imaginary planes passing through midpoints, located on the roadway center line, and perpendicular to both the axis of the road and *x*-*y* plane. The distinguished feature of the passing sight distance algorithm is that all the processes are independent of the orientation of the roadway. This made it effective as the basis for creating a computer-based model for determining the location of no-passing zones using GPS coordinates. By integrating the algorithms, a computer model was developed to locate passing and no-passing zones on two-lane highways. Also, a user-friendly

software package (NPZ program) was created based on the developed computer model to automate locating no-passing zones using GPS data. The program takes input data (GPS data points), processes the data, and generates output data. It identifies the start and end locations of no-passing zones (solid lines) in terms of the distances from the beginning of the highway under study.

MAIN FINDINGS

There are a few main findings summarized from the previous chapters of this dissertation:

1) The conventional models for evaluating passing sight distances on two-lane highways are based entirely on two-dimensional separate alignments. These models calculate sight distance based on horizontal and vertical geometry separately and retain the minimum of those two values at each point of interest. Such models do not consider the three-dimensional nature of the geometric design. Ignoring the three-dimensional nature of the highway alignment may overestimate or underestimate the available sight distance, resulting in serious consequences for the operation and safety of highways. Few models have been developed to work on three-dimensional alignments; however, one of the first steps in using those models is to compile data describing the highway to be evaluated. The models need exact design information including intensive detailed information about highway segment geometry (horizontal alignment, vertical alignment, and cross section). The developed model in this research

study deals with a minimum level of input data and doesn't require detailed information about highway and roadside geometry.

2) The development of the algorithm was based on the assumption of uniform visual clear zones with fixed distance boundaries. The assumption is quite reasonable when no data about discrete obstructions (such as buildings) exist and a fairly constant width of visual clear zones is expected. It hence checks for a minimum level of available horizontal sight distance which is sufficient for determining the horizontal passing sight distance and locating no-passing zones in two-lane highways.
3) The developed model can deal with any arbitrary alignments (individual horizontal or vertical alignments, as well as complex combined horizontal and vertical alignments) including the elements such as tangent segments, simple curves, reverse curves, spiral curves, and unsymmetric (compound) curves.
4) The analytical model not only determines the availability of passing sight distance along any arbitrary alignment, but can check the existence of sight-hidden dips (in vertical curves) and blind spots (in horizontal curves).
5) The available passing sight distance on a two-lane highway depends on the direction of the travel. The resulted no-passing zones for the traffic in both directions may overlap or there may be a gap between their ends. The traditional methods for determining the location of no-passing zones require measuring passing sight distance in the field for different directions of travel separately; which is time consuming. The three-dimensional passing sight distance algorithm, developed in this research study, evaluates the sight distance by having the geometry of the

roadway center line (coordinates of the points located on the roadway center line). The geometry of the roadway center line must be in the format of sets of data points sorted in one direction of the roadway. The algorithm analyzes the sight distance in that specific direction along the roadway alignment. However, the evaluation of available sight distance in the opposing direction is easily conducted by reversing the data points and applying the algorithm to the reversed data points. The capability means that data needs to be collected in only one direction of travel.

6) The computer program should be of great interest to highway agencies since it can have different applications. The NZP program can replace the current field measurement method for locating no-passing zones on existing highways. The implementation of this automated method would save time and costs, avoid human errors, and be safer compared to the current methods of no-passing zone location. Furthermore, by applying the program, the agencies will be able to oversee and check the accuracy of existing no-passing zones located and marked by the field crews. The third possible application of the program would be for evaluating sight distance in new design, and also selecting the optimal design since the values for passing sight distance in the 2011 AASHTO Green Book is now consistent with the MUTCD. It means that applying the program can provide the flexibility to change the alignments and analyze the resulting available passing sight distances during the design process.
7) GPS data were collected in three different two-lane highways using different GPS receivers. Finally, the output of the developed NPZ program was verified

by comparing to the existing field no-passing zones. The verification shows that the developed algorithm and computer program can be used to determine the available sight distance and locate no-passing zones.

8) As the NPZ program requires points further along the roadway to analyze passing sight distance for any particular point, calculations for points falling near the end of a finite length of road are unable to be completed. That is the reason, in some cases, the length of the last existing field no-passing zone of the roadway segment under study is longer compared to its corresponding calculated no-passing zone.
9) Comparing all the results to the existing no-passing zones, it seems that some adjacent no-passing zones were close enough that they were connected in the field, even though they might be far enough apart to exist as separate no-passing zones according to the MUTCD.
10) It happens that some segments of the roadway include horizontal curves or vertical crest curves, and the program calculates no-passing zones for these segments. However, there are no corresponding existing field no-passing zones for them showing in the graphs. The reason is there were no solid line pavement markings in the field in those segments of the roadway due to the junctions or railroad crossings.
11) The field observation showed that there were no solid line pavement markings in some segments of the roadways with horizontal and/or vertical crest curves. However, the NPZ program calculated no-passing zones for those segments of the roadways.

12) In this research effort, we do not necessarily need to know the exact location (coordinate) of each individual data point. But rather, knowing the relative position of sequential GPS data is sufficient to model the geometry of the roadway and determine the availability of sight distance. Therefore, the GPS receivers with a reasonable accuracy would be sufficient.
13) The results of the linear difference analysis calculations showed a consistent average of the maximum differences (24 feet) for the beginning and also the ending points of all the calculated no-passing zones. This means that adding a length of 24 feet to both the beginning and the end of each calculated no-passing zone does compensate for the variance in the results and the resulting uncertainties. The variance in the results is not due to the developed model. It is due to the inaccuracies in the GPS data points.
14) The main input for the developed model are coordinates of points located along the center of travel lanes. The GPS receiver provides this information. The developed analytical model is accurate provided that the GPS receiver used has reasonable accuracy. Technology advancement leading to the improvement of accuracy of future GPS receivers will provide even better results for the developed model.

FUTURE RESEARCH

Although the objectives of this research have been achieved, valuable extensions merit further study in the future. In this study, the author validated the performance of the

developed method by comparing it against the existing field no-passing zones and measuring the differences by calculating MAPD and RMSD. Therefore, there are two areas that should be the focus of future research. The first is selecting the ground truth by which the calculated no-passing zones were compared. In the comparison study, the calculated no-passing zones were compared to the existing no-passing zone markings; however, there is no guarantee that the existing no-passing zones are correct. Furthermore, in order to calculate MAPD and RMSD, the judgment was made by the author to group the no-passing zones where they seemed similar to the existing field no-passing zones. However, that may not be the most accurate method. As a follow-up to this research study, the author is working on a precise mathematical measurement that can measure the variability of the results of the NPZ program for each GPS receiver. The basic idea behind this measurement is to divide each existing field no-passing zone into segments, based on the calculated no-passing zones, and measure the difference between those segments and passing or no-passing zones that the program calculated. By taking into account the performance of each GPS receiver, this measurement will further validate the model.

REFERENCES

1. Fitzpatrick, K., A. H. Parham, and M. A. Brewer. *Treatment for Crashes on Rural Two-Lane Highways in Texas*. Report No. FHWA/TX-02/4048-2, Texas Transportation Institute, The Texas A&M University System, College Station, TX, 2002.
2. *Manual on Uniform Traffic Control Devices for Streets and Highways*. Federal Highway Administration (FHWA), U.S. Department of Transportation, 2009.
3. Waissi, G. R., and D. E. Cleveland. Sight Distance Relationships Involving Horizontal Curves. In *Transportation Research Record: Journal of Transportation Research Board*, No. 1122, Transportation Research Board of the National Academies, Washington, DC, 1987, pp. 96-107.
4. Hassan, Y., S. M. Easa, and A. O. Abd El Halim. Sight Distance on Horizontal Alignments with Continuous Lateral Obstructions. In *Transportation Research Record: Journal of Transportation Research Board*, No. 1500, Transportation Research Board of the National Academies, Washington, DC, 1995, pp. 31-42.
5. Lovell, D. J. Automated Calculation of Sight Distance from Horizontal Geometry. *ASCE Journal of Transportation Engineering*, Vol. 125, No. 4, 1999, pp. 297-304.
6. Nehate, G., and M. Rys. 3D Calculation of Stopping-Sight Distance from GPS Data. *Journal of Transportation Engineering*, Vol. 132, No. 9, 2006, pp. 691-698.
7. Leroux, D. Software Tool for Location of No-Passing Zones Using GPS Data. In *24th Annual Esri International User Conference*, 2004.

8. Namala, S. R., and M. J. Rys. *Automated Calculation of Passing Sight Distance Using Global Positioning System Data*. Report No. K-TRAN: KSU-03-02, Kansas State University, Manhattan, KS, and Kansas Department of Transportation, Topeka, Kansas, 2006.
9. Williams, C. *Field Location and Marking of No-Passing Zones Due to Vertical Alignments Using Global Positioning System*. Master of Science Thesis, Texas A&M University, 2008.
10. American Association of State Highway and Transportation Officials. *A Policy on Geometric Design of Highways and Streets*. AASHTO, Washington, DC, 2011.
11. American Association of State Highway and Transportation Officials. *A Policy on Geometric Design of Highways and Streets*. AASHTO, Washington, DC, 2004.
12. Harwood, D. W., D. K. Gilmore, K. R. Richard, J. M. Dunn, and C. Sun. *NCHRP Report 605: Passing Sight Distance Criteria*. TRB, National Research Council, Washington, DC, 2008.
13. American Association of State Highway Officials. *A Policy on Criteria for Marking and Signing No-Passing Zones on Two and Three Lane Roads*. AASHO, Washington, DC, 1940.
14. Glennon, J. C. New and Improved Model of Passing Sight Distance on Two-Lane Highways. In *Transportation Research Record: Journal of Transportation Research Board*, No. 1195, Transportation Research Board of the National Academies, Washington, DC, 1988, pp. 132-137.

15. Harwood, D. W., and J. C. Glennon. Passing Sight Distance Design for Passenger Cars and Trucks. In *Transportation Research Record: Journal of Transportation Research Board*, No. 1208, Transportation Research Board of the National Academies, Washington, DC, 1989, pp. 59-69.
16. Andrle, S. J., K. K. Keith, T. McDonald, and D. E. Smith. *Iowa Traffic Control Devices and Pavement Markings: A Manual for Cities and Counties*. Iowa State University, 2001. http://www.ctre.iastate.edu/pubs/itcd/itcd_whole.pdf. Accessed January 24, 2012.
17. *Iowa Traffic and Safety Manual*. Iowa Department of Transportation, Office of Traffic and Safety. http://www.iowadot.gov/traffic/manuals/pdf/07a-01.pdf. Accessed February 3, 2012.
18. *Traffic Control Devices Handbook*. Institute of Transportation Engineers (ITE), Publication No. IR-112, Washington, DC, 2001.
19. Brown, R. L., and J. E. Hummer. *Procedure for Establishing No-Passing Zones*. Final Report, FHWA/NC/95-007, FHWA and NCDOT, Raleigh, NC, 1996.
20. Brown, R. L., and J. E. Hummer. Determining the Best Method for Measuring No-Passing Zones. In *Transportation Research Record: Journal of Transportation Research Board, No. 1701*, Transportation Research Board of the National Academies, Washington, DC, 2000, pp. 61-67.
21. USU/NASA Space Grant/Land Grant Geospatial Extension Program. *High-End DGPS and RTK Systems*. Periodic Report, October 2005.

http://extension.usu.edu/nasa/files/uploads/GTK-tuts/RTK_DGPS.pdf. Accessed August 9, 2010.

22. *What is WAAS?* http://www8.garmin.com/aboutGPS/waas.html. Accessed August 10, 2010.
23. Young, S. E., and R. Miller. High-Accuracy Geometric Highway Model Derived from Multi-Track, Messy GPS Data. In *Proceedings of the 2005 Mid-Continent Transportation Research Symposium*, Ames, IA, August 2005.
24. Awuah-Baffour, R., W. Sarasua, K. K. Dixon, and W. Bachman. Global Positioning System with an Attitude, Method for Collecting Roadway Grade and Superelevation Data, In *Transportation Research Record: Journal of Transportation Research Board*, No. 1592, Transportation Research Board of the National Academies, Washington, DC, 1997, pp. 144-150.
25. Awuah-Baffour, R. Collecting roadway cross slope data using multi antenna-single receiver GPS configuration. In *Proceedings of the International Conference on Applications of Advanced Technology in Transportation Engineering*, 2002, pp. 354-361.
26. Roh, T. H., D. J. Seo, and J. C. Lee. An Accuracy Analysis for Horizontal Alignment of Road by the Kinematic GPS/GLONASS Combination, In *KSCE Journal of Civil Engineering*, Vol. 7, No. 1, 2003, pp. 73-79.
27. Ghilani, C. D., and P. R. Wolf. *Elementary Surveying, An Introduction on Geomatics*, 13th edition, Pearson, 2012.

28. Texas Administrative Code. *Geographic Information Standards*. Title 1, Part 10, Chapter 205, Rule §205.20 Geographic Information Standards. http://info.sos.state.tx.us/pls/pub/readtac$ext.TacPage?sl=T&app=5&p_dir=P&p_rloc=155447&p_tloc=&p_ploc=-1&pg=2&p_tac=155447&ti=1&pt=10&ch=206&rl=1. Accessed August 5, 2011.

29. Ben-Arieh, D., S. Chang, M. Rys, and G. Zhang. Geometric Modeling of Highways Using Global Positioning System Data and B-Spline Approximation. *ASCE Journal of Transportation Engineering*, Vol. 130, No. 5, 2004, pp. 632-636.

30. Makanae, K. An Application of Parametric Curves to Highway Alignment. *Journal of Civil Engineering Information Processing System*, Vol. 8, 1999, pp. 231-238.

31. Castro, M., L. Iglesias, R. Rodríguez-Solano, and J. A. Sánchez. Geometric Modeling of Highways Using Global Positioning System (GPS) Data and Spline Approximation. *Transportation Research Part C*, Vol. 14, No. 4, 2006, pp. 233-243.

32. Lovell, D. J., J. Jong, and P. C. Chang. Clear Zone Requirements Based on Horizontal Sight Distance Considerations. *Transportation Research Part A*, Vol. 35, No. 5, 2001, pp. 391-411.

33. Lovell, D. J., and T. Iida. The Exact Clear Zone Envelope for Piecewise-Linear Alignment Data. *Transportation Research Part B*, Vol. 37, No. 5, 2003, pp. 485-499.

34. Iida, T., and T. Lovell. Convergence of Piecewise-Linear Envelope Curves in Transportation Design. In *Transportation Research Part B*, Vol. 41, No. 5, 2007, pp. 527-539.

35. Hassan, Y., S. M. Easa, and A. O. Abd El Halim. Analytical Model for Sight Distance Analysis on Three-Dimensional Highway Alignments. In *Transportation Research Record: Journal of Transportation Research Board, No. 1523*, Transportation Research Board of the National Academies, Washington, DC, 1996, pp. 1-10.

36. Hassan, Y., S. M. Easa, and A. O. Abd El Halim. Automation of Determining Passing and No-Passing Zones on Two-Lane Highways. *Canadian Journal of Civil Engineering*. Vol. 24, No. 2, 1997, pp. 263-275.

37. Hassan, Y., A. O. Abd El Halim, and S. M. Easa. Application for Automated Determination of Passing and No-Passing Zones: A Case Study. *Canadian Journal of Civil Engineering*. Vol. 24, No. 2, 1997, pp. 276-287.

38. Ismail, K., and T. Sayed. New Algorithm for Calculating 3D Available Sight Distance. *ASCE Journal of Transportation Engineering*, Vol. 33, No. 10, 2007, pp. 572-581.

39. RTK DGPS Receivers, Hydro International Product Survey, October 2007. http://www.hydro-international.com/files/productsurvey_v_pdfdocument_18.pdf. Accessed August 10, 2010.

40. SparkFun Electronics. *GeoChron Blue Datasheet*. http://www.sparkfun.com/datasheets/GPS /geochronblue_datasheet.pdf. Accessed May 15, 2011.

41. GlobalSat Technology Corporation. *GPS Engine Board EM-408*. http://www.usglobalsat .com/store/download/47/em408_ug.pdf. Accessed May 15, 2011.

42. *Nu-metrics® NITESTAR® Model No. NS-50/NS-60 Operation Manual.* Nu-metrics, Uniontown, PA, 1999.

APPENDIX

NMEA SENTENCE INFORMATION

$GPRMC

Name	Example Data	Description
Sentence identifier	$GPRMC	
UTC time	170834	17:08:34 Z
Data status A = ok V = invalid		
Latitude	4124.8963, N	41° 24.8963' N or 41° 24' 54" N
Longitude	08151.6838, W	81° 51.6838' W or 81° 51' 41" W
Speed over ground in knots		
Course over ground in degrees		
Date		
Magnetic variation in degrees		
E or W		
Mode A = autonomous D = DGPS E = DR N = data not valid		
Checksum	*75	Used by program to check for transmission errors

$GPGGA

Name	Example Data	Description
Sentence identifier	$GPGGA	Global Positioning System Fix Data
UTC time	170834	17:08:34 Z
Latitude	4124.8963, N	41° 24.8963' N or 41° 24' 54" N
Longitude	08151.6838, W	81° 51.6838' W or 81° 51' 41" W
Fix quality (position fix indicator): 0 = invalid 1 = GPS fix 2 = DGPS fix	1	Data is from a GPS fix
Number of satellites used	05	5 satellites are in view
Horizontal dilution of precision (HDOP) in meters	1.5	Relative accuracy of horizontal position
Altitude (MSL)	280.2, M	280.2 m above mean sea level
Height of geoid above WGS84 ellipsoid (geoid separation) in meters	-34.0, M	-34.0 m
Time since last DGPS update (age of diff. corr.)	blank	No last update
DGPS reference station ID	blank	No station DI
Checksum	*75	Used by program to check for transmission errors

$GPGSA

Name	Example Data	Description
Sentence identifier	$GPGSA	
Mode: M = manual, forced to operate in 2D or 3D A = 2D automatic, allowed to automatically switch 2D/3D		
Mode: 1 = fix not available 2 = 2D (< 4 SVs used) 3 = 3D (> 3 SVs used)		
ID of SVs used in position fix (satellite used SV on channel 1)		
ID of SVs used in position fix (satellite used SV on channel 2)		
…		
Position dilution of precision (PDOP) in meters		
Horizontal dilution of precision (HDOP) in meters	1.5	Relative accuracy of horizontal position
Vertical dilution of precision (VDOP) in meters		
Checksum	*75	Used by program to check for transmission errors